Adult stem cell-derived secretome based strategies to promote myocardial regeneration

By

Renae Waters
B.Sc., South Dakota School of Mines and Technology, 2014

Submitted to the graduate degree program in Bioengineering and the Graduate Faculty of the University of Kansas in partial fulfillment of the requirements for the degree of Doctor of Philosophy.

_____

Chair: Dr. Arghya Paul

_____

Dr. Cory Berkland

_____

Dr. Steve Soper

_____

Dr. Clay Quint

_____

Dr. Elizabeth Friis

Date Defended: 25 January 2019

The dissertation committee for Renae Waters certifies that this is the approved version of the following dissertation:

Adult stem cell-derived secretome based strategies to promote myocardial regeneration

Chair: Dr. Arghya Paul

Date Approved: 25 January 2019

ABSTRACT

Restoring the functionality of the heart after the occurrence of an acute myocardial infarction requires the design of specific therapies aimed to induce an intricate cascade of biological events necessary to promote myocardium regeneration. To achieve such a challenging task, it is necessary to consider the milieu of proangiogenic, anti-inflammatory and anti-apoptotic paracrine molecules involved in the process of myocardial remodeling that occurs after an acute myocardial infarction. A potential approach is the use of stem cell-derived secretome-based strategies. The secretome is an array of multiple factors including growth factors, cytokines, microRNA (miRNA), and extracellular vesicles (EVs) that are secreted by stem cells to regulate tissue homeostasis. Several pre-clinical studies have shown that the secretome can be delivered to the peri-infarct area of the heart to improve cardiac function and prevent heart failure.

Unfortunately, the clinical translation of secretome-based therapies has been hampered by its heterogeneous nature and by the limited identification of key therapeutic factors responsible for its regenerative potential. Additionally, the lack of retention of the therapeutic factors at the damage site upon delivery imposes another obstacle. Therefore, it is necessary to identify new strategies to standardize the production of secretome and to develop new carriers that will allow the efficient delivery and retention of these therapeutic factors at the therapeutic site.

To address these challenges, the work presented in this thesis aimed to accomplish the following goals: (1) identify the optimal culture strategies for the production of a reproducible stem cell-derived secretome that exhibits cardioprotective and angiogenic properties *in vitro* and *in vivo* as well as, (2) to deliver them efficiently using hydrogels. Several methods have been investigated to reach this goal (1). The first strategy represented the use of stem cell spheroids to produce a

concentrated secretome enriched with angiogenic growth factors that could display a superior angiogenic and cardioprotective efficacy. Additionally, the work of this thesis has been focused on another approach in which stem cells were genetically modified to upregulate the production of a miRNA-146a (miR-146a) in the secretome to further enhance its therapeutic properties (proangiogenic and anti-inflammatory). Finally, to address goal (2), this thesis has also been focused on designing a suitable strategy for the delivery of secretome in a non-invasive manner to the peri-infarct area of the heart. Therefore, a novel nanocomposite injectable hydrogel has been designed as a delivery platform for the secretome and tested both *in vitro* and *in vivo* in an acute myocardial infarction rat model.

Overall, the strategies and findings of this thesis are beneficial to further advance the therapeutic efficacy of secretome-based therapies to promote myocardial regeneration by inhibiting of cardiomyocyte apoptosis, promoting angiogenesis, and modulating of inflammation.

ACKNOWLEDGMENTS

I would like to begin by thanking my advisor, Dr. Arghya Paul for his support and guidance throughout my research project and time at KU. I am extremely grateful for the freedom and flexibility you gave me to pursue my scientific interests in the lab as well as, various outreach and career development opportunities that have helped guide my career choices after graduate school. In addition, opening a new lab at a university is undoubtedly a huge challenge and I am grateful to have had the opportunity to work for someone with your level of enthusiasm and drive.

I would like to thank my committee members, Dr. Cory Berkland, Dr. Steve Soper, Dr. Elizabeth Friis and Dr. Clay Quint for their time and guidance which have brought immense value to my thesis and resulted in several meaningful scientific discussions. In particular, thank you Dr. Cory Berkland for always providing a comfortable place to share all the trials and tribulations I have faced in graduate school. I sincerely appreciate all the advice and support you have given me as I try to figure out my path. Lastly, thank you for the constant encouragement to have faith that everything will work out.

I could not have wished for better group of current and former labmates. In particular, I would like to thank Dr. Settimio Pacelli, Aparna Chakravarti, Saman Modaresi, Jon Whitlow, Vijayan Monoharan, Jeannie Salash and Sayantani Basu for their unwavering help with all the lab work, writing, editing and planning necessary to complete this thesis. You all are truly inspirational people who have a work ethic and dedication second to none and I feel so incredibly blessed to have worked beside you these past several years. Also, thank you for your friendship and enriching my life by sharing little pieces of your culture and traditions. I would like to specifically thank Dr. Settimio Pacelli for always going above the call of duty to support us graduate students. You are absolutely the glue that keeps us all together and I would not be where I am today without your support.

I have also had the opportunity to work with some hardworking and dedicated undergraduate students and research associates who were instrumental in completing the experiments outlined in this thesis including, Francisca Acosta, Siddharth Subham, Divya Murali, Keiko Suzuki, Kartikeya Jodha, Kyley Burkey, and Kyle Rampetsreiter. These students also provided me the opportunity to learn and grow as a mentor and teacher which is a privilege I am extremely grateful for. I would like to specifically thank Siddharth Subham for enduring the last semester of my thesis with me when each day required a unique level of perseverance. I am extremely grateful for your positive attitude, conversation, and willingness to always help no matter what the current unforgiving circumstances were.

In addition, there were many individuals that took the time to train me and help me learn techniques while using the facilities at KU including, Dr. Karen Peltier of the TORP lab, Dr. Prem Singh Thapa-Chetri of the Rosa-Molinar Lab, and Dr. Qingfu Zhu of the He Lab. I would also like to thank our collaborator, Dr. Rafeeq P.H. Ahmed, from the University of Cincinnati for providing the facilities and expertise to test what I had developed in animals.

I am indebted to all the professors associated with the NIH-sponsored Biotechnology Predoctoral Training Program including, Dr. Teruna Siahaan, Dr. David Volkin, Dr. Russ Middaugh, Dr. William Picking, Dr. Wendy Picking, Dr. John Stobaugh, and Dr. Michael Hageman. Thanks to their commitment to share their extensive knowledge of the biotech industry with the next generation of scientists, I received a grant that funded two years of my graduate career and provided me with unparalleled opportunities for training in science and leadership that is directly applicable to industry. This program exposed me to all the opportunities available for scientists to make a tangible impact on the development of live saving medication and has played a key role in deciding my plans after I graduate. In addition, the program allowed me to work at Genentech for

six months where I met several influential scientists that taught me how the drug development process works in industry and confirmed my aspirations to pursue a career in a similar department. I would like to specifically thank Dr. Ann Woys, Dr. Dan Zarraga, Dr. John Wang, Stephanie Yarborough, Alison Bailey, Sasha Howes and Sigurlín Björg Atladóttir for the friendship, support, and advice while I was there.

I am also grateful for the Bioengineering Graduate Program, which allowed me the flexibility to explore different research areas and gain the interdisciplinary training that aligned with my interests. To Denise Bridwell, thank you for all your support with everything from paperwork to the real life implications of graduate school. I would also like to thank Dr. Michael Detamore for his support, advice, and always being willing to assist me with my career and graduate school questions.

In addition to the people that have helped me in graduate school, there have been several teachers and professors that have made an enormous impact on my path to get me to where I am today. Specifically, I would like to thank my undergraduate advisors Dr. Dan Heglund, Dr. Linda DeVeaux, and Lori Coble for first introducing me to research and biomedical engineering. Also, I would like to thank Dr. Prajna Dhar for all her support and guidance while I worked as an undergraduate research associate at KU.

Lastly, I am deeply grateful for all of their love, support, and understanding my family and friends have given me throughout this roller coaster ride. To the women who somehow understand every piece of the puzzle, Jeannie Salash, Aparna Chakravarti, and Jordan Needens, thank you for always being there and listening when I felt like no one could possibly understand. You all have such caring hearts and fierce ambitions and I cannot thank you enough for being there for me throughout my graduate career.

To my mom, Juliann Hull, thank you for being an amazing role model and my biggest cheerleader. I am where I am today because of your sacrifices and for that I am eternally grateful. You were always available when I just needed to vent about my challenging day or needed a reminder of how far I had come. Thank you for always reminding me that nothing is impossible with hard work and faith. Last, but certainly not least, thank you for being my ride-or-die hiking buddy and knowing sometimes being at the top of a mountain is just what my soul needs.

To my two amazing sisters, Stephanie Waters and Stacie Hull, thank you for all your unique support and love that has kept me moving on the most challenging days. Stephanie, thank you for your surprise visits, long conversations on my commute, and always making me feel like I am some sort of superhero in my lab coat. Stacie, thank you for all the unparalleled joy your jokes and wit bring to my life as well as, giving me a fellow engineer companion in the family to talk math and science with.

To my husband, Marshall Davis, thank you for being my teammate on this journey and always saying yes to every adventure that comes our way. I can honestly say that your support is the reason I have taken advantage of several opportunities and cannot thank you enough for your unwavering faith in me and us. Thank you for being strong enough to love me on my worst days and always being up for a game of one-on-one when I need a stress relief. I can't wait to see what this next phase has in store for us.

Finally, I want to thank my two cats who are actually part dog, Fausto and Maya, for always bringing a smile to face and giving me a cuddle buddy at the end of the day.

Most of all, I thank God for all of these blessings.

TABLE OF CONTENTS

ABSTRACT iii
ACKNOWLEDGMENTS v
LIST OF FIGURES xii
LIST OF TABLES xiii
CHAPTER 1. INTRODUCTION TO THESIS 1
CHAPTER 2. STEM CELL-DERIVED SECRETOME FOR CARDIAC REGENERATION 5
ABSTRACT 5
2.1 Introduction 5
2.2 Stem Cell-Based Therapy for Cardiac Regeneration 9
2.3 Stem cell-derived secretome 14
2.3.1 Secretome composition and therapeutic action in cardiac regeneration 14
2.3.2 Methods of Modifying the Secretome Composition 15
2.3.3 Clinical Translation of secretome-based therapies 17
2.4 Injectable hydrogels 19
2.4.1 Natural vs. Synthetic Polymers 20
2.4.2 Composite hydrogels 22
2.4.3 Biomolecule delivery using injectable hydrogels 23
3. CONCLUSIONS 25
CHAPTER 3. STEM CELL SECRETOME-RICH NANOCLAY HYDROGEL: A DUAL ACTION THERAPY FOR MYOCARDIAL REGENERATION 27
ABSTRACT 27
3.1 INTRODUCTION 28
3.2 MATERIALS AND METHODS 30
3.2.1 Preparation of the nanocomposite hydrogels 30
3.2.2 Harnessing the MSC secretome using a microfluidic device 30
3.2.3 Characterization of nanocomposite hydrogels 31
3.2.4 Analysis of angiogenic potential of hydrogels 31
3.2.5 Analysis of the cardioprotective properties of hydrogels 32
3.2.6 Scanning Electron Microscopy (SEM) 33
3.2.7 Swelling studies 33
3.2.8 Statistical analysis 34

3.3 RESULTS AND DISCUSSION 34
3.3.1 Spheroid formation and secretome characterization 34
3.3.2 Nanocomposite hydrogel characterization 35
3.3.3 Angiogenic studies 36
3.3.4 Assessment of the secretome cardioprotective properties 37
3.4 CONCLUSIONS 39
CHAPTER 4. STEM CELL-DERIVED SECRETOME-RICH INJECTABLE HYDROGEL FOR MYOCARDIAL REGENERATION 40
ABSTRACT 40
4.1 INTRODUCTION 40
4.2 MATERIALS AND METHODS 43
4.2.1 Preparation and physical characterization of the nanocomposite hydrogels 43
4.2.2 Harnessing the hASCs secretome using a microchip device 45
4.2.3 Rheological analysis 46
4.2.4 Biocompatibility of the nanocomposite hydrogel *in vitro* 47
4.2.5 HUVEC proliferation, migration and tube formation assays 48
4.2.6 qPCR analysis of apoptotic and stress-related genes in spheroids 49
4.2.7 Biocompatibility assessment of nanocomposite hydrogel *in vivo* 50
4.2.8 *In vivo* acute myocardial infarction surgery 52
4.2.9 *In vivo* assessment of cardiac function 53
4.2.10 Immunostaining of heart sections 54
4.2.11 Statistics 54
4.3 RESULTS AND DISCUSSION 55
4.3.1 Secretome preparation and characterization 55
4.3.2 *In vitro* proangiogenic activity of secretome 57
4.3.3 Formation and characterization of the injectable nanocomposite hydrogel 58
4.3.4 *In Vivo* Biocompatibility of the injectable nanocomposite hydrogels 62
4.3.5. *In vivo* therapeutic efficacy in myocardial infarcted rat model 63
4.4 CONCLUSIONS 65
CHAPTER 5. DEVELOPMENT OF SUPERIOR THERAPEUTIC SECRETOME ENRICHED WITH MIR-146A FOR MYOCARDIAL REGENERATION 67
ABSTRACT 67
5.1 INTRODUCTION 68

5.2 MATERIALS AND METHODS 70
5.2.1 hASCs culture conditions and transfection with miR-146a 70
5.2.2 EV isolation from transfected cells and morphological characterization 71
5.2.3 Western blot analysis of isolated EVs 72
5.2.4 miRNA analysis of isolated EVs 73
5.2.5 Assessment of transfected cell-derived secretome protein composition 74
5.2.6 HUVEC proliferation assay with secretome^{146a} 74
5.2.7 HUVEC migration and tube formation assay with secretome^{146a} 75
5.2.8 Assessment of anti-inflammatory properties of secretome^{146a} on HUVECs 76
5.3 RESULTS AND DISCUSSION 77
5.3.1 Isolation and characterization of miR-146a enriched EVs derived from hASC 77
5.3.2 Angiogenic properties of secretome^{146a} 79
5.3.3 Immunomodulatory properties of secretome^{146a} 81
5.4 CONCLUSIONS 83
CHAPTER 6. CONCLUSIONS 85
REFERENCES 90
APPENDIX A: Figures 109
APPENDIX B: Tables 141

LIST OF FIGURES

CHAPTER 1

No Figures

CHAPTER 2

Figure 2.1 Schematic diagram of an acute myocardial infarction……..111

CHAPTER 3

Figure 3.1 Development of hMSC secretome-loaded hydrogel treatment schematic……...112
Figure 3.2 *In vitro* characterization of the developed nanocomposite hydrogel carrying secretome of hMSC spheroids……...…….……...113
Figure 3.3 Angiogenic potential the developed bioactive nanocomposite hydrogel…..…….....114
Figure 3.4 Cardioprotective nature of the developed bioactive nanocomposite hydrogel…….....115
Figure S3.1 SEM images of Gel-MA nanocomposite hydrogels having different concentration of Laponite……...……...116
Figure S3.2 Swelling equilibrium profiles of the different nanocomposite hydrogels over time……...……117
Figure S3.3 Calcein staining of HUVECs in 3D GelMA nanocomposite hydrogels containing different concentration of Laponite…..……...……118

CHAPTER 4

Figure 4.1 Preparation and characterization of secretome isolated from both hASC spheroids (3D secretome) and hASC monolayer (2D secretome)……..…….....119
Figure 4.2 *In vitro* superior angiogenic potential of hASCs spheroid-derived secretome.....120
Figure 4.3 Effect of Laponite® on the rheological properties of the nanocomposite hydrogel…….....121
Figure 4.4 Positive effect of the secretome loaded nanocomposite hydrogel on cardiac function *in vivo*..……..…….....122
Figure 4.5 Assessment of the *in vivo* proangiogenic and scar area reduction capability of the secretome loaded nanocomposite hydrogel.…….....123
Figure S4.1 Characterization of the injectable nanocomposite hydrogel ……..…...124
Figure S4.2 Effect of Laponite on nanocomposite hydrogel stiffness.……...….125
Figure S4.3 Influence of Laponite concentration on the injectable hydrogel stability and protein release.……..…….……126
Figure S4.4 Effect of secretome on *in vitro* tube network length using tube formation assay.....127
Figure S4.5 Biocompatibility assessment of the injectable nanocomposite hydrogels……....128
Figure S4.6 *In vivo* assessment of pro-inflammatory markers post nanocomposite hydrogel injections…….……..129
Figure S4.7 Cardiac damage assessment post *in vivo* nanocomposite hydrogel injections.....130
Figure S4.8 *In vivo* biocompatibility of the injectable nanocomposite hydrogel…….....131
Figure S4.9 Retention of cardiac function post intramyocardial injection of nanocomposite hydrogel.…….....132
Figure S4.10 *In vivo* cardiac function assessment after secretome delivery with and without the nanocomposite hydrogel……..…….....133

CHAPTER 5

Figure 5.1 Schematic representing the process of hASCs transfection with miR-146a…....134
Figure 5.2 Extracellular vesicle characterization.....135
Figure 5.3 Comparison of the growth factor composition and angiogenic properties of the secretome derived from transfected vs not-transfected hASCs with miR-146a.……...……..136
Figure 5.4 Tube formation assay of HUVEC to test the proangiogenic properties of the secretome...……....138
Figure 5.5 Assessment of the anti-inflammatory response of the secretome[146a]..……....139
Figure S5.1 SEM image displaying the morphological structure of EV.. ……..…....140

CHAPTER 6

No Figures

LIST OF TABLES

CHAPTER 1

No Tables

CHAPTER 2

Table 2.1 Clinical Trials Assessing Adult Stem Cell Therapy for AMI and IHD……...142
Table 2.2 Key Paracrine Molecules for Cardiac Regeneration……...……...…...144

CHAPTER 3

No Tables

CHAPTER 4

No Tables

CHAPTER 5

No Tables

CHAPTER 6

No Tables

CHAPTER 1. INTRODUCTION TO THESIS

The overall objective of this thesis was to develop an alternative treatment to stem cell therapy that would promote cardiac tissue regeneration for patients that have suffered from acute myocardial infarction. To achieve this goal the milieu of angiogenic, cardioprotective, and anti-inflammatory growth factors, cytokines and extracellular vesicles secreted by stem cells (secretome) was thoroughly investigated *in vitro* and tested *in vivo* to prove its efficacy. Precisely, stem cells culture conditions were varied and optimized to obtain a reproducible secretome composition with an angiogenic, anti-inflammatory and cardioprotective effect. In addition, a biocompatible, clinically feasible delivery vehicle that would be mechanically stable after placement into the myocardium was developed to retain the therapeutic secretome at the treatment site. The characterization and development of this treatment is comprised of the following three specific aims: (1) Identify an optimal method of stem-cell derived secretome production and characterize its cardioprotective and angiogenic properties *in vitro* by using a model nanocomposite hydrogel scaffold, (2) Develop an injectable nanocomposite hydrogel for the delivery of stem cell-derived secretome *in vivo* to assess its cardiac regeneration potential, and (3) Enhance the miRNA composition of stem cell-derived secretome and evaluate the angiogenic and anti-inflammatory efficacy *in vitro*.

The first aim was to identify an ideal method to culture stem cells that would cause the production of an angiogenic and cardioprotective secretome. Additionally, a hydrogel scaffold made of gelatin methacrylate (GelMA) and the nanosilicate (Laponite®) was developed and tested *in vitro* for its feasibility to deliver secretome in a controlled manner while maintaining their biological activity (angiogenic and cardioprotective). The second aim was to develop a hydrogel formulation that can be used *in vivo* for the delivery of the therapeutic secretome. To achieve this goal, a nanocomposite injectable hydrogel based on gelatin and the nanosilicate was developed and used as a carrier of

the secretome. The loaded hydrogels were tested *in vivo* in an acute myocardial infarction rat model and assessed for their cardiac regeneration efficacy. The third aim was to improve the angiogenic and anti-inflammatory efficacy of the secretome by transfecting stem cells with miR-146a, whose therapeutic efficacy for myocardial regeneration post-AMI has been well characterized.[1] The subsequent chapters reflect the chronological order of these aims and are organized as described below.

Chapter 2 provides a background of the pathophysiology of an acute myocardial infarction and subsequent ischemic heart disease. Then, a literature review on the pivotal clinical trials using adult stem cell therapy for myocardial regeneration in AMI and IHD patients is discussed with the intention of providing the scientific context that supports the widely accepted mode of action being largely mediated by the secretion of paracrine factors. Additionally, the chapter provides a literature review on the development of paracrine factors secreted by mesenchymal stem cells (MSC) (secretome) as an alternative treatment for myocardial regeneration. Lastly, injectable hydrogels are reviewed as potential delivery devices for MSC-derived secretome. Chapter 2 provides the necessary background knowledge to explain the scientific rationale that guided the choices to use the materials and techniques in each of the subsequent chapters. In addition, this chapter provides valuable insight on the complexity and challenges associated with the development and clinical translation of a treatment that efficiently regenerates the myocardium and restores proper heart function post-AMI.

Chapter 3 addresses the first aim of the thesis by describing different methods for stem cell-derived secretome production. The first strategy consisted of culturing bone marrow derived stem cells

(hMSCs) in spheroids using a polydimethylsiloxane (PDMS) microwell device, while the second method involved the traditional culture of hMSCs as a monolayer. The concentration of the angiogenic growth factors secreted by hMSCs using the two separate culture methods were compared to determine which had the greatest therapeutic potential. Furthermore, the chapter discusses the design of a model hydrogel delivery system to promote the sustained release of angiogenic growth factors present in the secretome. The hydrogel was fabricated using a photo-crosslinked network made of GelMA in combination with various concentrations of the nanosilicate. The release profile of key angiogenic growth factors from the secretome-loaded nanocomposite hydrogels were monitored to evaluate whether the nanosilicate had any effect in controlling the rate of diffusion of the loaded proteins. Lastly, the angiogenic and cardioprotective efficacy of the released growth factors were assessed upon delivery from the model hydrogel platform using several cell assays *in vitro*. Overall, this chapter provides the foundation for the subsequent thesis by confirming the angiogenic and cardioprotective potential of secretome isolated from stem cell spheroids and validate the selection of nanosilicate as an effective strategy to control the delivery of secretome-based angiogenic growth factors.

Chapter 4 addresses the second aim of the thesis by describing the development of an injectable nanocomposite hydrogel to serve as a secretome delivery device for *in vivo* cardiac regeneration. Gelatin was combined with various concentrations of nanosilicate and the biocompatibility, viscosity, stiffness, thixotropic behavior, ability to modulate protein release, and degradation of each of the resulting nanocomposite hydrogels were evaluated. Secretome was isolated from human adipose-derived stem cells (hASCs) due to their ease of harvest, high proliferation rate and inherent ability to produce angiogenic growth factors. hASCs were cultured as spheroids and the

secretome composition was evaluated by quantifying the concentration of the different key angiogenic growth factors and testing their proangiogenic efficacy using *in vitro* cell assays. Lastly, the secretome was loaded in the optimized nanocomposite hydrogel and assessed *in vivo* in an acute myocardial infarction rat model by confirming the biocompatibility and monitoring the improvement in heart function, increase in angiogenesis, and decrease in infarct size after treatment *in vivo*. These results were vital for moving forward to the third aim where the composition of the therapeutic ASC derived secretome was further refined.

Chapter 5 addresses the third aim by focusing on refining the miRNA composition of ASC derived secretome. A non-viral transfection method was used to increase the amount of a well-characterized therapeutic miRNA, miR-146a, within the exosomes present in the ASC derived secretome. The size, protein composition, and morphology of the extracellular vesicles within the secretome was characterized. In addition, the cytokines, angiogenic growth factors and extracellular vesicle miRNA composition within the secretome derived from non-transfected and transfected ASCs was compared. Finally, cell-based assays were used to evaluate the angiogenic and anti-inflammatory efficacy of the secretome.

Chapter 6 addresses the concluding statements of this thesis. The key findings from each aim are summarized and their contribution to the collective goal of identifying a therapeutic treatment for cardiac regeneration is elucidated. Finally, recommendations are made for future work using stem cell-derived secretome for cardiac regeneration. Overall, the work completed in this thesis is a proposed solution to overcome the drawbacks associated with traditional stem cell-based therapies for cardiac regeneration.

CHAPTER 2. STEM CELL-DERIVED SECRETOME FOR CARDIAC REGENERATION

ABSTRACT

The aim of cardiac regenerative medicine is to restore the structural and functional characteristics of the heart tissue in patients who have suffered an AMI by promoting myocardium and vascular tissue growth at the infarct site. This chapter first discusses the pathophysiology of an acute myocardial infarction and the current progress made in the field of stem cell-based therapies for cardiac regeneration. Next, the current insights, production methods and the clinical translation of stem cell-derived secretome as an alternative therapeutic tool for ischemic heart disease are explained. Lastly, the use of various types of injectable hydrogels as delivery strategies for proteins, cytokines, miRNA extracellular vesicles and other therapeutic molecules is described.

2.1 Introduction

On average, one person dies of a cardiovascular disease (CVD) every 40 seconds in the United States making CVD the leading cause of death in this country.[2, 3] Additionally, according to the American Heart Association Heart Disease and Stroke Statistics 2018 Update, the annual direct and indirect costs of CVD and stroke in 2013 and 2014 were $329.7 billion in the United States accounting for 14% of total health expenditures.[4] Specifically, ischemic heart disease (IHD) has a higher mortality rate than any other CVD accounting for one third of deaths worldwide [5, 6] This disease is caused by the inhibition of blood flow to the left ventricle (LV) due to plaque buildup within the coronary arteries (Fig. 2.1). The resulting inadequate perfusion of the LV causes a lack of delivered oxygen to the highly aerobic tissue causing

cardiomyocyte necrosis and a myocardial infarction (MI). Due to the inadequate regenerative capacity of the myocardium, adverse LV remodeling occurs after a MI which ultimately leads to ischemic heart failure caused by changes in LV size, shape, function, cellular and molecular composition.[7]

The intrinsic mechanism of chronic cardiac remodeling after an AMI consists of a complex cascade of events that involves interactions between several different cell types present in the heterogeneous heart tissue, including inflammatory cells, endothelial cells, fibroblasts, and myofibroblasts. Specifically, the mechanism can be divided into two distinct phases, the inflammatory and reparative phase.[8, 9] The hypoxia of IHD initiates a significant increase in necrotic, apoptotic and autophagic cardiomyocytes which begins within hours of the initial coronary artery occlusion. The subsequent release of substances called danger associated molecular patterns (DAMPs) from these cardiomyocytes robustly activates a cascade of inflammatory mediators, including inflammatory cytokines, chemokines, and cell adhesion molecules.[10-12] These DAMPs are also upregulated and released by damaged extracellular matrix, recruited and activated leukocytes, and fibroblasts. DAMPs are also responsible for endothelial activation that leads to the extravasation of recruited leukocytes, originating from the spleen, into the infarct area.[13, 14] Specifically, endothelial adhesion molecules are upregulated and facilitate the binding of leukocyte ligands. This leukocyte binding causes neutrophils and monocytes to roll along the venular endothelium, eventually firmly adhering to the endothelium, and ultimately transendothelial migration occurs by paracelluar trafficking between endothelial cells or intracellular trafficking through endothelial cytoplasmic pores.[15] Following leukocyte infiltration, neutrophils, monocytes and M1 macrophages orchestrate the complex inflammatory response which serves to clear damaged extracellular matrix tissue and cells by promoting phagocytosis of dying cells and tissue digestion via protease and oxidase release.[8] It should be emphasized that the importance of this inflammatory phase has been proven and is a necessary precursor for the subsequent reparative phase to occur.[16]

Inflammation resolution happens within the reparative phase and is also accompanied by myofibroblast proliferation, scar formation, and neovascularization. Specifically, neutrophil apoptosis is a critical

mechanism that facilitates the transition from an inflammatory to a reparative state. Apoptotic neutrophils induce the polarization of macrophages from M1 to M2 by two primary methods. First, the expression on the surface of phosphatidylserine signals on apoptotic neutrophils promotes the phagocytic clearance of the apoptotic cells by M1 macrophages. In addition, apoptotic neutrophils express scavenging cytokines and chemokine receptors that result in tissue depletion of these proteins.[17] Furthermore, the secretion of anti-inflammatory and profibrotic cytokines including IL-10 and TGF-β also are key regulators in the activation of intracellular signals that inhibit the innate immune response and promote tissue repair.

Neovascularization is another key process that occurs in the reparative phase and is crucial for supplying nutrients and oxygen to the infarct region. Vasculature growth into the infarct region is promoted by the upregulation of growth factors, such as vascular endothelial growth factor (VEGF), and growth factor receptors on endothelia cells within the peri-infarct region. Initially, the neo-vessels are formed by the migration, proliferation, and alignment of endothelial cells into tubular structures. In the later phases of healing, growth factors, such as the platelet-derived growth factor (PDGF), promote the reinforcement of the neo-vessels with a mural coating composed of pericytes and smooth muscle cells.[18] The formation of this mural coating is vital for infarct healing because the attenuation of vascular permeability leads to a reduction in leukocyte infiltration and facilitates the transition into the reparative phase of cardiac remodeling.

The increased presence of cardiac fibroblasts and subsequent transdifferentiation to myofibroblasts is a hallmark process of the reparative phase in cardiac remodeling. The origin of the fibroblast population that is recruited to the infarct region is unclear, however, experimental studies have suggested circulating bone marrow progenitors,[19] endothelial cells undergoing mesenchymal transdifferentiation,[20] pericytes,[21] resident fibroblasts,[22] and interstitial fibroblasts from viable periphery tissue are possible sources.[23] Once recruited to the infarct site, soluble factors, such as transforming growth factor beta (TGF-β), and mechanical stress cause fibroblast conversion to a

myofibroblast phenotype which induces proliferation and the promotion of the matrix synthesis.[24] Specifically, a temporary highly plastic matrix primarily comprised of collagen (types I, III, V), fibrin, fibronectin, and laminin is formed, which guides migrating cells, and provides a scaffold for proliferating cells and allows for the dynamic changes to occur throughout the remodeling process.[25] Furthermore, this ECM deposition is vital to maintain mechanical integrity of the LV after the removal of the necrotic tissue. Inadequate ECM accumulation has been shown to cause infarct wall thinning, LV dilation, rupture of the LV, and systolic and diastolic dysfunction post-MI.[25, 26] In addition, the upregulation of matricellular proteins in the infarct region provides binding sites for matrix proteins and cell receptors therefore, modulating the behavior of the heterogeneous cell population involved in cardiac remodeling.[27] Matricellular proteins have also been linked to the regulation of collagen fibrillogenesis which is ultimately a precursor to scar maturation.[28] The final step of the reparative phase is characterized by the maturation and stabilization of the scar tissue that has been deposited. This maturation includes the increased deposition of collagen I, degree of matrix crosslinking, deactivation of reparative cells, and the reduction in myofibroblasts within the infarct region.[29, 30]

Ultimately, the damage to the LV myocardium and subsequent scar formation causes a reduction in the cardiac output. Neurohormonal systems are subsequently activated in an effort to maintain adequate blood circulation to the body.[31] Two primary examples of these mechanisms are sodium and fluid retention driven by the release of angiotensin II and aldosterone, and vasoconstriction induced by activation of the adrenergic system to increase the blood pressure.[32, 33] Although these mechanisms initially compensate for the loss in the LV function, they become maladaptive, causing fluid overload, steady cardiomyocyte death, and myocardial hypertrophy, which promotes additional LV dysfunction and ultimate leads to hearth failure.

Although many patients survive the myocardial infarction (MI) caused by IHD, the absence of robust intrinsic regenerative responses in the heart ultimately leads to heart failure due to the left ventricular dysfunction caused by the replacement of functional myocardium with fibrotic scar tissue. Clinical

practices aim to limit infarction magnitude by providing timely coronary reperfusion, and reduction in microvascular obstruction using pharmacological interventions. These strategies along with significant advances in LV mechanical assistance devices have improved patient survival, however, the only definitive cure for IHD is heart transplantation which is plagued by the organ-donor shortage.[7, 34-36] Therefore, it is imperative that an alternative treatment option is developed to restore proper heart function.

The following sections review how adult stem cells (Table 2.1) and stem cell-derived secretome have been used in cardiac regeneration. In addition, a section will discuss the use of injectable hydrogels as delivery devices for growth factors, cytokines, and extracellular vesicles highlighting the criteria required for their design for secretome delivery.

2.2 Stem Cell-Based Therapy for Cardiac Regeneration

Within the last decade, the use of stem cells for cardiac regeneration has emerged as a leading strategy in the development of a novel treatment to prevent end-stage heart failure in IHD patients that have previously suffered from an acute MI.[37] Adult mesenchymal stem cells (MSCs) have emerged as an ideal option for clinical translation due to their relative ease of isolation from multiple tissue sources, including bone marrow, adipose tissue, umbilical cord blood, and Wharton jelly.[38] Furthermore, their ability to be expanded *ex vivo* and lack of major histocompatibility type II markers allows for the development of an off-the-shelf product from an allograft.[39] Lastly, they exhibit immunosuppressive properties and secrete an extensive profile of anti-apoptotic and angiogenic paracrine factors that can promote cardiac repair.[40] The identification of these positive attributes has led to dedicated efforts to assess the safety and efficacy of adult stem cell therapy in clinical trials.[41] Therefore, this section is dedicated to reviewing the clinical research that has framed the current knowledge on adult stem cell therapy for cardiac regeneration in acute MI and IHD patients. Specifically, the focus will be on the

promising results derived from Phase I-III clinical trials and how these results have caused a shift in the hypothesized mechanism of therapeutic action amongst the scientific community. Lastly, the early preclinical data supporting the current widely accepted paracrine mediated mechanism of action primarily responsible for the improvements in cardiac function observed after the administration of stem cells will be discussed.

The initial strategy of cell-based therapy for AMI was focused on an intracoronary infusion of bone marrow mononuclear cells (BMMNCs) in conjunction with percutaneous coronary intervention to prevent further myocardial damage by limiting cardiomyocyte necrosis.[42] BMMNCs were the predominant cell choice because they do not require *ex vivo* expansion therefore, they could be harvested, isolated, and refused into the same patient efficiently. Initial encouraging results from TOPCARE-AMI (Transplantation of Progenitor Cells and Regeneration Enhancement in Acute Myocardial Infarction)[43] and BOOST (Bone Marrow Transfer to Enhance ST-Elevation Infarct Regeneration)[44] clinical trials showed improvements in left ventricle ejection fraction (LVEF) and a reduction in infarct size after 4-6 weeks in the cell treated group however, these results were limited by the lack of a control group and the open label nature of the study, respectively. Despite the deficiencies in those initial trials, two double-blinded trials, Leauven-AMI[45] and FINCELL[46] (Finish Stem Cell study), also reported increases in LVEF amongst the cell treated group. These findings were further confirmed in the REPAIR-AMI (The Reinfusion of Enriched Progenitor Cells and Infarct Remodeling in Acute Myocardial Infarction),[47] study. This was a phase III, double-blinded, placebo-controlled clinical trial that reported an average 5.5% improvement in the LVEF of the BMMNC group compared with only 3.0% in the placebo group after 4 months. Furthermore, a reduction in composite of death, MI and need for repeat revascularization after 1 year, along with a reduction in mortality at 5 years was also reported. However, despite these results, the subsequent trials showed contradictory results, including the multicenter, double-blinded, placebo-controlled TIME (Use of Adult Autologous Stem Cells in Treating People Who Have Had a Heart Attack),[48] LateTIME (Use of Adult Autologous

Stem Cells in Treating People 2 to 3 Weeks After Having a Heart Attack),[49] SWISS AMI trial (Swiss Multicenter Intracoronary Stem Cells Study in Acute Myocardial Infarction),[50] BOOST-2 trial,[44] and MiHeart/AMI trial.[51] Given the inherent heterogeneity of BMMNCs, Quyyumi et al. selected a CD34+ subpopulation of endothelial progenitor cells isolated from bone marrow to study in their PreSERVE-AMI study (The NBS10 Versus Placebo Post ST Segment Elevation Myocardial Infarction)[52] trial. After 1 year, there was no significant improvement in LVEF or resting myocardial perfusion however, when the data was adjusted using duration of ischemia, a dose-dependent improvement in LVEF, infarct size, and mortality were observed indicating how a purified cell population may provide beneficial effects.

As the preclinical evidence on the immunomodulatory, anti-fibrotic, and angiogenic behavior of mesenchymal stem cells isolated from bone marrow, adipose tissue, umbilical cords, and Wharton's jelly has expanded, IHD clinical trials have conducted studies analyzing the safety and efficacy of mesenchymal stem cells as well. The majority of clinical trials have focused on bone marrow-derived stem cells (BMSCs). One of the initial clinical trials using BMSCs was a phase II randomized, placebo-controlled trial called TAC-HFT (Transendocardial Autologous Cells hBMC in Ischemic Heart Failure),[53] which compared autologous, BMSCs, BMMNCs and placebo. Despite the lack of significant improvement in LVEF in response to either cell treatment, several quality of life (QoL) scores significantly increased and an average reduction in infarct size of 19% was reported in the BMSC group while the BMMNC and placebo group remained the same. These results indicate that BMSCs may have had an anti-fibrotic effect causing a positive effect on exercise capacity. In addition, the results suggest that a significant reduction in LVEF may not be necessary for statistically significant improvements in QoL and function capacity. Another randomized, double-blinded trial called TRIDENT (Transendocardial Stem Cell Injection Delivery Effects on Neomyogenesis),[54] analyzed the effect of allogenic BMSC dose on LVEF. Although a larger follow-up clinical trial with definitive end points is needed, they observed a significant reduction of 3.7% in LVEF after 12 months only in the

group that received 100 million cells and not in the 20 million cell dose group. These results support the general understanding that a large cell dose will most likely be needed in order to overcome low engraftment and viability after cell delivery. The POSEIDON trial (Percutaneous Stem Cell Injection Delivery Effects on Neomyogenesis)[55] was the first to analyze the immune-privilege properties of BMSCs by comparing the safety and efficacy of autologous and allogeneic cells at 3 different doses in a randomized, double-blinded phase I/II trial. At 1 year, the scar size was 33% less than baseline and the left ventricular end-systolic volume (LVESV) and left ventricular end-diastolic volume (LVEDV) decreased in both groups. However, a significant reduction in the LVEDV was only detected in the allogeneic group therefore, supporting the hypothesis that the potency of MSCs derived from young, healthy donors is greater as compared with those from older patients with IHD. Finally, the MSC-HF trial assessed the transendocardial stem cell injection (TESI) of autologous BMSCs in a severe IHD patient population with LVEF <45%. There was a significant increase in the LVEF of 6.2% and reduction of LVESV in the BMSC group compared to the placebo. This difference in these results compared to the TAC-HFT and POSEIDON trails could be due to a higher baseline, difference in cell selection and dose. When taken together, the results from these 3 clinical studies have proven the safety of BMSCs and indicate that they may improve LVEF, functional capacity, cardiac remodeling, and QoL. Umbilical cord-derived mesenchymal stem cells (UC-MSCs) represent another MSC population that has clinical potential due to their high proliferative potential, longevity, immunomodulatory properties, and noninvasive isolation procedure.[56] The RIMECARD (Randomized Clinical Trial of Intravenous Infusion of Umbilical Cord Mesenchymal Stem Cells on Cardiomyopathy),[57] trial investigated the intravenous infusion of allogeneic UC-MSCs in a phase I/II randomized, double-blinded, placebo-controlled trial. After 1 year, the UC-MSC treated patients were the only group that showed a significant increase in LVEF of 7%, improvement in NYHA class, and QoL scores. Lastly, ASCs represent the third main clinically relevant source of MSCs for IHD due to their immunomodulatory, homing, angiogenic, and reparative properties as well as the relative ease of an

abundant isolation from subcutaneous tissue.[58] A small trial called the PRECISE trial (Randomized Clinical Trial of Adipose-Derived Stem Cells in Treatment of Non Revascularizable Ischemic Myocardium),[59] demonstrated the safety and feasibility of a TESI of autologous adipose-derived stem cells (ASCs). The larger Athena trials[60] that followed PRECISE assessed a similar protocol with 2 doses of autologous ASCs (40 and 80 million cells) versus a placebo however, the only improvement that was observed was in QoL scores in the cell treatment groups.

Despite the heterogeneity between the clinical trials summarized above, one consistent observation amongst the majority of the studies is the lack of cell retention and subsequent engraftment within the damaged myocardium. Regardless of the cell type, many studies have shown that the majority of cells that were successfully delivered to the heart die within the first weeks.[40, 61] Furthermore, in the trials that showed positive therapeutic results, the number of cells that actually differentiated into resident cell populations was not large enough to account for the observed clinical benefits.[62] Therefore, scientists began to formulate a new hypothesis behind the therapeutic MSC mechanism of action that did not focus on the delivered cells transdifferentiating into new functional tissue. In 2004, Kinnaird et al. showed that BMSCs secreted vascular endothelial growth factor (VEGF), basic fibroblast growth factor (bFGF) and other cytokines into culture medium.[63] These cells were used in a hindlimb ischemia preclinical model and showed a positive improvement in collateral perfusion that was presumably attributed to arteriogenic cytokines that were secreted by the injected cells. Then, in 2005 Gnecchi et al. demonstrated that an intracardiac injection of cell-free MSC culture medium modified to express the survival gene AKT1 could reduce the infarct size in rats with coronary occlusion.[64,65] This scientific evidence marks the conception of the paracrine hypothesis in which the primary MSC mechanism of therapeutic action for cardiac regeneration is the secretion of paracrine signals that promote several endogenous reparative processes.[66] Several studies have provided further support for this hypothesis and therefore, the paracrine hypothesis in now widely accepted as being primarily responsible for tissue regeneration and cardiac functional improvements observed after the administration of MSCs.[67]

2.3 Stem cell-derived secretome

As stated in the previous section, the current clinical evidence shows that the primary regenerative mechanism of action of MSCs is the secretion of paracrine molecules (cytokines, growth factors, metalloproteinases,[68, 69] mitochondrial transfer[70] and extracellular vesicles (EVs)) that modulate the damaged tissue regeneration and stimulate endogenous repair mechanisms rather than the engraftment and transdifferentiation of the MSCs at the therapeutic site.[62, 64, 65, 71] This mixture of bioactive paracrine molecules known as secretome can be isolated *in vitro* and has gained interest among scientists as a possible cell-free treatment option for tissue regeneration. The following sections will review the composition, therapeutic action and the available strategies to modulate secretome composition for cardiac regeneration post-AMI. The overview on secretome-based therapies will be concluded by a discussion on the vital aspects to consider to facilitate the translation of this type of treatment into the clinic. However, the discussion will not take into consideration the use of secretome paracrine factors to influence cardiac metabolism, contractility, stem or progenitor cell recruitment and cardiomyocyte proliferation since these topics are out of the scope of this thesis.[1, 72, 73]

2.3.1 Secretome composition and therapeutic action in cardiac regeneration

The broad repertoire of paracrine molecule types in secretome is ideal for the activation of multiple therapeutic pathways to address complex pathologies. This is particularly advantageous for myocardial regeneration because, although fibrotic scar formation is the ultimate result of LV remodeling caused by IHD, a complex series of interconnected processes are ultimately responsible for this outcome.[72] These processes include lack of proper blood supply to the LV, cardiomyocyte apoptosis followed by necrosis, inflammation, extracellular matrix degradation, and fibrosis.[74] To date, dedicated efforts investigating the MSC-derived secretome have been focused on identifying and promoting the secretion of growth factors, cytokines, miRNA, and extracellular vesicles that are of interest for

myocardial regeneration due to their anti-apoptotic, immunomodulatory, and angiogenic properties. The main components based on their relevance to promote cardiac regeneration are summarized in Table 2.2. These soluble proteins, small nucleic acids and vesicles are molecular signals that are secreted by cells to interact with other recipient cells either directly or indirectly. Precisely, secretome can influence intracellular pathways of damaged cells or indirectly can induce the secretion of other functional biomolecules from nearby cells.[72] Additionally, the secretome composition has been found to vary depending on the type of MSCs and their tissue of origin.[75-78]

2.3.2 Methods of Modifying the Secretome Composition

As stem cell therapy research has progressed, it has become clear that signaling cues can modify the composition of paracrine molecules secreted by stem cells in addition to influencing stem cell behavior. Therefore, scientists have used this knowledge to promote the *in vitro* production of MSC-derived secretome with a composition that has a higher therapeutic efficacy in promoting cardiac regeneration. One established method is defined as physiological conditioning in which MSCs are cultured in hypoxic (5% O_2) and serum deprived conditions (0% serum) to mimic the ischemic myocardium. Several studies have demonstrated that under these culture conditions MSCs will secrete a significantly higher concentration of angiogenic and cardioprotective growth factors, miRNA encapsulated in exosomes, and cytokines.[79-82] One specific study demonstrated that the secretome isolated from MSCs cultured in serum deprived conditions was able to exhibit proangiogenic and cardioprotective behavior *in vitro.* Similarly, the isolated secretome could, promote capillary formation within the peri-infarct region, reduce the infarct size and the extent of cardiomyocyte apoptosis, and limit ventricular remodeling *in vivo*.[83] In order to gain insight into the specific molecules that were responsible for these promising therapeutic results a gene array of the MSCs and cytokine array of the secretome were completed and compared to fibroblasts and secretome isolated from fibroblasts, respectively. In the

MSC group 32 overexpressed genes encoding for secreted factors and 15 cytokines were present at a higher concentration in the secretome.

Another method used to enhance the secretome composition is genetic manipulation.[84] In their seminal paper, Gnecchi *et al*. used this method to overexpress protein kinase B (Akt) in MSCs and observed after culturing these cells in hypoxic conditions that the resulting secretome had cardioprotective effects on isolated adult rat ventricular cardiomyocytes and significantly reduced the infarct size in a rodent AMI model after MSC delivery.[65] Specifically, the secretome was able to inhibit cardiomyocyte apoptosis and reduce Caspase 3 release. In later publications, these results were attributed to the presence of hypoxic induced Akt regulated stem cell factor in the secretome and upregulation of secreted frizzled related protein 2 in the Akt-MSCs.[85]

Molecular and pharmacological conditioning using cytokines, growth factors and lipopolysaccharides represents another method to modulate the secretome composition. Although there have been no studies to date assessing the myocardial regeneration efficacy of MSC-derived secretome using this conditioning method, MSC studies have shown that TNF-α increases the secretion of VEGF, antioxidants and angiogenic growth factors are secreted more after melatonin treatment causing increased angiogenic efficacy, and MSCs conditioned with lipopolysaccharides secreted a significantly greater concentration of anti-inflammatory cytokines.[86-88]

Additionally, cell-cell interactions and physical conditioning has been proven to have a profound impact on the MSC secretome profile. For example, by culturing MSCs in 3D spheroids scientists have shown a significant increase the secretion of proangiogenic and anti-inflammatory growth factors and cytokines including, VEGF, bFGF, angiogenin, HGF, FGF2, angiopoietin, STC1, PGE2 and TSG-6.[89-93] Ylostalo *et al*. reported that the secretome isolated from MSCs spheroids inhibited the pro-inflammatory behavior of lipopolysaccharide-stimulated macrophages. Specifically, the MSC spheroid-derived secretome inhibited the secretion of pro-inflammatory cytokines (TNFα, CXCL2, IL6, IL12p40, and IL23), promoted the secretion of anti-inflammatory cytokines (IL10 and IL1ra), and

modulated the expression of the activated M2 marker CD206.[93] These results were attributed to the presence of PGE2 in the MSC spheroid secretome through microarray analysis and PGE2 inhibitor studies using silencing RNA. This study proves that MSC secretome is individually capable of promoting anti-inflammatory processes under the optimal culture conditions. Furthermore, Skiles *et al*. determined that the cell number used to form each spheroid influenced both the VEGF concentration secreted and the angiogenic efficacy assessed by an *in vitro* HUVEC proliferation assay.[94] These results highlight the importance of optimizing and maintaining specific culture conditions to ensure a precise control over the MSC-derived secretome composition. Other physical conditioning parameters that have been studied for secretome production include, shear stress and substrate mechanical properities.[95, 96] Overall, this vast array of culture parameters that influence the profile of secreted paracrine factors by MSCs emphasizes the importance in thorough optimization and characterization of the MSC culture conditions for ideal therapeutic efficacy of MSC-derived secretome for myocardial regeneration.

2.3.3 Clinical Translation of secretome-based therapies

A secretome-based treatment has several advantages over traditional stem cell-based therapies, including potential *in vitro* modulation of paracrine molecule composition, reduced potential for an oncogenic response, greater ease of delivery, and lack of an immunogenic response allowing for an allogenic or off-the-shelf treatment option. Despite these advantages and the promising results described in the previous section, there are unresolved concerns associated with secretome-based therapies that will need to be addressed prior to clinical translation. One immediate challenge is the presence xenogeneic serum in the media used to culture MSCs for the production of a therapeutic secretome in preclinical studies. The presence of serum creates two main issues for clinical translation. First, from a regulatory and safety perspective, xenogeneic components pose a risk of contamination with infectious agents such as prions and viruses and therefore, their use as stem cell therapy products

is highly discouraged by the Food and Drug Administration (FDA), European Medicines Agency (EMA), and other regulatory bodies.[97, 98] Furthermore, serum is a highly abundant in proteins, which makes the identification and isolation of low-abundance secreted proteins challenging using analytical techniques.[99] In addition, although the complete removal of serum from the culture media would be an apparent solution, studies have shown that its removal impacts MSC behavior and the profile of secreted factors further emphasizing the importance of data-driven choices in auxiliary media component selection.[100]

As described in the previous section, the heterogeneous composition of MSC-derived secretome provides the opportunity to promote several different endogenous regenerative responses that would lead to a more holistic repair of the myocardium. However, this complex composition poses numerous translational challenges. One of the main challenges to date is the development of robust and accurate potency assays which accurately quantify the biological activity of the MSC secretome.[101] According to the International Conference on Harmonization (ICH), potency assays quantitatively measure the biological activity of a product based on the product attribute that has been correlated to the relevant biological properties.[102] Therefore, potency assays are mandated by the FDA and EMA as vital components of the drug approval process because they set the efficacy standard that ensures consistency from drug discovery to market release. The first step to the development of a potency assay is the identification of the main mode of action (MOA) of the secretome and the paracrine molecules that are responsible for this response. To date, the majority of the studies have focused on the therapeutic benefit of exosomes or complete secretome without characterizing the therapeutic efficacy of the individual components. Due to the proven pleiotropic nature of the paracrine molecules that are present in the MSC-derived secretome, it will be paramount to characterize the influence MSC-secretome has on each type of cell that collectively forms the heterogeneous myocardium.[72, 103] In addition, the development and use of animal models that accurately mimic current clinical protocols for AMI will be vital in obtaining representative data that can predict clinical trial success.[104]

Furthermore, this characterization will require intricate analytical separation and characterization techniques for the enrichment and purification of only essential components. The heterogeneous composition of MSC-secretome makes this challenging because these methods rely on specific chemical and physical characteristics of each molecule.[99] It is likely that there will be remaining non-essential components present in the final product which will need to be proven nontoxic in pre-clinical animal models.

Following robust preclinical results, clinical studies will require large scale manufacturing that will demand strict quality control guidelines to be established and maintained due to the sensitivity of the secretome composition in regards to changes in the MSC microenvironment.[101] Once the optimal therapeutic dose concentration, number of doses and time of administration after an MI have been identified, the stability over time and under distribution conditions will need to be studied. These stability studies will determine the formulation and storage methods that allows for the necessary shelf-life duration and distribution process which is ultimately determined by the treatment duration and location of the patient population. Once again, the complexity of the MSC secretome composition will pose a unique challenge in determining the optimal formulation that will retain the bioactivity of each crucial component and concessions will likely need to be made. Lastly, the cost of the treatment will be of the utmost importance throughout the entire development process to ensure the treatment is feasible for the patient population once it reaches the market.

2.4 Injectable hydrogels*

Injectable hydrogels represent an ideal strategy for the delivery of therapeutic secretome for cardiac regeneration due to several parameters required for hydrogel synthesis that can be modified in order to

* Sections published as Hasan, A., Khattab, A., Islam, M. A., Hweij, K. A., Zeitouny, J., Waters, R., ... & Paul, A. (2015). Injectable hydrogels for cardiac tissue repair after myocardial infarction. Advanced Science, 2(11), 1500122.

tune the delivery properties of the resulting hydrogel. These include the type of polymer, the degree of crosslinking and the mechanism of gelation, which provide great versatility in the design of the ideal hydrogel carrier for secretome delivery. Additionally, injectable hydrogels can be applied with minimally invasive procedures and can provide a spatio-temporal control over the dose released, which minimizes off target effects and associated risks to the patient. Precisely for AMI patients, intramyocardial injections are ideal because the dose can be delivered directly into the LV using an epicardial method or a catheter technique. The main factors that are essential to consider in the development of injectable hydrogels for myocardial regeneration are the physical and material properties, primarily related to hydrogel mechanics, and the biological properties involved in processes such as cell adhesion.[105] In the following sections the different types of polymers and hydrogels will be discussed with a particular focus on the benefits and drawbacks of using natural versus synthetic polymers. Then, the unique and beneficial properties of composite hydrogels will be reviewed with specific examples given. Lastly, the use of injectable hydrogels for the delivery of biomolecules will be discussed because these strategies can give insight into effective strategies for the delivery of stem cell-derived secretome.

2.4.1 Natural vs. Synthetic Polymers

Injectable hydrogels can be made from a vast range of polymers that can be classified as either natural or synthetic in origin.[106] Both natural and synthetic biomaterials present strengths and weaknesses in terms of biomedical applications that must be considered prior to the hydrogel synthesis. Naturally-derived hydrogels are largely biocompatible and supportive of cellular activities however, they exhibit low mechanical strength, may induce an immune response, and are subject to batch-to-batch variations. Furthermore, structural modification of natural polymers is difficult due to the complexity and relatively less amount of control over the degree of functionalization.[107] Despite these drawbacks, naturally-derived biomaterials continue to be a promising component of hydrogels due to their

bioactivity, biodegradability, and the fact that many of them are naturally present in the human body. This correlation can be extremely valuable because one of the major goals of hydrogel synthesis is to produce a structure or delivery device that is analogous to the native tissues. Some examples of natural polymers that have shown significant utility in regenerative medicine include collagen, gelatin, hyaluronic acid, fibrin, and decellularized extracellular matrix (ECM), among several others.[105] Collagen and gelatin exhibit ideal biocompatibility, and thermal reversibility however, their low physical strength can be a concern that is commonly overcome by using crosslinking mechanisms.[108] Hyaluronic acid is a component of glycosaminoglycans that is both biocompatible and biodegradable and has been investigated for wound healing applications. Fibrin hydrogels use the naturally occurring process of fibrinogen polymerizing with thrombin at ambient temperatures to form a crosslinked hydrogel.[109] Cell-associated enzymatic activity promotes the degradation of fibrin during cell migration facilitating matrix remodeling.[110] Lastly, ECM hydrogels have been used because they are capable of replicating the native cellular microenvironment with specific characteristics based on the tissue from which they are extracted. Their composition consists of native chemical and biophysical cues and therefore improve the attachment, survival and function of the transplanted cells. Besides, each tissue has a distinct composition of fibrous proteins, proteoglycans, and glycosaminoglycans that make up its ECM.[111] Conversely, synthetic hydrogels are particularly useful for tissue engineering and regenerative medicine applications because they traditionally exhibit strong mechanical properties and can be chemically modified with relative ease.[112] However, a significant drawback that needs to be properly accounted for is that synthetic polymers are also generally biologically inert because they lack cell binding motifs. Some of the most predominant synthetic polymers that have been used for delivery devices in regenerative medicine include poly(acrylic acid) derivatives (PAA), polyethylene glycol (PEG), and polypeptides.[105] For PAA hydrogels, the permeability and hydrophilicity can be tailored by selecting particular cross-linking mediators however, PAA is not completely biodegradable which can interfere with native tissue growth.[113] In contrast, PEG is a biocompatible and hydrophilic polymer

that has been approved by the FDA for several biomedical applications. PEG is specifically used to prepare biological conjugates,[114] modify surfaces,[115] and stimulate cell membrane synthesis.[113] It does not cause immune responses and has low cell adhesion and protein binding which can serve as a benefit or a hindrance depending on the application.[116, 117] Lastly, polypeptides can form nanofiber hydrogels by means of charge interactions, hydrogen bonding, and other interactions.[118] The use of peptides is very beneficial since they can act as a scaffold that mimics natural extracellular matrices (ECM).[119]

2.4.2 Composite hydrogels

In addition to various natural and synthetic polymer-based hydrogels, a number of hybrid and composite hydrogels have also been tested for application in cardiac repair. Some specific examples include ECM-fibrin hydrogels,[120] alginate-chitosan hydrogels,[121] and ECM-polyethylene glycol hydrogels.[122] More specifically, a fibrin-alginate composite hydrogel was injected into the heart of an AMI animal model and the results showed that the expansion of the infarcted region of the left ventricle stopped upon injection of the hydrogel. Additionally, myocardial stiffness was relatively higher than those of control groups and fibrous collagen in the myocardium border region was increased.[123] Hence, the soluble collagen content in the infarcted zone was decreased, which accounts for the deceleration of damaged tissue enlargement. Thus, injection of fibrin-alginate as well as other suitable composite hydrogels may provide an effective treatment to suppress the expansion of infarcted tissue. Another recent strategy for achieving multiple functionalities in hydrogels is to incorporate various nanoparticles within them, thereby developing nanocomposite hydrogels. The nanoparticles to be incorporated can be polymeric, metallic, ceramic, inorganic, or carbon-based while the strategies of incorporation can be physical entrapment, noncovalent immobilization, or covalent immobilization.[124, 125] The addition of such nanoparticles to a polymer network can improve the mechanical and electrical properties of the hydrogel to better align with the native tissue. Specifically, in the case of myocardial regeneration applications, carbon-based or metal nanomaterials have been incorporated in polymer

networks to match the electrical conductivity of the myocardium therefore, causing minimal disturbance to the heart beat and providing a representative environment for the MSCs that can guide them towards a cardiac lineage.[126, 127] The introduction of a nanomaterial within a polymer network can also modulate the physical properties of the hydrogel causing it to be thixotropic.[128] This is particularly advantageous for injectable hydrogels because it allows the treatment to be easily administered through a syringe but it regains its mechanical integrity once the sheer stress is removed. This effect helps to maximize the retention of the gel at the therapeutic site while minimizing undesirable off-target effects of the treatment. Scientists have successful formulated injectable nanocomposite hydrogels that exhibit these properties using nanosilicate and have used them to for the controlled delivery of therapeutic growth factors.[129, 130]

2.4.3 Biomolecule delivery using injectable hydrogels

The encapsulation of biomolecules within injectable hydrogels has been shown to result in the controlled release of molecules such as growth factors, chemokines, miRNA and EVs therefore, providing optimal sustained release while increasing the molecules half-life compared to a direct bolus injections.[106] An example of this is the use of a pH and temperature responsive hydrogel that increased the retention of bFGF in the acidic microenvironment of the ischemic heart.[131] After 28 days, there was a significantly greater increase in capillary density, arteriolar density, and fractional shortening in the growth factor-loaded hydrogel group indicating an improvement in angiogenesis and cardiac function. Another study using a thermosensitive hydrogel composed of poly δ-valerolactone and polyethylene glycol assessed how different VEGF loading methods effected the therapeutic efficacy of the resulting VEGF-loaded hydrogel *in vivo*.[132] They observed that when VEGF was conjugated, instead of being simply mixed into the hydrogel, there was a significant increase in blood vessel density and an improvement in heart function. These results further emphasize the influence of biomolecule release kinetics and hydrogel design has on the efficacy of regenerative treatments. As stated in the previous

section on stem cell-derived secretome, one major challenge associated with myocardial tissue regeneration is the heterogeneity of the native tissue. With regards to the use of biomolecules, scientists have focused on delivering more than one therapeutic factor per treatment in an effort to promote multiple endogenous regenerative processes. To support this multifactor delivery, scientists have developed hydrogels that will sequentially release therapeutic growth factors leading to a greater degree of spatio-temporal controlled delivery and therefore, a more favorable progression of myocardial regeneration.[133] Ruvinov et al. formulated an injectable affinity-binding hydrogel for the dual delivery of IGF-1 and HGF. This hydrogel design exploits the difference in heparin binding affinities between the two growth factors which directly correlates to their rate of release from the hydrogel. The resulting progressive release of IGF-1 followed by HGF lead to an attenuation of infarct expansion, reduced fibrosis, increased angiogenesis and induced cardiomyocytes cell cycle re-entry. In addition, the hydrogel matrix was able to protect the growth factors from proteolytic degradation. Similar outcomes in angiogenesis and decreases in infarct size were seen in another study with the dual delivery of SDF-1 and an angiogenic peptide (Ac-SDKP) when using a biomimetic hyaluronic acid (HA) injectable hydrogel as opposed to each of the therapeutic factors being delivered individually.[134] These studies highlight how beneficial a thorough hydrogel design can be to increase the therapeutic efficacy of biomolecule regenerative medicine strategies. Other examples of reported positive effects in myocardial regeneration resulting from the encapsulation of therapeutic factors within injectable hydrogels include the use of self-assembling peptides for PDGF-BB and FGF-2 delivery,[135] sonic hedgehog protein and IL-10 encapsulated in a PEG hydrogel,[136] recombinant TIMP-3 delivered using a HA hydrogel,[137] endothelial progenitor cell-derived extracellular vesicles delivered within a modified HA shear-thinning hydrogel,[138] miR-29B delivery using a hyaluronan-based hydrogel,[139] and miR-1825 encapsulation in a gelatin-silicate nanocomposite hydrogel.[140] Together, these studies highlight the broad array of biomolecules that can be released by injectable hydrogels formulated to overcome

specific drawbacks associated with the delivery of the free biomolecules therefore, promoting a more efficient myocardial regenerative response.

3. CONCLUSIONS

As the burgeoning field of myocardial regeneration advances and scientist's knowledge grows, the underlying goal to restore proper function to a damaged heart post-AMI remains. This chapter provided an appropriate overview of the complexity that encompasses this goal beginning with the pathophysiology of an AMI and IHD, largely focusing on the cellular biology. Salient phase I-III clinical trials using adult stem cells were highlighted and, although adult stem cell therapy has not been definitely shown to be effective in the treatment of AMI, together these studies did demonstrate that stem cells act via paracrine mechanisms and not through long-term engraftment.[66] Therefore, the subsequent sections of the chapter have emphasized the use of stem cell-derived secretome as an alternative treatment for myocardial regeneration in AMI patients with IHD. Several conditioning strategies are being used to alter and optimize the stem cell-derived secretome composition including, mimicking the physiological ischemic tissue, genetic modification, the addition of proteins and lipopolysaccharides to the culture media, and the promotion of cell-cell interactions by altering the physical arrangement of the stem cells in culture. Each of these techniques has been shown to promote the secretion of a greater concentration or more diverse composition of paracrine molecules into the stem cell secretome that are able to promote therapeutic processes such as angiogenesis, immunomodulation, cardioprotection and anti-fibrosis. Although promising, these studies largely lack a thorough characterization of the heterogeneous secretome composition and the effect these pleiotropic paracrine molecules have on each of the cell types that comprise the myocardium. This type of detailed characterization will be essential in identifying the secretome therapeutic MOA and therefore, the clinical translation of a MSC-derived secretome treatment for myocardial

regeneration.[101] In addition to the importance of a thorough understanding of the biological activity of the MSC-derived secretome, the development of the device that delivers a precise secretome dose to the damaged myocardium at the correct time is vital to ensure optimal therapeutic efficacy of the treatment. As previously mentioned, injectable hydrogel strategies have gained attention for this purpose due to the opportunity for more minimally invasive, clinically relevant delivery procedures.[105] However, it is important to note that an ideal injectable hydrogel formulation should be composed of materials that produce a hydrogel which is biocompatible, regains mechanical integrity after injection and can modulate the release of the diverse paracrine molecules present in the MSC-derived secretome. Thus, nanocomposite hydrogels that fulfill these criteria may provide the ideal delivery vehicle for MSC-derived secretome to promote myocardial regeneration.

CHAPTER 3. STEM CELL SECRETOME-RICH NANOCLAY HYDROGEL: A DUAL ACTION THERAPY FOR MYOCARDIAL REGENERATION[†]

ABSTRACT

Several strategies can be adopted to augment the secretome composition in angiogenic growth factors. For example, it is well known that stem cells when cultured in stressful condition such as hypoxia and serum deprivation can secrete a larger amount of angiogenic growth factors leading to the production of a more beneficial secretome. Another effective approach to induce stress in the cells, which has been investigated in this study, consists of culturing stem cell as spheroids. Precisely, human bone marrow derived stem cells (hMSCs) have been cultured as spheroids using a polydimethylsiloxane (PDMS) microwell device. The concentration of the angiogenic growth factors secreted by hMSCs spheroids has been compared to the secretome produced by hMSCs cultured in a traditional monolayer. Subsequently, the secreted growth factors have been loaded in a nanocomposite scaffold composed of gelatin methacrylamide (GelMA) and nanosilicate with the goal of identifying a model hydrogel delivery system to promote the sustained release of angiogenic growth factors present in the secretome. The release profile of key angiogenic growth factors from the secretome-loaded nanocomposite hydrogels was evaluated and it was confirmed that nanosilicate could control the rate of release of the loaded proteins. Finally, the angiogenic and cardioprotective properties of the released growth factors were confirmed upon delivery from the model hydrogel platform using several angiogenic and cardioprotective cell assays *in vitro*.

[†] Published as Waters, R., Pacelli, S., Maloney, R., Medhi, I., Ahmed, R. P., & Paul, A. (2016). Stem cell secretome-rich nanoclay hydrogel: a dual action therapy for cardiovascular regeneration. Nanoscale, 8(14), 7371-7376.

3.1 INTRODUCTION

Nanocomposite hydrogels have emerged as a valuable tool in tissue engineering and regenerative medicine as they provide tunable platforms to facilitate the formation of functional tissues.[141-143] In addition, they can be used as a carrier of drugs or growth factors by selecting a suitable nanomaterial, which can efficiently interact with the loaded biomolecule.[144] Specifically, the surface area, charge density and presence of reactive functionalities of the nanomaterial are the major parameters that dictate the loading efficiency and release kinetics. A variety of nanoscale materials are available for these applications, such as synthetic polymers, carbon-based nanotubes (CNTs), graphene oxide (GO) and nanodiamonds.[145-148]

These nanomaterials have been successfully embedded in polymeric networks as a delivery platform for therapeutics. However, their clinical potential in regenerative medicine, particularly for carbon based materials, is currently limited by inefficient loading of multiple therapeutic molecules, non-ideal release kinetics, biodegradability and associated cytotoxicity.[149, 150]

A possible alternative to address these problems is the use of biodegradable, biocompatible, two dimensional synthetic nanoclay materials.[151] Laponite ($Na^{+0.7}$ $[(Si_8Mg_{5.5}Li_{0.3})O_{20}(OH)_4]^{-0.7}$) is an example of synthetic clay from the smectite family that consists of disk-shaped particles with a diameter of approximately 25 nm and a 1 nm thickness.[152, 153] These nanoparticles provide superior physical, chemical, and biological utility when compared to other 2D nanoparticles, such as graphene oxide, due to their uniform shape, discotic charged surface, and high surface-to-volume ratio.[152] These properties allow for anisotropic interactions with anionic, cationic, and neutral polymers to form physically crosslinked networks. In addition, these same interactions can be useful in modulating the release kinetics of drugs and biomolecules.[154] A previous study has reported successful retention and controlled release of vascular endothelial growth factors (VEGF) by adsorbing the bioactive Laponite surface through electrostatic interactions.[155] The

VEGF/Laponite complex was then encapsulated in a collagen scaffold showing enhanced angiogenesis *in vivo* when compared to a collagen scaffold just containing VEGF. This result was attributed to the sustained release in the presence of the synthetic clay.

Nonetheless, scientists have proven that the delivery of multiple growth factors simultaneously can provide an increased therapeutic benefit when compared to monotherapy.[133, 156, 157] This is particularly true for cardiovascular diseases in which a mixture of paracrine growth factors has been shown to promote local angiogenesis and regenerate myocardial tissue. A natural way of producing growth factor-rich conditioned media, also known as secretome, is culturing mesenchymal stem cells (MSCs) under specific stressful conditions such as hypoxia and serum deprivation.

The secretome, isolated from MSCs, has been shown to have cardioprotective abilities, as well as, promote angiogenesis when injected into the peri-infarct area.[158-160] However, the efficacy of this treatment has been hindered by the lack of retention of the secretome components at the site of injury. A nanocomposite hydrogel platform may offer a possible solution to achieve its full therapeutic benefits. This method will also offer an alternate strategy to the widely used stem cell transplantation approach for delivering the paracrine factors.

Here we investigated the possibility of using Laponite nanosilicates and gelatin methacrylate (GelMA) to form a nanocomposite hydrogel for controlled release of stem cell secretome. The overall efficacy of this therapeutic device will be determined following the assessment of two main objectives. First, the effect of nanoclay in controlling the release kinetics of the growth factors present in the secretome needs to be assessed. Second, the proangiogenic and cardioprotective ability of the bioactive nanocomposite hydrogel had to be determined. These two aspects are

necessary for the successful application of this nanocomposite hydrogel for cardiac regeneration as shown in the schematic (Fig 3.1).

3.2 MATERIALS AND METHODS

3.2.1 Preparation of the nanocomposite hydrogels

Synthetic silicate nanoplatelets (Laponite XLG) SiO_2 (59.5%), MgO (27.5%), Na_2O (2.8%) and Li_2O (0.8%) with low heavy metals content were supplied by Southern Clay Products, Inc. (Louisville). Gelatin type A from porcine skin, methacrylic anhydride, Irgacure 2959, were used without further modification from the manufacturer (Sigma-Aldrich, St Louis, MO).

Nanocomposite hydrogels were prepared by mixing a GelMA solution (5% w/v) with different concentrations of Laponite (0.4, 0.8, and 1.0% w/v). Irgacure 2959 (0.5% w/v) was added prior to photoirradiation under UV light. In order to load the nanocomposite hydrogels with secretome 250 μL of polymeric mixture was combined with the 250 μL of media containing secretome prior to photoirradiation. Hydrogels with a thickness of approximately 3.5 mm and a diameter of 4 mm were photocrosslinked at 5 mW/cm^2 for 10 minutes for mechanical testing. Young's Modulus was calculated using the slope of the stress strain curve in the region up to 10% of strain[161].

3.2.2 Harnessing the MSC secretome using a microfluidic device

A microfluidic device was fabricated using a method previously reported.[162] hMSCs were first cultured in 2D conditions using DMEM supplemented with 1% L-glutamine, 1% penicillin/streptomycin, and 10% FBS. hMSCs (passage 2-5) were then trypsinized and a 250 μL solution with a cell density of 5 x 10^6 cells ml^{-1} was injected into the device ensuring an even distribution throughout all the wells. The hMSCs were incubated in a vertical position at 37ºC incubator for 48h to allow formation of spheroids and secretion of paracrine factors in conditioned

media (secretome). Quantification of the growth factors in the secretome was carried out using respective ELISA kits (R&D Systems).

3.2.3 Characterization of nanocomposite hydrogels

Compression studies of the nanocomposite hydrogels were investigated using an RSA-III dynamic mechanical analyser (TA Instrument; New Castle, NE). Samples were cyclically compressed (n=2) up to 25% of their original height at a rate of 0.005 mm/s in order to obtain stress versus strain curves. Then, the compressive modulus was calculated as the slope of the stress versus strain curve from 0% to 10% strain. After the mechanical characterization, secretome release kinetic studies were carried out. The secretome loaded nanocomposite hydrogels were incubated at 37°C in 100 µL of phosphate buffer solution (PBS) for 15 days. The PBS was changed every 3 days and ELISA was used to quantify the amount of VEGF and FGF2 in the PBS incubation solution at each time point.

3.2.4 Analysis of angiogenic potential of hydrogels

For cell study purposes, HUVECs were cultured in normal endothelial growth medium with growth supplements (EGM-2 BulletKit without additional VEGF and FGF, Lonza, Walkersville, MD) and 1% penicillin/streptomycin. Passage 6-9 HUVECs were used in all 3D encapsulation experiments. Prior to encapsulation experiments, HUVECs were trypsinized, centrifuged to obtain a pellet, and mixed with GelMA/Laponite polymeric solution under sterile conditions. The HUVEC cell density in the polymer solution was $3x10^6$ cells per mL. Each gel was fabricated in a 96 well plate by adding 50 µL of the cell suspended hydrogels from different groups (equal volume of secretome and prepolymer gel for NS+ group). After photocrosslinking for one minute, the gels

containing cells were grown for 3 days. Calcein staining was performed to investigate the morphology of the cells and the stained gels were washed with DPBS and high-resolution z-stack images were obtained using a confocal microscope (Olympus FV1200). For the microchannel migration assay, HUVECs were suspended in culture media (without VEGF and FGF) and seeded inside the microchannels. After 36 hours, photomicrographs were taken and analysed in Image J for percentage of area covered by adhered and migrated HUVECs in the different experimental groups[163].

3.2.5 Analysis of the cardioprotective properties of hydrogels

All experimental procedures were performed in accordance with the standard human care guidelines of the Guide for the Care and Use of Laboratory Animals published by the US National Institutes of Health (NIH Publication No. 85-23, revised 1996) and protocol No. 15-06-17-01 approved by the Institutional Animal Care and Use Committee, University of Cincinnati. The neonatal CMs used for this study were isolated from newborn (1–3 day) Fisher-344 rat pups using the Worthington Neonatal CMs Isolation System (Worthington Biochemical) following the manufacturer's protocol and earlier published work[164]. Minced harvested hearts were enzymatically digested by incubation overnight at 4° C in trypsin 50 mg/mL. The tissue was then oxygenated for 1 min and incubated with 5 mL collagenase at a concentration of 300 U/mL on the shaker (2–4 rounds/min) for 30–45 min at 37° C. Following this, the tissue was oxygenated and triturated several times, and undigested tissue was filtered out. The cells were allowed to settle for 20 min at an ambient temperature and centrifuged at 100 x g for 5 min before preplating twice (45 min each) in DMEM media (Hyclone), supplemented with 10% FBS (Hyclone) and Penicillin/Streptomycin at 37°C.

After culturing CMs for 48 hours on the hydrogels in 10% FBS and 5% O_2, the culture conditions were changed to 0% FBS and 1% O_2 for 24 hours to induce cell apoptosis. The resulting cell apoptosis was quantified by monitoring Caspase 3/7 activity using an Apo-ONE ® Caspase-3/7 Assay (Promga) for 12 hours and using a Dead EndTM Colorimetric TUNEL Assay (Promega)[165, 166]. Cell necrosis was quantified using an MTS assay. ROS production under previously mentioned stressed condition on different hydrogel formulations was determined by Intracellular ROS assay at 0 hour and 24 hour using fluorescence imaging.

3.2.6 Scanning Electron Microscopy (SEM)

Hydrogels in fully swollen state were frozen in nitrogen liquid and lyophilized afterwards. Subsequently, the lyophilized samples were cut to expose their cross-sections and coated with gold using a sputter coater. The detailed structure of the sample cross-sections was imaged using an SEM (Hitachi Model S4700, Japan).

3.2.7 Swelling studies

Swelling studies were performed on freeze-dried nanocomposite hydrogels in phosphate buffer (PBS, pH 7.4, ionic strength I = 0.1). Aliquots (20 mg) of the gels were placed in the buffer and allowed to swell at 37.0±0.1°C. After defined intervals of time the hydrogels were weighed and placed back in the media. The results were expressed as swelling ratio over time according to this formula:

$$\text{Swelling ratio (\%)} = ((W_s - W_d) / W_d) \times 100 \qquad \text{[Eq 1]}$$

where W_s and W_d are the weights of the swollen and dry hydrogels, respectively. Each experiment was carried out using 4 sample for each group.

3.2.8 Statistical analysis

Quantitative variables are presented as mean ± Standard Deviation (SD) from independent experiments as described in the figure legends. Statistics were performed using two-way and/or one-way Analysis of variance (ANOVA) by Bonferroni's multiple comparison post-hoc test. All statistical analyses were performed with Prism 5 (GraphPad Software). P value <0.05 was considered significant.

3.3 RESULTS AND DISCUSSION

3.3.1 Spheroid formation and secretome characterization

To efficiently harness a high concentration of secretome, hMSC spheroids were prepared. This method was chosen because spheroid culture provides a high ratio of cells to media volume that allows for the production of a highly concentrated secretome. Microfabrication technology was used to develop microscale arrayed wells in order to generate the human bone marrow-derived mesenchymal stem cell (hMSC) spheroids.[162] Concave microwells (300 μm wide) were fabricated starting from microfluidic channels combined with pentagonal chambers using polydimethylsiloxane (PDMS). Subsequently, a PDMS solution was introduced into the microfluidic channel filling these chambers. Finally, using suction and a pressing and rolling technique the excess PDMS solution was removed from the chambers. This leads to the production of the concave microwells after curing of the remaining PDMS solution. The formation of this final product is directly attributed to the surface tension of PDMS (Fig 3.2A). An hMSC suspension was introduced into the culture device through the inlet port which resulted in a uniform

number of cells trapped in each concave well (Fig 3.2B). Spheroids were cultured for 48 hours in order to promote the secretion of paracrine factors. The amount of growth factors in the media was quantified using ELISA and compared to hMSCs cultured in 2D under the same conditions. Specifically, the amount of vascular endothelial growth factor (VEGF), fibroblast growth factor 2 (FGF2), angiogenin, and bone morphogenetic protein 2 (BMP2) were found to be significantly higher in the spheroid culture (Fig 3.2C). Among all the bioactive molecules, these were chosen due to their integral role in cardiac regeneration by promoting angiogenesis, attenuating apoptotic pathways, and remodeling the damaged myocardium.[167]

3.3.2 Nanocomposite hydrogel characterization

A possible strategy to improve their therapeutic efficacy is to design a delivery platform that can control their release over time in the site of cardiac injury. For this reason, different nanocomposite photochemical hydrogels based on GelMA and Laponite were fabricated for the delivery of secretome. GelMA is a chemically modified version of gelatin that can easily form a photo-crosslinkable hydrogel due to the presence of methacrylic groups. The systems tested in this study were prepared using GelMA (5.0% w/v) with a medium degree of methacrylation (~50% amine substitution)[168]. The presence of a microporous network was confirmed by scanning electron microscopy (SEM) (Fig 3.2D). The concentration of Laponite was shown to have no effect on the porosity of the hydrogel network (Fig S3.1). The influence of Laponite over the mechanical properties of the photo-crosslinkable hydrogel was investigated through unconfined uniaxial cyclic compression studies (Fig 3.2E). As the concentration of Laponite in the GelMA hydrogel was increased from 0.4% to 1% w/v a corresponding enhancement in the mechanical properties was observed. As expected, GelMA hydrogels with the highest concentration of nanoclay showed the greatest Young's Modulus value (Fig 3.2F). This observed increase in stiffness is comparable to

previously reported results using the same nanocomposite system.[152] These results can potentially be attributed to the electrostatic interactions between the surface of the clay and the polymer chains.[169] The very same electrostatic interactions can play a fundamental role in modulating the release of the previously mentioned growth factors. For this reason, the *in vitro* release studies in PBS were carried out for VEGF and FGF2 to assess how the concentration of Laponite could affect their release kinetics (Fig 3.2G and H). A better control over the release of VEGF and FGF2 was observed in the formulations containing the higher amount of clay although no significant difference in the swelling behavior was detected between the groups (Fig S3.2). Specifically, Laponite was able to slow down the amount of growth factors released over time (15 days). This observed effect was directly dependent on clay concentration. We hypothesize that the mechanism responsible for the controlled release of VEGF and FGF2 is mainly due to electrostatic interactions between the growth factors and Laponite, however, hydrogen bonding and ion-dipole interactions could also be involved. In addition, the nanocomposite hydrogels (0.8% and 1.0 % w/v), minimized the initial amount of growth factor detected (t=0). This indicates that the increase in Laponite concentration leads to a more compact matrix capable of better retaining the growth factors for a prolonged period of time. For this reason nanocomposite hydrogels with a concentration less than 0.8% w/v were not further considered in the study.

3.3.3 Angiogenic studies

Next, the angiogenic potential of the hydrogels was tested in order to evaluate the bioactivity of the nanocomposite hydrogel using HUVECs as a model cell line. In particular, nanocomposite hydrogels loaded with secretome were further tested to prove their ability to influence HUVEC proliferation overtime. Growth factors were loaded by mixing the secretome solution with GelMA prior to UV gelation, therefore, it was necessary to verify whether the therapeutic ability of

secretome is maintained after the photo- crosslinking process. HUVEC (3 x 10^6 cells ml^{-1}) were encapsulated in three different groups: GelMA hydrogel (Ctrl Gel), GelMA/Laponite hydrogel (NS Gel), and GelMA/Laponite secretome loaded hydrogel (NS Gel+). All of the studies reported used a nanocomposite hydrogel with a Laponite concentration of 0.8% w/v. Results using 1.0% w/v of Laponite were included in the supporting information as the stiffness of the matrix hindered the HUVEC spreading in the 3D polymeric network (Fig S3.3).

At day 3 a statistically significant increase in HUVEC proliferation was observed for the NS Gel+ (Fig 3.3A) with respect to the other groups. In addition, the formation of tubular-like structures was more evident in the NS Gel+ system (Fig 3.3B) indicating the formation of a more mature cell network. HUVECs were able to spread throughout the total thickness of the NS Gel+ at day 3 (Fig 3C) as shown by the 3D reconstruction of the gel using confocal imaging. Subsequently, a microchannel migration assay was used to further assess the angiogenesis potential of the NS Gel+ system. The microchannel was fabricated throughout the thickness of the hydrogels by inserting a 200 μm needle into the polymeric solution prior to gelation (Fig 3.3D). NS Gel+ showed the greatest potential for lumen formation due to a significant increase in percentage of microchannel area covered (53.5±11.7%) when compared to the Ctrl Gel (25.4±3.3%) and NS Gel (22.6±6%). Overall these findings suggest that the bioactivity of the loaded secretome was not lost after gel formation as demonstrated by the positive influence on HUVEC proliferation and their reorganization into monolayers. These two factors represent fundamental aspects of angiogenesis, which is essential for the regeneration of cardiac tissue.

3.3.4 Assessment of the secretome cardioprotective properties

Apart from angiogenesis, another important mechanism influencing the recovery of cardiac function is the prevention of cell apoptosis and necrosis. Soluble paracrine factors present in

secretome have been shown to have an anti-apoptotic paracrine effect essential for the improvement of heart function post-infarction[170]. For this reason, the anti-apoptotic paracrine effect of the secretome loaded nanocomposite hydrogels was another focus of this study.

Cardiomyocytes (CMs) were seeded on the NS Gel+ in 24 well plate (10^5 cells/well) and cultured for 3 days (Fig 3.4A). Fluorescent phalloidin (F-actin) and DAPI (nuclei) staining showed morphology indicative of healthy CMs. (Fig 3.4B). Then an induction of cell apoptosis was necessary in order to mimic the conditions present in the post-infarct myocardium. This was accomplished by culturing the cells in hypoxia (1% O_2) and serum deprived conditions (0% FBS) for 24 hours after the confirmation of their beating functionality. A TUNEL assay was used to detect the presence of apoptotic cells on the different hydrogels characterized by double-stranded DNA breaks (Fig 3.4C). In the Ctrl Gel and NS Gel an increase in the presence of red staining was observed, which is indicative of apoptotic cells. On the contrary CMs seeded on the NS Gel+ showed a minimal amount of red staining. This result confirms the cardioprotective ability of secretome which is capable of increasing cardiomyocyte survival and preserving CMs morphology. Specifically, the percentage of apoptotic cells was significantly lower in the NS Gel+ (15.7±3.4%) than the other groups (Ctrl Gel: 28.6±1.8%; NS Gel: 27.1±4.9%) (Fig 3.4D). However, MTS assay showed no significant difference in the amount of necrotic cardiomyocyte cells. Another method to confirm the beneficial anti-apoptotic ability of the loaded secretome in the nanocomposite hydrogels is to quantify the production of reactive oxygen species (ROS). An increase in relative fluorescence intensity, indicative of ROS production, was observed only in the Ctrl Gel and NS Gel, whereas no significant change was detected for the NS Gel+ system after 24 hours of induced apoptosis (Fig 3.4E). In addition, activity of Caspase 3/7 was evaluated for 12 hours, as they represent important proteases involved in the execution-phase of cell apoptosis.

Throughout the experiment a higher enzymatic activity was detected for the Ctrl Gel and NS Gel compared to the NS Gel+ confirming the protective ability of the loaded secretome in reducing the apoptosis process (Fig 3.4F).

3.4 CONCLUSIONS

In conclusion, we report two principal findings. First, nanoclay can modulate the controlled release of multiple key growth factors present in stem cell derived secretome. The possible mechanism dictating this release profile is electrostatic interactions between the highly charged surface of Laponite nanoplatelets and the growth factors of the secretome. Second, a stem cell derived secretome loaded nanocomposite hydrogel provides a dual action therapeutic system through its proangiogenic and cardioprotective ability. After the hydrogel is implanted into the damaged myocardium, this approach has the potential to increase the therapeutic efficacy of stem cell derived secretome for cardiac regeneration by increasing its retention in the site of injury. Therefore, the encapsulation of stem cell derived secretome in a nanocomposite hydrogel provides a promising alternative to stem cell therapy for the regeneration of cardiac tissue post myocardial infarction.

CHAPTER 4. STEM CELL-DERIVED SECRETOME-RICH INJECTABLE HYDROGEL FOR MYOCARDIAL REGENERATION[‡]

ABSTRACT

The objective of this study was to develop an injectable and biocompatible hydrogel that can deliver a cocktail of therapeutic biomolecules (secretome) secreted by human adipose-derived stem cells (hASCs) to the peri-infarct myocardium. Gelatin and Laponite® were combined to formulate a shear-thinning, nanocomposite hydrogel (nSi Gel) as an injectable carrier of secretome (nSi Gel+). The growth factor composition and the proangiogenic activity of the secretome were tested *in vitro* by evaluating the proliferation, migration and tube formation of human umbilical endothelial cells. The therapeutic efficacy of the nSi Gel+ system was then investigated *in vivo* in rats by intramyocardial injection into the peri-infarct region. Subsequently, the inflammatory response, angiogenesis, scar formation, and heart function were assessed. Biocompatibility of the developed nSi Gel was confirmed by quantitative PCR and immunohistochemical tests which showed no significant differences in the level of inflammatory genes, microRNAs, and cell marker expression compared to the untreated control group. In addition, the only group that showed a significant increase in capillary density, reduction in scar area and improved cardiac function was treated with the nSi Gel+. Our *in vitro* and *in vivo* findings demonstrate the potential of this new secretome-loaded hydrogel as an alternative strategy to treat myocardial infarction.

4.1 INTRODUCTION

On average, one person dies of cardiovascular disease (CVD) every 40 seconds in the United States [2] making CVD the leading cause of death in this country. [3] Specifically, ischemic heart disease

[‡] Published as Waters, R., Alam, P., Pacelli, S., Chakravarti, A. R., Ahmed, R. P., & Paul, A. (2018). Stem cell-inspired secretome-rich injectable hydrogel to repair injured cardiac tissue. Acta biomaterialia, 69, 95-106.

(IHD), characterized by myocardium necrosis initiated by a lack of oxygen supply to the left ventricle, has a higher mortality rate worldwide than any other CVD. [5] Although many patients survive the myocardial infarction (MI) caused by IHD, the absence of robust intrinsic regenerative responses in the heart ultimately leads to heart failure due to the replacement of functional myocardium with fibrotic scar tissue.

To overcome this adverse remodeling of the myocardium and restore proper heart function, scientists have aimed to promote myocardial regeneration using adult mesenchymal stem cells (MSCs). Promising results have been reported in preclinical and early phase clinical trials using MSCs which demonstrated their therapeutic ability by promoting cardioprotection, endogenous cardiac stem cell stimulation, angiogenesis, and antifibrosis. [171] However, recent evidence indicates that several of these positive outcomes are likely not due to the transdifferentiation and engraftment of the MSCs at the therapeutic site but mainly because of the release of paracrine factors (cytokines, growth factors, and exosomes) from the cells. [62, 65, 71] This mixture of bioactive molecules known as secretome can be isolated *in vitro,* and the biomolecule composition has been shown to greatly depend on the culture conditions that the stem cells are subjected to. Scientists have proven that several parameters such as oxygen percentage, serum concentration, and degree of cell-cell interactions can cause diverse biomolecule secretion profiles. [99, 172] Therefore, significant efforts have been dedicated to characterizing and optimizing the regenerative potential of stem cell-derived secretome, which has several advantages over traditional stem cell therapy. These include the lack of immunogenic rejection allowing for an off-the-shelf product, minimized concern of an oncogenic response, and the possible control over the protein milieu contents through the use of multiple *in vitro* techniques. [72] However, much like traditional stem cell therapy, a simple injection of secretome in the peri-infarct area without any additional carriers often results

in a lack of retention at the delivery site. In fact, therapies based on the bolus injection of multiple growth factors are generally associated with an insufficient local regenerative response along with undesirable off-target effects. [173] Therefore, a method that provides a prolonged retention of secretome at the injection site represents an essential requirement to observe optimal therapeutic efficacy. [174-177]

Injectable hydrogels developed from synthetic and natural biomaterials can potentially provide a method to achieve this goal. [105] Various physical and chemical crosslinking mechanisms can be used to develop hydrogel networks that respond to different stimuli including mechanical stress, pH, enzyme, ionic strength, and temperature variation. [178] Additionally, the introduction of a nanomaterial within the network can modulate their physical properties causing them to exhibit thixotropic behavior. [128] For instance, the formation of nanocomposite hydrogels through the incorporation of various carbon-based, polymeric, and inorganic nanomaterials within the polymeric network has emerged as a valuable method to achieve this desired behavior. [179-183] Among them, synthetic nanoclay, specifically Laponite® ($(Na^{0.7+}[(Si_8Mg_{5.5}Li_{0.3})O_{20}(OH)_4]^{0.7-}$), represents an ideal choice for regenerative medicine applications. Laponite® is a smectite nanoclay comprised of disk-shaped nanoparticles with a diameter of approximately 25 nm and a 1 nm thickness. These nanoparticles overcome biocompatibility concerns associated with some carbon-based nanoparticles while maintaining superior growth factor loading capabilities due to their high surface-to-volume ratio and discotic charged surface. [184, 185] In addition, Laponite® can modulate the release of biomolecules loaded in the hydrogel through electrostatic interactions allowing the use of this type of hydrogel in regenerative tissue applications. [185] Following this strategy, recent studies have demonstrated how the presence of this nanosilicate can help control

the release of growth factors at the site of administration and promote significantly more tissue regeneration than corresponding bolus injections of proteins. [155, 186, 187]

Previously, we have used these nanocomposite hydrogel characteristics to our advantage for the controlled delivery of stem cell derived secretome *in vitro*. [185] We demonstrated that a photocrosslinkable, methacrylated gelatin based nanocomposite scaffold containing Laponite® can control the release of key therapeutic growth factors present in bone marrow-derived mesenchymal stem cell secretome over a prolonged period of time. In addition, *in vitro* cell based assays showed that the secretome loaded nanocomposite hydrogel has both proangiogenic and cardioprotective ability. Building on these encouraging results and recent literature highlighting the proangiogenic potential of hASC-derived secretome in comparison to secretome from bone marrow and Wharton's jelly derived stem cells, we aimed to develop an injectable nanocomposite hydrogel for the delivery of hASC-derived secretome to promote myocardial regeneration post myocardial infarction. [76] We hypothesized that the secretome loaded nanocomposite hydrogel would efficiently promote key therapeutic mechanisms including angiogenesis, scar area reduction, and cardioprotection. Through this strategy, we sought to improve cardiac function and demonstrate the potential of stem cell-derived secretome as an alternative to traditional stem cell therapy for myocardial regeneration.

4.2 MATERIALS AND METHODS

4.2.1 Preparation and physical characterization of the nanocomposite hydrogels

Synthetic silicate nanoplatelets (Laponite® XLG) containing SiO_2 (59.5%), MgO (27.5%), Na_2O (2.8%), Li_2O (0.8%) and a low content of heavy metals were supplied by Southern Clay Products, Inc. (Louisville). Gelatin type A from porcine skin bloom grade 300 was used without further

modification from the manufacturer (Sigma-Aldrich, St Louis, MO). Phosphate buffer saline (PBS) was purchased from Sigma-Aldrich.

A stock solution of 10% w/v gelatin was prepared by dissolving the protein in PBS (pH=7.4) at 37 °C. Stock suspensions of 1, 2, 3, and 4% w/v Laponite® were prepared in ultrapure water at room temperature. The nanocomposite hydrogels were formed by mixing equivalent volumes of the gelatin stock and the corresponding nanoplatelet suspensions in order to obtain a final concentration of 5% w/v gelatin and 0.5, 1, 1.5, and 2% w/v nanosilicates. The hydrogels were used immediately after their preparation unless otherwise specified. Hydrogels were also frozen and freeze dried prior further characterization using elementary Energy-dispersive X-ray spectroscopy (EDX) and Fourier transform infrared spectroscopy (FT-IR). To carry out SEM and EDX characterization, freeze dried samples were mounted on a holder with double sided conductive carbon tape and sputter-coated with gold. SEM images were obtained at an acceleration voltage ranging from 1 to 10 kV with an in-lens detector. For FT-IR spectra analysis, the gels were mixed in KBr tablet, and spectra were recorded in the range of 400 to 4000 cm^{-1} (resolution of 1 cm^{-1}) using a Bruker Vector-22 FTIR spectrophotometer (PIKE Technologies, USA). [188]

Degradation studies were carried out to assess the stability of the nanocomposite hydrogels containing either 0, 1, or 2% (w/v) Laponite®. Each nanocomposite hydrogel was initially freeze dried and weighed prior to the study which was performed in PBS (pH 7.4) at 37 °C while shaking the gel at 60 rpm for 2 weeks. The PBS was replaced every two days. At various time points five samples of each Laponite® concentration were freeze dried and weighed to calculate the percentage of degradation indicated by weight loss using the following equation (1):

$$W_L(\%) = \frac{W_i - W_f}{W_i} \times 100$$

W_i and W_f are the initial and final weight of the nanocomposite hydrogel after degradation, respectively.

Finally, myoglobin was used to determine whether the Laponite® concentration within the nanocomposite hydrogel effected the release profile of a loaded protein.

Nanocomposite hydrogels containing either 1 or 2% Laponite® were loaded with 5 mg/mL myoglobin and subjected to shaking of 60 rpm at 37 °C in the presence of PBS. The concentration of myoglobin within the PBS was determined at various time points by measuring the absorbance at 410 nm.

4.2.2 Harnessing the hASCs secretome using a microchip device

StemFIT 3D microwell® culture dishes were used to culture hASCs spheroids. Each culture dish was 300 mm in diameter containing 389 wells with a diameter of 600 µm. The hASCs used were purchased from Rooster Bio and originated from female donors between the ages of 31-45 years old. Flow cytometry was used by the company to determine that less than 20% of the cells expressed CD14, CD34, CD45 and greater than 70% of the cells expressed CD166, CD105, CD 90, and CD73. In addition to a phenotype confirmation, the multipotency of the cells was tested using 3 week cell differentiation studies. Positive Oil Red O and Alizarin Red staining confirmed the adipogenic and osteogenic differentiation abilities of the cells. These polydimethylsiloxane (PDMS) concave microwells were purchased from Prodizen (Seoul, Korea) and used according to the manufacture's protocol. hASCs (passage 2-6) were initially cultured in traditional 2D conditions (3.3×10^3 cells/cm^2) using hASC High Performance Media (Rooster Bio). The hASCs were then trypsinized and resuspended in serum-free α-MEM media supplemented with 1% L-glutamine and 1% penicillin/streptomycin. hASCs were seeded in the microchips at a cell density of 0.8×10^6 cells per milliliter. The cells were allowed to settle into the microwells of the

microchips for 20 minutes prior to removing all the media being cautious not to withdraw any of the cells in the microwells. This step is necessary to remove all the cells on the periphery of the wells and ensure optimal spheroid formation in the microwells. Finally, 1 mL of serum-free α-MEM media supplemented with 1% of L-glutamine and 1% penicillin/streptomycin was added to each microchip. The hASCs were incubated for 72 hours at 37° C to allow spheroid formation and the secretion of paracrine factors into the media (secretome). The resulting spheroids were fluorescently stained with ethidium bromide (0.2% v/v) and calcein (0.05% v/v) dye to visualize dead and living cells, respectively and assess whether the culture conditions caused any significant cell death. After 72 hours the secretome was collected from the chips, centrifuged at 1000 RPM for 5 minutes, and the secretome supernatant was collected to ensure there was no cellular debris in the secretome. A human angiogenesis antibody array and cytokine array (R&D Systems) were used to detect the relative levels of 55 angiogenic-related proteins and 36 different cytokines, chemokines and acute phase proteins in the secretome. More specifically, images were taken of each chemiluminescent blot, and the mean spot pixel densities for each protein were calculated using ImageJ software. To quantify specific angiogenic growth factors such as VEGF and Angiogenin, their respective ELISA kits were used according to the manufacture's protocols (R&D Systems and System Biosciences).

4.2.3 Rheological analysis

An AR2000 rheometer (TA Instruments, New Castle, DE) was used for mechanical characterization of the nanocomposite hydrogels containing varying concentrations of Laponite®. Viscosity measurements were performed immediately after the Laponite® was homogeneously distributed into the gelatin polymeric solution. The test was carried out using a cone-plate geometry (cone with 20 mm diameter, 1° angle) in the range of shear rates varying from 0.001 to

1000 s^{-1}. The study was conducted at the temperature of 25 °C (n=3). To study the hydrogel mechanical properties, cylindrical hydrogels were formed by introducing 0.5 mL of the gelatin-silicate mixture into in a 24 well plate and allowed to gel overnight at 4 °C. Prior to testing, all gels were removed and allowed to reach 20°C. All tests were performed at 25 °C using a roughened plate geometry (20 mm diameter). An initial strain sweep from 0.1% to 100% at 1 Hz was performed to determine the linear viscoelastic region of the hydrogel that was used for subsequent frequency sweep tests carried out in the range from 0.01 to 10 Hz (n=3). Recovery testing was conducted at 1 Hz by subjecting the hydrogels to 3 consecutive cycles of 5 minutes at 1% strain (within the linear viscoelastic region) and 5 minutes at 100% strain (outside the linear viscoelastic region) (n=3). Temperature sweeps from 25 °C to 40 °C were conducted at 1 Hz and 1% strain (n=3).

4.2.4 Biocompatibility of the nanocomposite hydrogel *in vitro*

Human umbilical vein endothelial cells (HUVECs) (8 x 10^4) were seeded in chamber slides with 10% of the media volume replaced with the gelatin-silicate mixture deriving from each of the different test groups (Lap 0, 1, and 2% w/v). The positive control group (Cntrl+) contained only media. As a negative control (Cntrl-), camptothecin at a concentration of 50 µM was added to the media. After 24 hours, cells were fixed in 4% paraformaldehyde for 5 minutes at 37 °C. Diamidino-2-phenylindole dilactate (DAPI, Invitrogen, USA) and phalloidin-AlexaFluor488 (Invitrogen, USA) were used to counterstain nuclei and actin, respectively. Immunofluorescence images were taken to observe whether or not the addition of the hydrogel had any effect on cell morphology.

Additionally, HUVECs were seeded in a 24 well plate and allowed to reach confluency in endothelial growth medium (EGM-2 BulletKit Lonza, Waldersville, MD) at 37°C and 5% of CO_2. Subsequently, to assess the cytotoxicity of the nanocomposite hydrogel, a Falcon® Permeable

Support (3.0 μm transparent PET membrane) containing 200 μL of the respective nanocomposite hydrogel from each of the different test groups (Lap 0, 1, and 2% w/v) was added to each well. As a control group, HUVECs were not treated with any gels. After 1 day, 3 days, and 5 days of gel exposure, cells were washed with fresh media and an MTS assay was carried out according to the manufacturer's instructions. [189] The absorbance of each well was measured at 490 nm to determine the HUVECs' mitochondrial activity (Cell Titer 96 Aqueous Non-Radioactive Assay, Promega). The number of cells was determined using a calibration curve in the range from 5 x 10^3 up to 2 x 10^5 cells.

4.2.5 HUVEC proliferation, migration and tube formation assays

To assess the proangiogenic ability of the secretome, HUVECs (1 x 10^4 cells/well) were seeded in a 48 well plate and allowed to grow in the media (200 μL) without the addition of VEGF and human fibroblast growth factor-B (hFGF-B). After 3 hours, one-fourth of endothelial growth medium (50 μL) was replaced by secretome derived from the 2D monoculture (2D secretome) or the spheroids (3D secretome) providing a VEGF concentration of 0.15 ng/mL and 1.2 ng/mL, respectively. This volume of secretome was determined to be the optimal volume of α-MEM media tolerated by the HUVECs to allow for the observation of the proangiogenic ability of each type of secretome. As a negative control, cells were not supplemented with any growth factor in the media (Cntrl (-)). The degree of HUVEC proliferation in the presence of the secretome was assessed by MTS cell proliferation assay (n=5) after 24 hours as described in the previous section.

Additionally, HUVECs were also cultured in a 24 well plate (2 x 10^4 cells/well) and allowed to become confluent in endothelial growth medium (400 μL) without the addition of VEGF and hFGF-B. Then, scratches were made in the cell monolayer using a cell scraper followed by several washes with PBS to remove the detached cells. 2D secretome and 3D secretome were

supplemented in the media (100 µL), and HUVECs were allowed to migrate through the scratch for 24 hours. Cells were stained with calcein, and fluorescent images were taken in the same positions along the scratch before and after the 24 hour migration period in all the groups. The cells that did not receive any growth factor supplement served as the negative control. The percentage of area recovered during the migration was calculated using Image J software. The original wound area was determined from the preliminary images and the area recovered was defined as the total wound area that was occupied by cells post 24-hour incubation. [179]

Finally, to determine the ability of the secretome to induce the formation of tubular-like structures, HUVECs were seeded on a growth factor depleted Matrigel-based on the manufacturer's protocol (Matrigel matrix, Basement Membrane, BD). Briefly, 289 µL of growth factor depleted Matrigel Matrix (10 mg/mL) previously cooled to approximately 5 °C was added to a 24 well culture plate on ice. The plate was then incubated at 37°C for 60 minutes to allow the gel to form. Then, HUVECs (1.2×10^5) were seeded on each gel with either endothelial growth medium without growth factors (Cntrl (-)) or supplemented with 2D and 3D secretome. After 10 hours, bright field images of the endothelial networks were taken for each group and the number of complete tubes formed, total network length and total segment length were determined using the Angiogenesis Analyzer for ImageJ. The average numbers from three independent wells were reported. [190]

4.2.6 qPCR analysis of apoptotic and stress-related genes in spheroids

RNeasy Mini Kit (Qiagen, Germany) was used to extract mRNA from the hASCs spheroids and hASCs cultured in well plates following the manufacturer's protocol. The total RNA concentration and purity were determined by measuring the optical density at 260 nm using a spectrophotometer (Nanodrop ND-1000; Thermo Scientific, USA). Complementary DNA (cDNA) was synthesized starting from the isolated RNA using the High-Capacity cDNA Reverse Transcription Kit (Applied

Biosystem, USA). The qPCR analysis was performed in triplicate for each test group on a Mastercycler Realplex (Eppendorf, Germany) using predesigned primers and KiCqStart SYBR Green qPCR Ready Mix (Sigma-Aldrich, USA). Fold expression levels of BCL-2, EPAS1 and HIF1A were calculated using the relative ΔΔCt method, using GAPDH as the housekeeping gene. The gene expression of the hASCs grown in traditional 2D tissue culture flasks was used as a reference group.

4.2.7 Biocompatibility assessment of nanocomposite hydrogel *in vivo*

In vivo biocompatibility experiments were performed using male adult Fischer 344 rats (~8 weeks), each weighing 250–300 g. [179] Animals were anesthetized with isoflurane gas followed by tracheal intubation and ventilation using Rodent Ventilator (Minivent, Type 845 Germany). Animal body temperature was maintained at 37ºC during the surgery. Nanocomposite hydrogels were formulated in accordance with the procedure used for the *in vitro* studies. The hearts were exposed by minimal left-sided thoracotomy and 100 µl of nanocomposite hydrogel (nSi Gel) [5.0% (w/v) Gelatin, 2.0% (w/v) Silicate] or PBS (Control) was intramyocardially injected at multiple sites (5 sites/heart). A total of 10 rats were used (n=5). The chest was closed, and animals were allowed to recover. The animals were maintained on buprinex after surgery for 24 h.

For immunostaining paraffin embedded heart sections were deparaffinized by Xylene to 100% ethanol change (5 min each) and antigen retrieval was done using citrate buffer according to standard protocols. Heart sections were blocked by CAS-block Histochemical Reagent (Thermo Fischer Scientific, USA) for 2 hours at room temperature followed by three PBS washes for 5 minute each. Primary antibodies for TnC (Sigma-Aldrich, USA) and TNFα (Sigma-Aldrich, USA) were used in a working dilution of 1:200 with CAS-Block and individually incubated for overnight at 4°C followed by three PBS washes for 5 minute each. The corresponding secondary antibodies

were used in a working dilution of 1:200 with CAS-Block and individually incubated for 2 hours at room temperature followed by three 5 minute PBS washes. Nuclei were stained by DAPI (Sigma-Aldrich, USA). Images were analyzed using fluorescent microscopy. In addition to immunostaining, A TUNEL assay was performed on deparaffinized 5 μm thick sections with an In-Situ Cell Death Detection Kit, TMR Red (Roche Inc) according to the manufacturer's instructions. [191] Nuclei were stained by 4′,6-diamidino-2-phenylindole (DAPI). The degree of apoptotic cell death was evaluated by calculating the ratio of TUNEL-positive cells to the total number of cells.

Lastly a qPCR analysis of cardiac function and cardiomyocyte cell cycle genes was performed on the myocardium. The frozen tissue samples were homogenized by The Bullet Blender homogenizer (Next Advance, Inc, USA) followed by the total RNA isolation by using Ambion™ TRIzol™ Reagent (Fisher Scientific, USA). Quantification of RNA was done by NanoVue™ Plus Spectrophotometer (GE Healthcare, Buckinghamshire, UK) and RNA quality was checked on 1.0% agarose gel. cDNA synthesis was performed with 1μg total RNA of each sample by using Omniscript Reverse Transcription kit (QIAGEN, USA) following the manufacturer's protocol. RT-PCR expression analysis for APC, TNFα, CyclinD1, Rb1, and Meis2 was performed using specific RT-PCR primer pairs for each gene (Fig S4.8C). RT-PCR primers were synthesized by using Primer3web version 4.0.0 (http://bioinfo.ut.ee/primer3/), and primer quality was checked by UCSC In-Silico PCR (http://rohsdb.cmb.usc.edu/GBshape/cgi-bin/hgPcr). Amplification reactions were performed in duplicate in CFX Connect™ Real-Time PCR Detection System (Bio-Rad, California, USA) using Applied Biosystems® SYBR Green PCR Master Mix (Thermo Fischer Scientific, USA) following the manufacturer's amplification conditions. Quantification of RT-PCR data was performed by using the ΔΔCt method and β-actin served as control. [191] For the

miRNA qPCR, total RNA was isolated by Trizol method, as previously described. The miRNA cDNA synthesis was performed using the miScript II RT Kit dual-buffer system (Qiagen) and miScript HiSpec Buffer. The subsequent miRNA quantification was performed by using miScript Primer Assays according to the manufacturer's protocol. Specific forward primers (Figure S4.8C) with a universal reverse primer were used for the RT-PCR reaction. (http://sabiosciences.com/manuals/BRO_GEF_miRNA_0212_lr.pdf). RT-PCR reactions were performed according to the standard manufacturer's protocol. RNU6 served as internal control. The quantification of miRNA expression was performed using the ΔΔCt method previously described.

4.2.8 *In vivo* acute myocardial infarction surgery

According to established protocols and in compliance with NIH Guide care and Use of Laboratory animals, *in vivo* experiments were performed using a myocardial infarction rat model with adult (~8 weeks) male Fischer 344 rats, each weighing 250–300 g. [179] Animals were anesthetized with isoflurane gas followed by tracheal intubation and ventilation using Rodent Ventilator (Minivent, Type 845 Germany). Animal body temperature was maintained at 37ºC during the surgery. Nanocomposite hydrogels were formulated in accordance with the procedure used for the *in vitro* studies. The hearts were exposed by minimal left-sided thoracotomy and an occlusion of the left ascending coronary artery was used to induce an acute MI according to conventional laboratory procedures. [140, 192, 193] Lyophilized 3D secretome was resuspended in PBS (0.125 mL) and mixed with Gelatin 20% w/v (0.125 mL) and Laponite 4% (0.25 mL) to obtain nSi Gel+. The nSi Gel was formulated using PBS in place of secretome. Then, 15 minutes post infarction 100 µL of either the nanocomposite hydrogel (nSi Gel) or the 3D secretome loaded nanocomposite hydrogel (nSi Gel+, 8 ng VEGF/ rat, 5 ng ANG/rat) was injected in five different sites within the peri-infarct

region of the heart using a 28 gauge syringe (20 µL/injection) (n=5). The control group received an injection of PBS 15 minutes post infarction (n=5). As an additional control group, a secretome was also included and was injected with a secretome solution containing the same amount of VEGF and ANG in the nSi Gel+ 15 minutes post infarction (n=5). A total of 20 rats were used (n=5). The chest was closed, and animals were allowed to recover. The animals were maintained on buprinex after surgery for 24 h. For the heart function assessments, transthoracic echocardiography was performed at day 0, 3, 7, 14, and 21 after surgery for therapeutic efficacy studies. After day 21, the animals were sacrificed, and hearts were frozen or fixed with 4% formalin solution for molecular and histological studies.

4.2.9 *In vivo* assessment of cardiac function

Cardiac function was assessed by transthoracic echocardiography 0, 3, 7, 14, and 21 days after surgery using Vevo®2100 Imaging System, Visualsonics with a 24-MHz transducer, MS250 followed an established protocol. [194, 195] Animals were anesthetized with isoflurane gas, 2-D imaging of hearts was performed and recorded for M-modes through the anterior and posterior left ventricle (LV) walls. Anterior and posterior wall thickness (end-diastolic and end-systolic), LV internal dimensions, LV end-systolic (LVESd) and end-diastolic (LVEDd) diameters were measured from at least 3 consecutive cardiac cycles. Indices of LV systolic function including left ventricle ejection fraction (EF), left ventricle fractional shortening (FS) and cardiac output (CO) were calculated as follows:

$$EF\ (\%) = \frac{(LVEDd^3 - LVEDSd^3)}{LVEDd^3} \times 100$$

$$LVFS = \frac{(LVEDd - LVESd)}{LVEDd} \times 100$$

Cardiac output = heart rate x stroke volume. The results were expressed as percentage ± standard deviation.

4.2.10 Immunostaining of heart sections

Paraffin-embedded heart sections were deparaffinized by introducing the slides in xylene followed by a wash with 100% ethanol. Both steps were carried out for five minutes. Antigen retrieval was done using a standard citrate buffer protocol. [195] Heart sections were blocked by CAS-block Histochemical Reagent (Thermo Fischer Scientific, USA) for 2 hours at room temperature followed by three PBS washing with 5 minutes interval between each wash. Primary antibodies for von Willebrand Factor (vWF) (catalog # A0082, Dako, Agilent Pathology Solutions, USA) and smooth muscle actin (SMA) (catalog # A2547 SIGMA, Sigma-Aldrich, USA) were used at a working dilution of 1:200 with CAS-Block. Both antibodies were individually incubated overnight at 4°C followed by three PBS washing with 5 minutes interval within each wash. The corresponding secondary antibodies were used at a working dilution of 1:200 with CAS-Block and individually incubated for 2 hours at room temperature followed by three PBS washing with 5 minutes interval within each wash. The nuclei were stained using DAPI (Sigma-Aldrich, USA). Images were analyzed using fluorescent microscopy. The results were compared by student's t-test and a p value ≤ 0.05 was considered as significant. Results were represented as mean ± standard deviation.

4.2.11 Statistics

All quantitative data are presented as mean ± standard deviation from individual experiments. A two-way or one-way analysis of variance (ANOVA) by Tukey's multiple comparison posthoc test

was performed to assess statistical significance with a p-value of <0.05 considered significant. Prism 5 (GraphPad Software) was used to carry out all statistical analysis.

4.3 RESULTS AND DISCUSSION

4.3.1 Secretome preparation and characterization

Several different *in vitro* cell culture techniques have been used to modulate the concentration and composition of growth factors and cytokines present in the secretome to promote specific regenerative responses. [172] Here we used polydimethylsiloxane (PDMS) microwell culture devices to form hASCs spheroids for secretome production. The green fluorescent images of the spheroids showed that the spheroids were largely composed of living hASCs with a minimal presence of dead cells in each spheroid (Fig 4.1A). This technique was chosen based on the generally accepted idea that spheroid culture techniques promote a cellular environment more representative of an *in vivo* setting than traditional 2D monolayer culture. This assumption is based on the greater amount of cell to cell interactions and cellular interfaces with extracellular matrix components which occur within spheroids. [196] In addition, the spheroid structure relies on diffusion to control the transport of nutrients, oxygen, and waste throughout the entirety of the sphere. This diffusion limitation provokes a state of stress within the cells which has been shown to alter the growth factor secretion. [91, 197] Lastly, the high ratio of cells to media used allows for the collection of a highly concentrated secretome. [185]

After 72 hours of culture, the hASCs spheroids showed an increased expression of the anti-apoptotic gene BCL-2 as well as, the stress related gene HIF1A when compared to traditional 2D monolayer culture (Figure 4.1B). The increased gene expression has been previously reported to occur within spheroids and has been shown to be linked to hypoxia and hypoxia-dependent

pathways. [89] In addition to the difference in gene expression between the two culture techniques, a human antibody array was carried out to evaluate the composition of therapeutic growth factors, cytokines, and proteins present in the secretome (Figure 4.1C and D). The protein endostatin/collagen XVIII and the hepatocyte growth factor (HGF) were only detected in the spheroid secretome (Figure 4.1D). Recently, endostatin/collagen XVIII has been linked to the suppression of type I collagen expression in cardiac fibroblasts which is a vital component of scar formation post myocardial infarction. [198] Additionally, the inhibition of endostatin/collagen XVIII in a rat MI model was shown to cause an increase in matrix metalloproteinases (MMP) activity of MMP2 and MMP9, angiotensin converting enzyme activity, and collagen deposition. [199] These findings suggest that endostatin/collagen XVIII may have a significant cardioprotective ability and a precise role in limiting myocardium remodeling. The second component that was exclusively detected in the spheroid secretome, HGF, is an effective agonist for the tyrosine kinase surface receptor c-MET. [200] This cytokine has been documented to exhibit proangiogenic, anti-fibrotic, and cardioprotective ability *in vitro* and *in vivo* MI models. [201-204] Along with the previously discussed therapeutic biomolecules only being secreted by the spheroids, there were also several growth factors present at a greater concentration in the spheroid secretome when compared to the 2D monolayer secretome. Specifically, the concentration of vascular endothelial growth factor (VEGF) and angiogenin was approximately eight and four times greater in the spheroid secretome, respectively (Figure 4.1E). These proteins are potent proangiogenic growth factors with a proven ability to promote endothelial proliferation, migration, and survival as well as, facilitate new blood vessel formation within the peri-infarct zone post-MI. [205-208] These results confirm that culturing hASCs in spheroids rather than a monolayer changes the genetic profile of the cells and

subsequently provokes the cells to secrete a greater amount and variety of therapeutic molecules involved in angiogenesis, cardioprotection, and improvement of the heart function post-MI.

4.3.2 *In vitro* proangiogenic activity of secretome

As mentioned previously, MI is initiated by the obstruction of blood flow to the myocardium as the result of an occlusion of the coronary arteries leading to the walls of the heart. The resulting ischemia causes several pathological changes within the myocardium such as hypoxia, inflammation, ventricular dilation, compromised contractile function, cardiomyocyte death, and tissue necrosis. [209, 210] Therefore, regardless of the method used, in order to repair the infarcted myocardium the reestablishment of sufficient vascularization throughout the heart is essential to ensure proper metabolic and structural homeostasis of the myocardium. [211] Therapeutic angiogenesis is an essential process involved in the revascularization, and consequently, the angiogenic potential of the hASCs derived secretome was characterized using several *in vitro* cell based assays.

Initially, angiogenesis relies on endothelial cell migration and proliferation to form capillary sprouts [212]. To assess cell proliferation, endothelial cells were seeded at a sub-confluent density in growth factor depleted endothelial growth media. Then, the two different hASCs derived secretome isolated respectively from 2D monoculture (2D secretome) and spheroids (3D secretome) were added to the media in different groups, and the cell number was quantified after 24 hours.

As a control group (Cntrl (-)), cells were grown in endothelial growth media without the addition of VEGF and human fibroblast growth factor-B (hFGF-B). The 3D secretome caused a significant increase in cell proliferation when compared to 2D secretome (Fig 4.2A). Next, an *in vitro* scratch

assay was performed to assess whether the secretome was able to promote endothelial cell migration.

After 16 hours of treatment, differences in cell migration could be observed within the scratch that was made prior to the addition of secretome. Specifically, treatment with the 3D secretome resulted in a 75.7% wound closure which was significantly higher than the 2D secretome group (Fig 4.2B and D). These results align with previous reports of endothelial migration induced by angiogenic protein-based treatments. [181, 213] Lastly, a tube formation assay was carried out. This assay is essential because, following the formation of capillary sprouts via endothelial cell migration and proliferation, cellular alignment into tubules is essential for lumen formation of a functional capillary. [214] After 10 hours of exposure to the secretome, the test groups containing the 2D secretome as well as the 3D secretome showed an increase in tube formation. The groups that received the 2D and 3D secretome showed approximately four and five times more tubes per field when compared to the control, respectively (Fig 4.2C and E). In addition, the 2D and 3D secretome induced the formation of longer tube segments and a larger total tube length (Fig S4.4). Based on the results obtained from these three cell-based assays, the prediction that the secretome composition derived from hASCs spheroids has superior proangiogenic properties when compared to the secretome isolated from the hASCs cultured in a traditional monolayer can be confirmed. [215]

4.3.3 Formation and characterization of the injectable nanocomposite hydrogel

Strategic combinations of polymers and nanoparticles allow scientists to develop injectable physically crosslinked hydrogels to control the delivery of several types of biomolecules and therapeutic agents for tissue regeneration. Polymers and nanomaterials can be mixed before the gelation to form nanocomposite systems that can be easily injected through a needle. This avoids

the use of complex fabrication methods that can be difficult to translate into the clinic, as well as, the need for invasive surgery for their administration. [216] In this study, fully exfoliated Laponite® (0, 1, 2% w/v) was combined with gelatin (5% w/v) to form an injectable hydrogel for the delivery of stem cell derived secretome (Fig 4.3A). After the hydrogel was formed, FT-IR spectra of Laponite®, gelatin, and the nanocomposite hydrogel confirmed the polymer clay interactions through a slight shift in the characteristic Si-O stretching peak from 1013 cm^{-1} to a lower frequency of 1006 cm^{-1} (Fig S4.1A). This peak shift has been reported to be seen from other nanocomposite hydrogels containing Laponite®, as well. [217, 218] A complimentary analysis of the nanocomposite hydrogel's elemental composition using energy-dispersive X-ray spectroscopy (EDS) established the presence of silicon (Si) and magnesium (Mg) therefore, confirming the contribution of the Laponite® nanoparticles to the structural network of the hydrogel (Fig S4.1B and S4.1C). [219] To assess the effect of Laponite® on the viscoelastic behavior of the nanocomposite hydrogel several rheological techniques were used. Initial strain sweeps were carried out to determine the linear viscoelastic region for each of the Laponite® concentrations (Fig S4.2A). Frequency sweep measurements from 0.01 to 10 Hz at a strain of 1% showed consistent storage moduli (G') approximately one magnitude higher than loss moduli (G''), irrespective of the frequency (Fig S2B). This behavior indicates that, at the concentrations used, gelatin and Laponite® are able to form hydrogel networks that exhibit solid-like behavior (G'>G''). [220] However, at higher oscillatory strain percentages the material begins to flow (G'<G'') illustrating yielding behavior which is an important parameter for designing injectable hydrogel systems. The yield stress approximately doubled as the concentration of Laponite® increased from 1% to 2% within the nanocomposite hydrogel (Fig 4.3B). In addition, a similar trend was seen in the viscosity testing where an increase from 1% w/v to 2% w/v Laponite® caused the viscosity to rise by an order of

magnitude (Fig 4.3C). One probable cause for this direct correlation between the increased viscosity and the Laponite® concentration is the physical crosslinking occurring between the predominately negatively charged Laponite® disks and the positive charges of lysine ε-amino groups of gelatin. This crosslinking can be confirmed by monitoring the change in the loss factor, tan δ = G''/G', over a range of oscillatory frequencies. As the concentration of Laponite® increased from 1% w/v to 2% w/v, there was also a slight decrease in tan δ at a frequency of 0.1 to 10 Hz (Fig 4.3D). This reduction in tan δ, combined with the significant rise in G' with greater concentrations of Laponite®, confirms that Laponite® increases the crosslinking density within the nanocomposite hydrogel. This behavior has been observed with several other nanocomposite hydrogels containing various hydrophilic polymers and Laponite®. [221, 222] Although the exact interactions are not known, generally researchers consider hydrogen bonding, dipole, and ionic interactions to play a significant role in the physically crosslinked networks between polymers and nanosilicates. [186, 221]. These interactions are more likely to occur at higher concentrations of Laponite® dictating a difference in the degradation profiles as observed in this study. Specifically, after 2 weeks the nanocomposite hydrogels containing 1% nanoclay were significantly degraded unlike the 2% nanoclay hydrogels which showed minimal degradation (Fig S4.3A). As well as improving the stability of the hydrogel, Laponite® can also influence the retention of proteins within the hydrogel matrix. This control over the amount of protein released is beneficial to treat cardiovascular injuries that require a prolonged presence of bioactive molecules consistently delivered to the damaged tissue. To prove this concept, we studied the influence of Laponite® concentration on the release of the model protein (myoglobin) and observed that a concentration of 2% nanoclay was able to reduce the percentage of protein released when compared to the formulation containing the lower Laponite® concentration (Fig S4.3B). As mentioned previously,

the ability for a hydrogel to pass readily through a needle is an important parameter to enable a straightforward delivery to the therapeutic site. The shear thinning behavior exhibited by this nanocomposite hydrogel at shear rates greater than 0.1 s^{-1} confirms its injectability (Fig 4.3D). However, after injection rapid recovery of the hydrogel stiffness is imperative to prevent the material from flowing out of the therapeutic site. Therefore, recovery testing was carried out with each nanocomposite hydrogel by monitoring the G' during three cycles of high (100%) followed by low (1%) oscillatory strain for five minutes each (Fig 4.3E). At the beginning of each high strain cycle, all of the G' values dropped to below 100 Pa, however, the hydrogels that contained 1% w/v and 2% w/v of Laponite® regained a significant amount of their stiffness directly after the strain was decreased to 1% w/v. Specifically, after the first high strain cycle, the nanocomposite hydrogel that contained 1% w/v Laponite® exhibited a G' value that was only 20% lower than the initial value during the primary low strain cycle. Despite this recovery behavior, after three cycles of high strain the hydrogel was only able to recover 66% of the original G' value. Interestingly, this reduction in G' values after multiple cycles of high strain was not observed in the nanocomposite hydrogel containing 2% w/v Laponite®. This hydrogel was able to recover to 98-99% of the initial G' value after each high strain cycle. These results confirm the thixotropic behavior of the hydrogel systems containing Laponite® previously observed with similar physically crosslinked hydrogel systems. [220, 222] In addition to the recovery studies, the stiffness of the hydrogel system was monitored from 25 °C to 40 °C in order to evaluate the mechanical integrity of the nanocomposite hydrogel at the physiological temperature of 37°C (Fig S4.2C). As expected there was a slight decrease in the G' among all the groups at temperatures above 35°C however, this decrease was less pronounced in the hydrogels containing 2% Laponite® (Fig S4.2D). This indicates that the Laponite® is crucial in maintaining the integrity of the hydrogel

even at temperatures where gelatin is known to be in a sol state. Taken together, these studies further established that gelatin and Laponite® have the ability to form a robust injectable hydrogel network for regenerative medicine applications. Lastly, *in vitro* biocompatibility testing with the different hydrogel formulations was carried out using an MTS assay. Briefly, HUVECs were seeded with complete endothelial growth media and allowed to reach confluency prior the addition of the respective nanocomposite hydrogel. After 1 day, 3 days and 5 days, no significant difference in cell number between the groups was observed indicating that the hydrogel did not produce any cytotoxic effects irrespective of the concentration of Laponite® included in the network (Fig S4.5A). These results were also supported by immunofluorescent staining for F-actin of the HUVECs which showed no morphological difference between the groups (Fig S4.5B). Overall, due to the superior rheological properties and absence of cytotoxicity, the nanocomposite hydrogel containing 2% w/v of Laponite® was chosen for further *in vivo* testing.

4.3.4 *In Vivo* Biocompatibility of the injectable nanocomposite hydrogels

To ensure that no significant immune response was induced by the nanocomposite hydrogel, preliminary *in vivo* biocompatibility tests in immunocompetent rats were performed (n=5). Immunohistochemical staining of the myocardium indicated that there was no substantial inflammation (TNFα) or cardiomyocyte damage (TUNEL) caused by the hydrogel injections (Fig S6 and S7), 14 days post infarction. Similar results were obtained by qPCR that indicated that there was no significant difference in pro-inflammatory (TNFα, miR-146, miR-155) or cardiomyocyte apoptotic (miR-145, Cyclin D1, Rb1) gene and miRNA expression between the control and animals injected with the hydrogel (Fig S4.8). Lastly, upon injection of the nanocomposite hydrogel, no inhibition of proper cardiac function was observed (Fig S4.9).

Therefore, based on these combined results we can conclude that the nanocomposite hydrogel is biocompatible as seen in previous regenerative medicine studies. [186]

4.3.5. *In vivo* therapeutic efficacy in myocardial infarcted rat model

Despite the multiple clinical trials and preclinical studies investigating stem cell therapy for the treatment of AMI, outcomes thus far have been sub-optimal due to the complex pathology resulting from this CVD and the lack of retention of the cells at the delivery site. Recent research has established paracrine signaling as the widely accepted mediator of the positive outcomes that have been observed from stem cell therapy in the heart. [65, 172] However, using the cocktail of therapeutic biomolecules produced by stem cells *in vitro* (secretome) to promote myocardial regeneration post acuteMI is still in its infancy. [83, 223] Specifically, there are few publications dedicated to using biomaterials in combination with secretome despite the well-established importance of biomaterial use in initiating an optimal local regenerative response in the heart upon cell, gene, or growth factor delivery. [105, 185] Therefore, in this study, we aimed to develop a biocompatible, injectable hydrogel containing stem cell-derived secretome for acute MI therapy. Taking advantage of the relatively high protein adsorption capacity of Laponite® and its ability to contribute to hydrogel stiffness we developed a nanocomposite hydrogel loaded with stem cell derived secretome and hypothesized that it would successfully treat pathologies associated with acute MI *in vivo*.

Subsequent studies to investigate the therapeutic efficacy of the secretome loaded nanocomposite hydrogel were assessed in an acute MI rat model using established methods (Fig 4.4A). [179, 192] Preliminary baseline echocardiographs (Fig 4.4A and B) were collected (EF% ≈ 50, FS% ≈ 27, and CO ≈ 42 L/min for all groups) and subsequent echocardiographs were taken at day 3, 7, 14 and 21 (Fig 4.4A). Initially, there was no significant difference in heart function observed on day

3 (Fig 4.4 C and E). However, on day 7 all three cardiac function parameters were significantly increased in the nSi Gel+ group (EF%=56.9, FS%=31.1, CO=10.9 L/min) with respect to the control and nSi Gel groups (Fig 4.4C and E). This trend continued on day 14 with the exception of the cardiac output (EF%= 57.0±4.6, FS% = 31.1±3.3) (Fig 4.4C and E). Once again on day 21, all three heart function parameters significantly improved in the nSi Gel+ group (EF%= 62.8±3.0, FS% = 33.8±2.8, CO = 66.7±6.6) with respect to the control (EF%= 45.2±5.0, FS% = 23.5±3.1, CO = 48.3±7.6) and the nSi Gel (EF%= 46.7±6.8, FS% = 23.4±3.8, CO = 50.2±13.2) groups (Fig 4.4C and E). These three assessments are vital systolic functional parameters that are commonly used to assess the extent by which acute MI pathologies have affected myocardial function. [223-226] Therefore, we can confidently conclude that the secretome loaded nanocomposite hydrogel is able to improve heart function after the characteristic initial decline caused by acute MI cardiac remodeling. In addition, we observed that the secretome loaded nanocomposite hydrogel was able to improve cardiac function significantly better than the injection of the secretome solution alone indicated by the EF% of 62.8±3.0 % and 50.5±3.2 % at day 21 (Fig S4.10), respectively. This confirms the importance of the hydrogel delivery vehicle for a greater therapeutic outcome.

As mentioned previously, vascular repair mechanisms constitute a paramount means to reduce myocardial injury and therefore, they are necessary for the improvement of the heart function after acute MI. [83, 223] In order to assess the therapeutic potential of the nSi Gel+ to promote angiogenesis within the infarcted heart (Fig 4.5A) of an acute MI rat model, the animals were sacrificed, and the myocardium was stained for vWF and SMA within the peri-infarct region (Fig 4.5B). A significantly larger density of vWF and SMA positive vessels was seen in the animals treated with the nSi Gel+ when compared to the nSi Gel and control group (Fig 4.5C). In addition, the increased presence of SMA staining was also observed in the nSi Gel+ group (Fig 4.5B).

These results indicate that there was not only more capillary formation within the nSi Gel+ group but also the presence of more mature vessel morphology shown by the SMA staining. These results indicate that the proangiogenic growth factors and cytokines detected within the stem cell derived secretome were indeed able to promote angiogenesis in the heart post-acute MI when delivered using the nanocomposite hydrogel. Another result of acute MI that impairs proper myocardial function is the replacement of functional myocardium with fibrous scar tissue known as cardiac remodeling that is caused by cardiomyocyte necrosis. [83, 131, 179] A histological analysis of the hearts from each group was used to assess if the nSi Gel+ was able to reduce the extent of this cardiac remodeling (Fig 4.5D). The results showed that the nSi Gel+ was able to significantly limit the infarct size to 15.6±4.5% of the total heart while the infarct accounted for 38.4±9.0% and 31.6±9.0% of the control and nSi Gel hearts, respectively (Fig 4.5E). These results were further supported by the calculated heart weight to body weight ratios that indicated the ratio obtained from the nSi Gel+ group hearts was significantly greater (Fig 4.5F). This decrease in cardiac fibrosis combined with an increase in angiogenesis has been associated with the improvement of the cardiac function post-acute MI in other studies, [83, 131, 179, 223] and may represent the potential mechanisms that likely facilitated the improvement in cardiac function that we observed in this work.

4.4 CONCLUSIONS

We have successfully designed an injectable therapeutic nanocomposite hydrogel that represents a promising alternative to traditional stem cell therapy for the treatment of acute myocardial infarction. The shear thinning hydrogel was made by mixing the gelatin solution with a Laponite® dispersion and was used as a carrier for the delivery of stem cell derived-secretome. As expected,

the increase in Laponite® concentration up to 2% w/v was responsible for the formation of a highly physically crosslinked gel which could sustain high strain and recover its original stiffness once the strain was reduced to 1%. This property is essential to prevent the material from flowing out of the therapeutic site once injected and thus enabling longer retention of the secretome.

Additionally, the secretome was easily isolated from hASCs cultured as spheroids using PDMS microwell devices. Spheroids secreted a more concentrated and diverse composition of proangiogenic and cardioprotective growth factors, proteins, and cytokines when compared to cells grown in a traditional 2D monolayer environment. Therefore, spheroid culture provides an ideal opportunity to deliberately adjust the secretome composition to directly promote key therapeutic processes needed for cardiac regenerative medicine applications. The injection of the secretome loaded hydrogel in the peri-infarct area in an acute myocardial infarction rat model promoted increased angiogenesis, reduction in cardiac remodeling, and cardioprotection *in vitro* and *in vivo*. Overall these results suggest that the stem cell-derived secretome loaded hydrogel represents a viable option for the promotion of myocardial regeneration and myocardial therapy post-acute MI.

CHAPTER 5. DEVELOPMENT OF SUPERIOR THERAPEUTIC SECRETOME ENRICHED WITH MIR-146A FOR MYOCARDIAL REGENERATION[§]

ABSTRACT

Secretome-based therapies have the promising potential to become the next generation of viable treatments to restore a proper cardiac function after acute myocardial infarction (AMI). However, to advance their translation into the clinic, it is important to design precise strategies aimed to refine and control the secretome composition to further enhance their therapeutic regenerative potential. Here in this chapter, we present a possible approach in this direction by describing a method to enhance the secretome composition. Specifically, this control was achieved by transfecting human adipose-derived stem cells (hASCs) with the well-characterized microRNA-146a (miR-146a), which is a potent regulator of several processes including angiogenesis and inflammation. The preliminary hypothesis was that by transfecting hASCs with this type of microRNA (miRNA) it is possible to obtain a stem cell-derived secretome with a superior angiogenic and anti-inflammatory response. To test this hypothesis, the composition of the secretome obtained from the transfected hASCs (secretome^{146a}) was thoroughly characterized to evaluate possible changes in angiogenic and anti-inflammatory growth factor, cytokine and miRNA composition in comparison to the secretome retrieved from non-transfected hASCs. Then to confirm the superior angiogenic response of secretome^{146a}, several *in vitro* assays were carried out to test the proangiogenic effect on the proliferation, migration and tubular morphogenesis of human umbilical vein endothelial cells (HUVECs). Finally, HUVECs were exposed to IL-1β to

[§] Submitted as Waters R., Subham S., Pacelli S., Modaresi S., Chakravarti A., and Paul A. (2019 Development of microRNA-146a enriched stem cell secretome for superior myocardial therapy. *Biotechnology and bioengineering*.

induce a state of endothelial cell activation similar to the initial stages of the inflammatory response and evaluate the anti-inflammatory effect of the secretome[146a]. Specifically, the gene expression and protein activity of key mediators involved in endothelial cell activation were monitored before and after secretome treatment. Overall, the findings of this study serve to validate whether this strategy can potentially be applied to design a secretome with superior therapeutic response for the treatment of myocardial infarction.

5.1 INTRODUCTION

Ischemic heart disease resulting from AMI remains the leading cause of death in the United States, accounting for approximately 16% of total deaths worldwide.[4] Survival rates have improved significantly after AMI due to surgical revascularization and percutaneous coronary intervention. However, despite advancements in the pharmacological treatment of the symptoms, heart transplantation remains the only solution to prevent heart failure. This is caused by the lack of an intrinsic regenerative response within the heart, which leads to the myocardium being replaced with fibrotic scar tissue that inhibits a proper cardiac function. Therefore, over the past two decades scientist have focused their efforts in using stem cells as a strategy to regenerate the myocardium and restore the heart function.[66]

To accomplish this goal, several adult stem cell types have been used in clinical trials based on the hypothesis that stem cells would induce the formation of a new functional tissue upon long-term engraftment in the myocardium.[66] However, this hypothesis does not align with the results reported in several preclinical and small scale clinical trials because of the lack of observed stem cell retention, engraftment and transdifferentiation in these studies. Based on this evidence, the positive therapeutic effect has been attributed to the secretion of therapeutic paracrine molecules that promote endogenous reparative and regenerative responses within the infarcted myocardium. This

pivotal discovery has led to a significant effort in identify novel cell-free treatments which are based on the delivery of key angiogenic, anti-apoptotic, anti-inflammatory and anti-fibrotic paracrine factors. This milieu of therapeutic factors, known as secretome, has been proven to be effective in promoting an intrinsic regenerative response in the myocardium by restoring the functionality of the damaged tissue[101, 172, 227].

The secretome is a complex array of pleiotropic molecules secreted by stem cells which includes growth factors, cytokines, miRNA, and extracellular vesicles (EVs).[1, 211] Specifically, EVs are small bi-layered particles that have been originally identified as a strategy of stem cells to discard undesired cellular material. However, in recent studies, EVs have been identified as regulators of cell-cell communication by carrying essential paracrine factors.[228] There are two types of EVs regularly secreted by healthy cells. The first ones are known as exosomes (30-150 nm) and the second type are defined as micro-vesicles which possess a broader size distribution (100-1000 nm). Both types of EVs are composed of a phospholipid bilayer membrane containing ligand receptors and major histocompatibility complex molecules which facilitate binding to cell receptors that are necessary to trigger signaling cascades within the target cell. In addition, EVs have also been shown to transport an array of RNA types including, messenger RNA (mRNA),[229, 230] and, of particular note, miRNA[1, 229, 231]. miRNA are small (21-23 nucleotides), endogenous, non-coding RNAs that negatively regulate gene expression on a posttranscriptional level and act as powerful regulators of pathophysiological processes.[232] In the context of cardiovascular regeneration, stem cell-derived EVs have been shown to promote angiogenesis, modulate inflammation, inhibit apoptosis, and induce proliferation due to the presence of specific miRNA types loaded within their bilayer structure.[228, 233] Precisely, among the different types of miRNA, miR-146a has been shown to be a potent regulator of inflammation[234, 235] in addition to, its ability

to promote angiogenesis and inhibit cardiomyocyte apoptosis.[236, 237] Based on these studies, it is evident that optimizing the miRNA composition within EVs represents an innovative strategy to develop a cell-free therapeutic treatment that exhibits a greater therapeutic efficacy for cardiac regeneration.

In this study, we aimed to enhance the therapeutic efficacy of hASC-derived secretome by transfecting the cells with miR-146a to induce the secretion of EVs carrying this therapeutic miRNA. A schematic representing the overall strategy is reported (Fig 5.1). The hypothesis was that the presence of the miR-146a within the EVs would cause an increase in the proangiogenic and anti-inflammatory response of the secretome in comparison to the one produced by hASCs that were not transfected. To test this hypothesis, the angiogenic and anti-inflammatory growth factor, cytokine, and miRNA composition of the two types of secretome were compared to identify changes in therapeutic paracrine molecule composition after transfection. Finally, the angiogenic and anti-inflammatory properties of the two different types of secretome were tested and compared *in vitro* by evaluating their modulation on endothelial cell proliferation, migration, tube formation, inflammatory activation, gene expression and protein activity.

5.2 MATERIALS AND METHODS

5.2.1 hASCs culture conditions and transfection with miR-146a

hASCs were purchased from Rooster Bio and originated from female donors between the ages of 31 and 45 years old. Passages 2-6 were used for all the experiments, and cells were cultured in traditional 2D conditions (3.3×10^3 cells/cm2) using hASC High performance media (Rooster Bio media) at 37℃ and 5% CO_2.

hASCs were seeded in 6 well-plates (1×10^5 cells/well) and cultured 24 hours in Rooster Bio media containing 10% of fetal bovine serum (FBS). Upon 70% of confluency, cells were washed three times with phosphate buffer saline (PBS) at pH 7.4. The media was then switched to endothelial growth medium (EGM-2 BulletKit, Lonza), without the addition of FBS and angiogenic growth factors including the vascular endothelial growth factor (VEGF) and human fibroblast growth factor-B (hFGF-B). hASCs were then transfected with the XMIR-146a-5p RNA Oligo (10 µM) (System Bioscience) using the Purefection Transfection Reagent (System Bioscience). Specifically, 30 µL of the oligonucleotide suspension and 7.5 µL of the transfection reagent were mixed prior addition to the cells in 200 µL of DMEM media without any FBS. The mixture was vortexed briefly and incubated at room temperature for 15 minutes. Then, the complex was added to the cells to reach a final concentration of 100 nM of oligonucleotide in each well. The well plate was kept on a shaker incubator for 30 minutes followed by incubation at 37℃ for 24 hours according to the manufacturer's protocol. As a control group, hASCs were treated in the same culture condition without being transfected with the oligonucleotide miR-146a. The media was collected from both groups, centrifuged at 16,000 x g for 10 minutes at 4℃ to remove cellular debris, and used fresh or stored at -20℃ for further analysis.

5.2.2 EV isolation from transfected cells and morphological characterization

The secretome^{146a} and the control group (secretome) was collected as reported in the previous sections. After centrifugation, the exosomes were isolated using the exoEasy Maxi Kit (Qiagen). Briefly, the supernatant was mixed with an equal volume of the XBP buffer (Qiagen) and centrifuged at 500 x g for 1 minute followed by subsequent washing steps according to the manufacturer's protocol. The isolated exosomes were retrieved in the XE elution buffer in a final volume of 400 µL.

Exosomes morphological analysis was carried out by transmission electron microscopy (TEM) and scanning electron microscopy (SEM) analysis. TEM and SEM samples were prepared by adding 5 μL of the exosome sample onto the carbon-coated 200-mesh copper grids for 5 minutes to allow the exosomes to adsorb to the surface. The grids were dried for several hours in a desiccator. The dried grids were analyzed with a Philips CM100 microscope operated at 100 kV. High-resolution TEM images were recorded on FEI Tecnai F20XT, 200 kV (FEI, Hilsboro, OR). SEM images were obtained at an acceleration voltage ranging from 1 to 10 kV with an in-lens detector of a FEI Versa 3D Dual Beam microscope.

Finally, the exosome size distribution and concentration were assessed by nanoparticle tracking analysis (NTA) using a Malvern Panalytical NanoSight LM10. Exosomes samples were suspended in PBS and injected into the sample chamber using sterile syringes. The samples were loaded by filling the chamber without the introduction of air bubbles. The detection threshold was fixed to 60 particles per field of view and camera level was set in standard mode. All measurements were performed in triplicate at room temperature with every measurement lasting for 1 minutes. The concentration values and the particle sizes were determined using the NanoSight software.

5.2.3 Western blot analysis of isolated EVs

Western blot analysis was carried for both the exosomes and the cell lysates samples to verify the presence of specific protein markers in the exosome population. hASCs were cultured following the cell culture conditions described in the section 5.2.1 and the exosomes were isolated based on the procedure described previously in 5.2.2. The cell lysate was prepared by treating hASCs with RIPA buffer containing Tris-HCl (pH 7.6, 25 mM), NaCl (150mM), NP-40 (1% w/v), sodium deoxycholate (1% w/v) and sodium dodecyl sulfate (0.1% w/v). The protein concentration was determined by measuring the optical density at 280 nm using a spectrophotometer (Nanodrop ND-

1000; Thermo Scientific). The exosomes samples were normalized using the same sample volume in the pre-casted gel for western blot analysis (29 µL).

The protein samples (80 µg of cell protein or 29 uL of exosomes in each well) were resolved by SDS-PAGE (BoltTM 4-12% Bis-Tris Plus) at 180V for 42 minutes. The proteins bands were transferred to PVDF membranes (Immobilon-P Transfer Membranes), blocked in 0.5% Tween 20 and probed with antibodies which were diluted in the corresponding blocking buffer. The cellular protein cytochrome c was resolved under reducing conditions while the exosome protein CD63 was resolved under non-reducing conditions. The antibodies used were anti-CD63 antibody (ab59479) dilution 1:2000, and anti-cytochrome c antibody (ab110325) dilution 1:2000 in the blocking buffer. Goat anti-Mouse IgG H&L (HRP) (ab205719) was used as the secondary antibody at dilution of 1:4000. The protein band signals were detected using an X-ray film and enhanced by a chemiluminescent reagent. The signals were detected using an ECL Plus detection system according to the manufacturer's protocol.

5.2.4 miRNA analysis of isolated EVs

Exosomes isolated from the transfected and the non-transfected groups, as reported in section 5.2.2, were assessed to evaluate their miRNA content and composition. miRNA was isolated from the exosomes using the exoRNeasy Serum/Plasma Maxi Kit (Qiagen). The total RNA concentration and purity were determined by measuring the optical density at 260 nm using a spectrophotometer (Nanodrop ND-2000; Thermo Scientific). Complementary DNA (cDNA) was synthesized starting from the isolated RNA using the miScript II RT Kit (Qiagen). The qPCR analysis was performed in triplicate for each test group on a Mastercycler Realplex4 (Eppendorf) using predesigned primers and miScript SYBR Green PCR Kit (Qiagen). Fold expression levels of miR-146a in the transfected group (secretome^{146a}) were calculated using the relative ΔΔCt

method, using *RNU6* as the housekeeping gene. Similarly, following the same protocol, qPCR analysis was carried out using a miSCript miRNA PCR array 96 well-plate (Qiagen) to detect the composition of the miRNA present in the exosomes samples upon transfection compared to the non-transfected group.

5.2.5 Assessment of transfected cell-derived secretome protein composition

The secretome obtained from the transfected (secretome^{146a}) and non-transfected hASCs (secretome), was assessed using a human angiogenesis antibody array and human cytokine array (R&D Systems). The two arrays were used to detect the differences in composition between the two different types of secretome by analyzing the relative levels of 55 angiogenic related proteins and 36 different cytokines, chemokines and acute phase proteins, respectively. The studies were carried out according to the manufacturer's protocols. Images of the corresponding chemiluminescent dot blots were taken and the mean spot pixel density for each protein was calculated using ImageJ software.

5.2.6 HUVEC proliferation assay with secretome^{146a}

Furthermore, angiogenic studies were carried out to assess the superior proangiogenic ability of the secretome^{146a}. Immortalized HUVECs were cultured in endothelial basal medium [EGM-2 BulletKit, (Lonza), 2% FBS, and 1% penicillin/streptomycin] with complete endothelial growth supplements. HUVECs from passage 2-5 were used in all the *in vitro* angiogenic studies. HUVECs (0.2×10^5 cells/mL) were seeded in a 48 well plate and allowed to grow overnight in EGM-2 media, without the addition of FBS and angiogenic growth factors, VEGF and hFGF-B. The cells were then washed with PBS and the media was then replaced with media supplemented with different type of secretome as described in section 5.2.1. Precisely, three groups were tested: a negative

control consisting of HUVECs cultured in EGM-2 media without growth factors (Ctrl (-)), endothelial cells cultured in the same media supplemented with secretome isolated from non-transfected ASCs (secretome), and a test group where the media without growth factors was supplemented with secretome isolated from transfected ASCs (secretome^{146a}) (n=5). The final volume in each well was 200 µL and the volume of secretome for both test group was 100 µL. The degree of HUVEC proliferation in the presence of the secretome was assessed by MTS proliferation assay (Promega) after 24 hours using a standard calibration curve in the range of $5x10^3$ up to $1x10^5$ cells. The absorbance measurements were carried out at 490 nm according to the manufacturer's protocol

5.2.7 HUVEC migration and tube formation assay with secretome^{146a}

HUVECs (3×10^5 cells/mL) were seeded in Ibidi 3-well culture inserts within a 24 well plate as per the company's protocol to perform a cell migration assay (n=3). Specifically, 70 µL of the cell suspension was added to each well and the cells were allowed to culture overnight in EGM-2 media. Next, the inserts were removed, and the media was changed according to same groups used in the proliferation assay reported in the previous section. Brightfield images were taken in the same positions along the scratch at 0, 6 and 24 hours after treatment to monitor HUVEC migration into the gap for each group. The average percentage of area recovered during the migration was calculated using Image J software considering 10 images per group. The area of the original gap was determined from the images taken at the 0 hour time point.

Finally, to determine the ability of the secretome to induce the formation of tubular-like structures, HUVECs were seeded on a growth factor depleted Matrigel-based on the manufacturer's protocol (Matrigel matrix, Basement Membrane, BD). Briefly, 289 mL of growth factor depleted Matrigel Matrix (10 mg/mL) previously cooled to 5℃was added to a 24 well culture plate on ice. The plate

was then incubated at 37℃ for 60 min to allow the gel to form. Then, HUVECs (1.2×10^5 cells/mL) were seeded on the Matrigel matrix and treated with one of the same three treatment groups used for the proliferation and migration assays. After 10 hours, bright field images of the endothelial networks were taken for each group and the number of nodes, number of meshes, the total segment length, number of segments and number of isolated segments were determined using the Angiogenesis Analyzer in ImageJ. Results are reported as mean ± deviation standard considering at least 10 images per group.

5.2.8 Assessment of anti-inflammatory properties of secretome^{146a} on HUVECs

HUVECs were seeded in 24 well plates at the cell density of $5x10^4$ cells/well and cultured for 24 hours using EGM-2 media without any angiogenic growth factor. Then, cells were treated with interlukin-1 (IL-1β) at the concentration of 10 ng/mL to induce an endothelial cell activation similar to the endothelial cell state in the early stages of inflammation. Three groups were tested in this study: a positive control where HUVECs were left untreated, and two test groups were the media was supplemented with the secretome derived from hASCs non-transfected (secretome), and the one obtained from hASCs transfected with miR-146a (secretome^{146a}), respectively. Half of the volume of the media in each well was replaced with secretome for both test groups.

After 4 and 24 hours the mRNA was extracted from the HUVECs using the RNeasy Mini Kit. The total RNA concentration and purity were determined by measuring the optical density at 260 nm. cDNA was synthesized starting from the isolated RNA using the miScript II RT Kit (Qiagen). The qPCR analysis was performed in triplicate for each test group on a Mastercycler Realplex4 (Eppendorf) using predesigned primers and miScript SYBR Green PCR Kit (Qiagen). Fold expression levels of several genes including vascular cellular adhesion molecule-1 (VCAM-1), intracellular adhesion molecule-1 (ICAM-1), tumor necrosis factor receptor associated factor 6

(TRAF6), and monocyte chemoattractant protein-1 (MCP1) were evaluated at 4 and 24 hours post-treatment. The data was analyzed using the relative ΔΔCt method, and GAPDH was used as the housekeeping gene.

In addition to the gene analysis, the anti-inflammatory effect of the two types of secretome was investigated by studying the expression of ICAM and the secretion of MCP-1 by the IL-1β activated HUVECs. HUVECs were washed with PBS three times after 8 hours post-treatment with one of the secretomes. Cells were blocked with 5% w/v goat serum for 15 minutes, followed by incubation for 30 minutes with primary antibody against ICAM (2µg/mL in 1% goat serum). Cells were then washed three times with PBS and incubated for 30 minutes with the secondary antibody Anti-Mouse IgG H&L (Alexa Fluor® 488) (ab150113) for ICAM stained samples at the of dilution 1:2000. Cells were washed with PBS three times, recovered using trypsin, resuspended in PBS and FACs analysis was carried out to quantify the amount of fluorescent positive stained cells in the three different groups using the Attune NxT flow cytometer (Thermo Fischer Scientific).

Finally, HUVECs secretion of MCP-1 was assessed using an ELISA kit for MCP-1 (R&D Systems). A standard curve in the range of 31.3 pg/ml to 1000 pg/mL was used to correlate the absorbance values at 450 nm with the amount of protein present in each sample.

5.3 RESULTS AND DISCUSSION

5.3.1 Isolation and characterization of miR-146a enriched EVs derived from hASC

The regenerative potential of mesenchymal stem cell (MSC)-derived secretome in restoring proper heart function within the damaged myocardium after AMI relies on the combination of multiple paracrine molecules secreted by MSCs. These include an array of angiogenic, anti-inflammatory, cardioprotective, and anti-fibrotic growth factors, cytokines, and EVs.[172] Specifically, EVs are

emerging as key components of the MSC therapeutic paracrine mechanism due to their ability to carry proangiogenic, anti-inflammatory and anti-apoptotic miRNA. Therefore, tailoring their miRNA content represents an ideal approach to increase the therapeutic efficacy of secretome leading to a superior regenerative response in the myocardium.

In the present study, hASCs were successfully genetically modified to overexpress miR-146a in the secreted exosomes. We chose to use hASCs over other MSC sources because their minimally invasive isolation technique has a low morbidity and produces a high cell yield making this method more clinically feasible than other MSC isolation procedures.[77] Specifically, hASCs were transfected with a miR-146a oligonucleotide fused to a RNA sequence tag that specifically targets small RNAs into exosomes for packaging (Fig 5.1). After transfection, the hASCs were cultured for 24 hours and the resulting secretome[146a] was isolated for characterization and therapeutic assessment. EVs within the hASC-derived secretome were separated to characterize their size, morphology, protein composition, and miRNA content. Electron microscopy images showed that the hASC-EV particles had bilayer membrane with a primarily uniform circular morphology (Fig. 5.2A and B, Figure S5.1). NTA analysis revealed that the average diameter of the EVs was 201.2 ± 12.7 nm with 90% of the population having a diameter less than 360.3 nm (range 60-600 nm) (Fig. 5.2C). In addition, the most prevalent subpopulation within the EVs had a diameter of 138.1 nm indicating an exosome-enriched EV population with generally limited size heterogeneity.[238] Western blot of hASCs and hASC-EVs confirmed the presence of transmembrane tetraspanin protein CD63 and absence of the mitochondrial protein cytochrome c within the hASC-EVs (Fig. 5.2D). These results confirm the endosomal origin of the EVs.[239] Tetraspanins have been shown to bind several integrins and MHC molecules therefore, the enrichment of CD63 is important for potential protein-protein interactions between EVs and cellular membranes.[230, 240]

Lastly, the transfection efficiency was confirmed by comparing the miRNA composition of the EVs isolated from secretome (hASCs not transfected) and secretome^{146a} using RT-qPCR, which revealed that EVs from secretome^{146a} were highly enriched with miR-146a ($p < 0.001$) (Fig. 5.2E).

5.3.2 Angiogenic properties of secretome^{146a}

An efficient secretome-based therapy aimed to restore myocardial function after AMI needs to provide the necessary angiogenic cues required to re-establish proper blood perfusion to the damaged myocardium. The secretome obtained from non-transfected hASCs displayed a slightly greater amount of angiogenin and VEGF however, the secretome^{146a} contained larger amounts of several key angiogenic growth factors including, urokinase-type plasminogen activator (uPA), dipeptidyl peptidase IV (DPP IV), endothelin 1, hepatocyte growth factor (HGF), and fibroblast growth factors 1 and 2 (FGF-1 and FGF-2) (Fig. 5.3A). Specifically, uPA regulates angiogenesis through proteolytic degradation of the extracellular matrix that facilities the subsequent proliferation and migration of endothelial cells.[241, 242] FGF-2 has been shown to induce proliferation, promote migration, and inhibit apoptosis of endothelial cells *in vitro* in addition to, improve revascularization, cardiac function and reduce in infarct size in AMI *in vivo* studies.[211, 243, 244] Similarly, HGF has been proven to promote endothelial cells proliferation and migration as well as, improve heart function post-AMI attributed to induced angiogenesis. [202, 211, 245] In addition to a greater presence of angiogenic growth factors in the secretome^{146a}, several proangiogenic miRNAs were significantly more concentrated in the secretome^{146a} EVs when compared to the EVs in the secretome including, miR-126-3p ($p < 0.01$), miR-210 ($p < 0.01$), miR-143-3p, and miR-130a-3p ($p < 0.05$) (Fig. 5.3B). These specific miRNAs have been shown to increase endothelial cell proliferation, promote neovascularization, and improve cardiac function post-AMI.[1, 193, 246, 247] Lastly, the secretome^{146a} EVs also contained significantly less anti-angiogenic

miRNA compared to the secretome including, miR-26a-5p ($p < 0.05$), miR-92a-3p ($p < 0.05$), miR-15-5p ($p < 0.01$), and miR-222-3p ($p < 0.05$) (Fig. 5.3C).[103, 248]

The angiogenic efficacy of the two groups was assessed using three different *in vitro* HUVEC assays. HUVECs cultured in endothelial growth media without the addition of VEGF and FGF-B was used as the control group (Ctrl (-)). Angiogenesis is a tightly regulated multistep physiological process that begins with the migration and proliferation of activated endothelial cells through the perivascular tissue to form capillary sprouts originating from existing vessels.[211] Therefore, first an MTS assay was used to determine the effect each secretome type had on HUVEC proliferation. After 24 hours, a higher cell number was observed in the secretome^{146a} group when compared to the control and the secretome group ($p < 0.05$) (Fig. 5.3E). Next, the ability of the secretome to promote HUVEC migration was determined using silicone inserts that allowed the formation of a defined cell-free gap of 1 mm in the center of a confluent HUVEC monolayer. After 6 hours minimal migration had occurred in all three groups however, at 24 hours the HUVECs treated with the secretome^{146a} had migrated to cover 55% of the cell-free area as opposed to the HUVECs in the Ctrl (-) and secretome groups which only covered 27% and 37%, respectively ($p < 0.001$ and $p < 0.05$, respectively; Fig. 5.3D and F).

After the formation of the capillary sprouts, it is necessary for endothelial cells to properly align and form tubes with a patent lumen that can provide the scaffold needed for basement membrane deposition.[214] The capacity of the secretome to induce the formation of tube-like structures by HUVECs was evaluated using a Matrigel assay. HUVECs were culture on Matrigel-coated wells either in the presence of secretome or secretome^{146a} for 16 hours before images were taken (Fig. 5.4A). Similar to the proliferation and migration assay, the secretome^{146a} caused the formation of significantly greater number of nodes ($p < 0.01$; Fig. 5.4B), complete tubes ($p < 0.01$; Fig. 5.4C),

and segments ($p < 0.001$; Fig. 5.4D) as well as longer segment lengths ($p < 0.001$; Fig. 5.4E). Additionally, a reduction in the number of isolated segments ($p < 0.001$; Fig. 5.4F) was also observed in the secretome^{146a} group compared to the secretome group. Similar trends were seen when comparing the secretome^{146a} to the Ctrl (-) group ($p < 0.001$; Fig. 5.2B-F). These three assays together confirmed the superior angiogenic efficacy of secretome^{146a}. Therefore, based on these results and the composition analysis, the transfection of hASCs with miR-146a resulted in the production of a secretome with superior proangiogenic efficacy compared to the one isolated from non-transfected hASCs. These results are in agreement with a previous study that correlated the improvement of cardiac function, cardioprotection and angiogenesis post-AMI after treatment with exosomes that displayed an abundant presence of miR-146a.[236]

5.3.3 Immunomodulatory properties of secretome^{146a}

After AMI, an acute inflammatory response is needed for proper clearance of damaged extracellular matrix and necrotic cardiomyocytes. However, the intensity and duration of this inflammatory response must be tightly regulated to prevent further damage to the tissue. Therefore, a potential strategy for an efficient secretome-based therapy could also be to modulate the inflammatory response to promote cardiac regeneration.[249]

We compared the cytokine and miRNA composition of the two different types of secretome to identify paracrine molecules that could potentially modulate an inflammatory response. The comparison of the inflammatory cytokine composition of each secretome indicated that only one cytokine, granulocyte colony-stimulating factor (G-CSF), was expressed exclusively in the secretome^{146a} (Fig 5.5A). Despite the fact that G-SCF has not been shown to have anti-inflammatory properties, its known ability to recruit stem/progenitor cells, inhibit apoptosis and promote angiogenesis in the context of myocardial regeneration could support any enhanced

therapeutic efficacy observed with secretome^{146a} treatment.[250, 251] The remaining cytokines including CCL-1, CCL-2, TRAP, and IL-4 were detected at comparable levels in the two different secretomes. Furthermore, the miRNA present in the EVs originating from the two different secretomes was compared and showed that several anti-apoptotic miRNA were significantly upregulated in the secretome^{146a} (miR-22-3p ($p < 0.05$), miR-214-5p ($p < 0.05$), miR-24-3p ($p < 0.01$)) in addition to, a significant downregulation in multiple pro-apoptotic miRNAs (miR-29b-3p ($p < 0.05$), let-7c ($p < 0.01$), and let-7b-5p ($p < 0.05$)) (Fig. 5.5B and C).[252-255] Therefore, the miRNA in the secretome^{146a} EVs represent an ideal treatment for the inhibition of inflammation within the myocardium due to the fact that the damage-associated molecular patterns (DAMPs) released by apoptotic and necrotic cardiomyocytes are key regulators in the activation of endothelial cells to an inflammatory state.

A key target of the inflammatory process within the damaged myocardium is the endothelium, which directly controls the extravasation of leukocytes that are recruited to the infarct area from the spleen.[7] Precisely, in the initial stages of inflammation, an upregulation of leukocyte adhesion molecules (VCAM, ICAM, E-selectin) on endothelial cells is vital for efficient capture of neutrophils and subsequent mediation of their tethering and rolling process along the venular endothelium.[7] To mimic the process of endothelial cells inflammatory activation by circulating cytokines, we exposed HUVECs to the pro-inflammatory cytokine, IL-1β, and assessed the ability of the secretome to modulate the subsequent HUVEC inflammatory activation.

The anti-inflammatory efficacy of the secretome and secretome^{146a} was then assessed evaluating the gene expression of several genes involved in the regulation of the inflammatory response in HUVECs. First, IL-1β was shown to cause an upregulation in the gene expression of *ICAM*, *MCP-1*, and *VCAM* and there was no difference in gene expression between all three test groups 4 hours

after treatment (Fig. 5.5D). However 24 hours after treatment, the secretome^{146a} was shown to significantly decrease the gene expression of *ICAM* ($p < 0.01$), *MCP-1* ($p < 0.01$), and *VCAM* ($p < 0.05$) compared to the secretome treated group (Fig. 5.5E).

In addition to the gene upregulation of adhesion molecules for leukocytes, activated endothelial cells also serve as an important source of cytokines and chemokines within the infarct zone.[7, 256] Therefore, we also studied the effect the two different types of secretome had on MCP-1 secretion by IL-1β activated endothelial cells. Secretome^{146a} was also able to significantly suppress the secretion of MCP-1 by HUVECs after IL-1β treatment compared to the Ctrl (-) and secretome group ($p < 0.001$ and $p < 0.05$, respectively; Fig. 5.5F). The expression of adhesion protein ICAM was also shown to decrease upon secretome treatment with the secretome^{146a} group, which exhibited the lowest expression amongst the three test groups (Fig. 5.5G).

Together these results demonstrate that secretome^{146a} has the capacity to modulate several of the inflammatory responses exhibited by endothelial cells upon activation by inflammatory cytokines such as IL-1β. Additionally, these results confirm that the secretome retrieved from transfected hASCs has superior anti-inflammatory properties and could potentially be used in late stage resolution of the acute inflammation post-AMI to downregulate endothelial cell activation and therefore, inhibit excessive transmigration of neutrophils into the myocardium.

5.4 CONCLUSIONS

In this study we have successfully enhanced the therapeutic efficacy of hASC-derived secretome by transfecting hASC with miR-146a. By using this specific miRNA sequence tagged oligonucleotide we efficiently caused the EVs secreted by hASC to be enriched with the known therapeutic miRNA. The resulting EV population exhibited a size and protein composition

indicative of an exosome-enriched population, a subpopulation of EVs that have been implicated in an increase in cardiac function post-AMI. Within the EVs secreted by the transfected hASCs, we detected an increased concentration of proangiogenic and anti-apoptotic miRNAs as well as, a decreased concentration of anti-angiogenic and pro-apoptotic miRNAs when we compared them to the EVs secreted by non-transfected hASCs. Furthermore, the growth factor and cytokine composition of this secretome showed a significantly higher concentration of several key proangiogenic, chemotactic, and anti-apoptotic proteins which are shown to improve cardiac function post-AMI. The enhanced composition of therapeutic paracrine molecules present in the secretome^{146a} also corresponded to a superior therapeutic efficacy *in vitro*. Specifically, the secretome^{146a} was shown to significantly upregulate the proliferation, migration and tube formation of endothelial cells proving enhanced proangiogenic properties. Additionally, the secretome^{146a} was able to suppress the pro-inflammatory behavior of IL-1β activated endothelial cells by reducing the expression of leukocyte adhesion molecules and the secretion of pro-inflammatory cytokines. Overall these results suggest that the secretome^{146a} represents a viable treatment option for the promotion of angiogenesis and modulation of the inflammation and therefore, could potentially be used to promote myocardial regeneration post-AMI.

CHAPTER 6. CONCLUSIONS

Secretome represents a promising alternative to traditional stem cell therapy due to its observed therapeutic efficacy in pre-clinical studies that have been attributed to the presence of specific paracrine molecules secreted by adult stem cells *in vitro*.[172, 257] Several conditioning strategies are currently being investigated to modify the growth factor, cytokine, miRNA, and EV composition of the secretome with the final goal being to optimize its therapeutic efficacy. Specifically, these methods include hypoxia, serum deprivation, genetic manipulation, molecular and pharmacological agents, and the promotion of cell-cell interactions.[73, 172] Despite the success in using these methods, the clinical translation of secretome-based therapies has been hindered by its inherent heterogeneity, pleiotropic nature and the lack of studies characterizing its complete composition to thoroughly identify the components that are responsible for the positive outcomes.[101] In addition, the lack of retention at the delivery site reduces the therapeutic response.[105] Therefore, the work in the current thesis aimed to address these two concerns by using different secretome production methods and by designing an injectable hydrogel-based delivery device to promote the efficient retention at the therapeutic site.

Initially, we cultured hMSC in spheroids to induce a mild state of stress and promote cell-cell interactions in an effort to promote the production of a more therapeutic secretome composition. We observed that the secretome isolated from hMSC spheroids contained a greater concentration of proangiogenic growth factors including VEGF, FGF2, and angiogenin when compared to secretome produced by hMSCs cultured in a traditional 2D monolayer. Then, we developed photo-crosslinkable hydrogel composed of GelMA (5% v/v) and varying concentration of Laponite® (0.4, 0.8, 1.2% w/v) for the delivery of the isolated secretome. Higher Laponite® concentrations were shown to control the release of key angiogenic growth factors present in the loaded secretome. These results are likely due to electrostatic interactions between the surface of the clay,

and the growth factors.[220, 258] Aside from the release study, the model nanocomposite hydrogel was used as a platform to determine the therapeutic efficacy of the secretome-loaded hydrogel *in vitro*. Specifically, HUVECs were encapsulated in the nanocomposite hydrogels containing GelMA and Laponite® and two different groups were compared including, the nanocomposite hydrogel containing the secretome (NS Gel+) and without the secretome (NS Gel). The studies showed that the NS Gel + promoted greater HUVEC proliferation, migration and tube formation therefore, exhibiting superior proangiogenic efficacy compared to the NS Gel. This enhanced therapeutic efficacy of the NS Gel+ was also observed in cardioprotective assays. Specifically, the NS Gel+ inhibited apoptosis, ROS production and Caspase 3/7 activity of cardiomyocytes. Together this study demonstrated hMSCs spheroids produce superior angiogenic and cardioprotective secretome and Laponite® can effectively modulate the release of therapeutic growth factors contained in the secretome.

The next goal of the thesis was to formulate a secretome-based treatment that was more clinically feasible by developing an injectable nanocomposite hydrogel for the delivery of stem cell-derived secretome to the myocardium. To accomplish this goal, while leveraging the knowledge gained in the previous study, we combined gelatin (5% w/v) with varying concentrations of Laponite® (0, 1, 2% w/v). Rheological testing of the resulting nanocomposite hydrogels was done to assess the effect Laponite® had on the mechanical properties and to ensure their thixotropic behavior. The results indicated a positive correlation between the increase in Laponite® concentration and the resulting rheological properties including an improvement in yield stress, viscosity, and thixotropic behavior. One of the likely causes for this direct correlation can be explained by the possible electrostatic interactions occurring between the predominately negatively charged Laponite® disks and the positive charges of lysine ε-amino groups of gelatin. This hypothesis was confirmed

by the observed decrease in the loss factor, tan δ = G''/G', between the hydrogel containing 1% (w/v) versus 2% (w/v) Laponite® over a range of oscillatory frequencies from 0.01 to 10 Hz. This reduction in tan δ coupled with the significant increase in G' at greater concentrations of Laponite®, confirms that Laponite® increases the crosslinking density within the nanocomposite hydrogel. Similar results have been observed with several other nanocomposite hydrogels containing various hydrophilic polymers and Laponite® therefore, further validating our observations.[221, 222] Although the exact interactions were not studied in this current thesis, this type of physical crosslinking between polymers and nanosilicates is generally attributed to hydrogen bonding, dipole, and ionic interactions.[186, 221]. An increase in the Laponite® concentration also caused a reduction in the degradation rate of the hydrogel and superior control over the release of an encapsulated model protein. Therefore, we have concluded based on these studies that a nanocomposite hydrogel containing gelatin and Laponite® has the ideal properties to support the delivery of stem cell-derived secretome to the heart. Furthermore, similar to the previous study and in order to produce a therapeutic secretome, hASCs were cultured in a microwell device in order to form spheroids. The hASC spheroid-derived secretome (3D secretome) contained key angiogenic growth factors that were not present in the hASC monolayer-derived secretome (2D secretome) including, endostatin/collagen XVIII and HGF. In addition, the superior angiogenic efficacy of the 3D secretome was confirmed using several HUVEC cell assays *in vitro*.

Due to the positive *in vitro* studies, an AMI rat model was used to assess the therapeutic efficacy of the 3D secretome-loaded injectable nanocomposite hydrogel (nSi Gel+). Preliminary tests of the nanocomposite hydrogel (nSi Gel) showed no difference between the pro-inflammatory or cardiac stress proteins and the miRNA of the nSi Gel compared to the PBS treated group, which confirmed the biocompatibility of the nSi Gel. Furthermore, in the following therapeutic

assessment studies, after injection into the peri-infarct region 15 minutes post-AMI induction, the group treated with the nSi Gel+ exhibited a significant increase in heart function demonstrated by the increase in ejection fraction, fractional shortening, and cardiac output after 7, 14, and 21 days. The histological analysis of the peri-infarct region after 21 days showed significantly more expression of SMA+ and VWF+ in the nSi Gel+ group compared to the control groups in addition to a significant reduction in infarct size. Together these results indicate that the nSi Gel+ was indeed able to improve cardiac function post-AMI by promoting angiogenesis and limiting fibrotic scar development within the per-infarct region.

As previously mentioned, the inherent heterogeneity and pleiotropic nature of the secretome's paracrine molecule composition poses a challenge for clinical translation.[101] Therefore, the use of precise methods for promoting the secretion of therapeutic paracrine molecules and a thorough characterization of the secretome composition is vital to facilitating the transition of secretome-based treatments into the clinic. Therefore, for the final study we genetically modified hASCs to cause the enrichment of a well characterized therapeutic miRNA, miR-146a, within EVs present in the resulting secretome. The EV population present in the isolated secretome contained an exosome-rich population as demonstrated by a prevalent vesicle diameter of 138.1 nm and the confirmed CD63 protein composition. The transfection of hASCs was verified by the observed significant enrichment in miR-146a within the secretome (secretome^{146a}) prior the therapeutic assessment *in vitro*. The focus of this study was to address two essential regenerative processes within the myocardium that are mediated by ECs. First, we observed the superior angiogenic efficacy of secretome^{146a} compared to the secretome originating from non-transfected cells (secretome). Precisely, a significant increase in HUVEC proliferation, migration and tube formation was observed in the secretome^{146a} group. The analysis of the proangiogenic composition

of growth factors and miRNA showed that the secretome^{146a} contained a significantly larger concentration of uPA, DPPIV, endothelin 1, HGF, FGF-1, FGF-2, miR-126-3p, miR-210, miR-143-3p, and miR-130a-3p in addition to, the decreased concentration of anti-angiogenic miR-26a-5p, miR-92a-3p, miR-15-5p, and miR-222-3p compared to the secretome obtained from not transfected hASCs. These two analysis further supported our cell assay findings that the secretome^{146a} has a superior angiogenic efficacy.

In addition to angiogenesis, the endothelium plays a crucial role in regulating the inflammatory response by controlling the extravasation of leukocytes into the damaged myocardium. Therefore, we studied whether secretome^{146a} was capable of inhibiting hallmark EC behavior that is indicative of ECs being in an activated inflammatory state that could facilitate these initial stages of inflammation after the commencement of cardiomyocyte apoptosis. To mimic this activation HUVECs were treated with IL-1β and two different responses were studied; the expression of leukocyte adhesion molecule ICAM and secretion of pro-inflammatory cytokine MCP-1. Interestingly, secretome^{146a} was able to significantly inhibit both processes compared to secretome from not transfected hASCs which implies that secretome^{146a} has superior anti-inflammatory properties. An analysis of the inflammatory cytokine and miRNA composition of the secretome^{146a} did not show any significant presence of anti-inflammatory paracrine molecules. However, several well characterized anti-apoptotic paracrine molecules were significantly more concentrated in the secretome^{146a} including, G-SCF, miR-22-3p, miR-214-5p, miR-24-3p. Furthermore, similar to the angiogenic paracrine molecule analysis, several pro-apoptotic miRNA were downregulated in the secretome^{146a} including, miR-29b-3p, let-7c, and let-7b-5p. These results support the idea that secretome^{146a} is a viable proangiogenic and anti-inflammatory treatment option and therefore, could potentially be used to promote myocardial regeneration post-AMI.

REFERENCES

1. Boon RA and Dimmeler S. MicroRNAs in myocardial infarction. *Nature Reviews Cardiology*. 2015;12:135.
2. Mozaffarian D, Benjamin EJ, Go AS, Arnett DK, Blaha MJ, Cushman M, de Ferranti S, Després J-P, Fullerton HJ and Howard VJ. Heart disease and stroke statistics—2015 update. *Circulation*. 2015;131:e29-e322.
3. Pagidipati NJ and Gaziano TA. Estimating deaths from cardiovascular disease: a review of global methodologies of mortality measurement. *Circulation*. 2013;127:749-756.
4. Benjamin EJ, Virani SS, Callaway CW, Chamberlain AM, Chang AR, Cheng S, Chiuve SE, Cushman M, Delling FN and Deo R. Heart disease and stroke statistics—2018 update: a report from the American Heart Association. *Circulation*. 2018;137:e67-e492.
5. Moran AE, Forouzanfar MH, Roth G, Mensah GA, Ezzati M, Flaxman A, Murray CJ and Naghavi M. The global burden of ischemic heart disease in 1990 and 2010: the Global Burden of Disease 2010 study. *Circulation*. 2014:CIRCULATIONAHA. 113.004046.
6. Roth GA, Johnson C, Abajobir A, Abd-Allah F, Abera SF, Abyu G, Ahmed M, Aksut B, Alam T, Alam K, Alla F, Alvis-Guzman N, Amrock S, Ansari H, Ärnlöv J, Asayesh H, Atey TM, Avila-Burgos L, Awasthi A, Banerjee A, Barac A, Bärnighausen T, Barregard L, Bedi N, Belay Ketema E, Bennett D, Berhe G, Bhutta Z, Bitew S, Carapetis J, Carrero JJ, Malta DC, Castañeda-Orjuela CA, Castillo-Rivas J, Catalá-López F, Choi J-Y, Christensen H, Cirillo M, Cooper L, Criqui M, Cundiff D, Damasceno A, Dandona L, Dandona R, Davletov K, Dharmaratne S, Dorairaj P, Dubey M, Ehrenkranz R, El Sayed Zaki M, Faraon EJA, Esteghamati A, Farid T, Farvid M, Feigin V, Ding EL, Fowkes G, Gebrehiwot T, Gillum R, Gold A, Gona P, Gupta R, Habtewold TD, Hafezi-Nejad N, Hailu T, Hailu GB, Hankey G, Hassen HY, Abate KH, Havmoeller R, Hay SI, Horino M, Hotez PJ, Jacobsen K, James S, Javanbakht M, Jeemon P, John D, Jonas J, Kalkonde Y, Karimkhani C, Kasaeian A, Khader Y, Khan A, Khang Y-H, Khera S, Khoja AT, Khubchandani J, Kim D, Kolte D, Kosen S, Krohn KJ, Kumar GA, Kwan GF, Lal DK, Larsson A, Linn S, Lopez A, Lotufo PA, El Razek HMA, Malekzadeh R, Mazidi M, Meier T, Meles KG, Mensah G, Meretoja A, Mezgebe H, Miller T, Mirrakhimov E, Mohammed S, Moran AE, Musa KI, Narula J, Neal B, Ngalesoni F, Nguyen G, Obermeyer CM, Owolabi M, Patton G, Pedro J, Qato D, Qorbani M, Rahimi K, Rai RK, Rawaf S, Ribeiro A, Safiri S, Salomon JA, Santos I, Santric Milicevic M, Sartorius B, Schutte A, Sepanlou S, Shaikh MA, Shin M-J, Shishehbor M, Shore H, Silva DAS, Sobngwi E, Stranges S, Swaminathan S, Tabarés-Seisdedos R, Tadele Atnafu N, Tesfay F, Thakur JS, Thrift A, Topor-Madry R, Truelsen T, Tyrovolas S, Ukwaja KN, Uthman O, Vasankari T, Vlassov V, Vollset SE, Wakayo T, Watkins D, Weintraub R, Werdecker A, Westerman R, Wiysonge CS, Wolfe C, Workicho A, Xu G, Yano Y, Yip P, Yonemoto N, Younis M, Yu C, Vos T, Naghavi M and Murray C. Global, Regional, and National Burden of Cardiovascular Diseases for 10 Causes, 1990 to 2015. *Journal of the American College of Cardiology*. 2017;70:1-25.
7. Prabhu SD and Frangogiannis NG. The biological basis for cardiac repair after myocardial infarction: from inflammation to fibrosis. *Circulation research*. 2016;119:91-112.
8. Frangogiannis NG. Regulation of the inflammatory response in cardiac repair. *Circulation research*. 2012;110:159-173.
9. Nahrendorf M, Pittet MJ and Swirski FK. Monocytes: protagonists of infarct inflammation and repair after myocardial infarction. *Circulation*. 2010;121:2437-2445.
10. Timmers L, Pasterkamp G, de Hoog VC, Arslan F, Appelman Y and de Kleijn DP. The innate immune response in reperfused myocardium. *Cardiovascular research*. 2012;94:276-283.
11. Mann DL. The emerging role of innate immunity in the heart and vascular system: for whom the cell tolls. *Circulation research*. 2011;108:1133-1145.

12. Ghigo A, Franco I, Morello F and Hirsch E. Myocyte signalling in leucocyte recruitment to the heart. *Cardiovascular research*. 2014;102:270-280.
13. Zhu M, Goetsch S, Wang Z, Luo R, Hill JA, Schneider JW, Morris SM and Liu Z-P. FoxO4 promotes early inflammatory response upon myocardial infarction via endothelial Arg1. *Circulation research*. 2015:CIRCRESAHA. 115.306919.
14. Cahill TJ, Choudhury RP and Riley PR. Heart regeneration and repair after myocardial infarction: translational opportunities for novel therapeutics. *Nature Reviews Drug Discovery*. 2017;16:699.
15. Frangogiannis NG, Smith CW and Entman ML. The inflammatory response in myocardial infarction. *Cardiovascular research*. 2002;53:31-47.
16. Saxena A, Russo I and Frangogiannis NG. Inflammation as a therapeutic target in myocardial infarction: learning from past failures to meet future challenges. *Translational Research*. 2016;167:152-166.
17. Mantovani A, Cassatella MA, Costantini C and Jaillon S. Neutrophils in the activation and regulation of innate and adaptive immunity. *Nature Reviews Immunology*. 2011;11:519.
18. Zymek P, Bujak M, Chatila K, Cieslak A, Thakker G, Entman ML and Frangogiannis NG. The role of platelet-derived growth factor signaling in healing myocardial infarcts. *Journal of the American College of Cardiology*. 2006;48:2315-2323.
19. Möllmann H, Nef HM, Kostin S, von Kalle C, Pilz I, Weber M, Schaper J, Hamm CW and Elsässer A. Bone marrow-derived cells contribute to infarct remodelling. *Cardiovascular research*. 2006;71:661-671.
20. Zeisberg EM, Tarnavski O, Zeisberg M, Dorfman AL, McMullen JR, Gustafsson E, Chandraker A, Yuan X, Pu WT and Roberts AB. Endothelial-to-mesenchymal transition contributes to cardiac fibrosis. *Nature medicine*. 2007;13:952.
21. Hinz B, Phan SH, Thannickal VJ, Galli A, Bochaton-Piallat M-L and Gabbiani G. The myofibroblast: one function, multiple origins. *The American journal of pathology*. 2007;170:1807-1816.
22. Yano T, Miura T, Ikeda Y, Matsuda E, Saito K, Miki T, Kobayashi H, Nishino Y, Ohtani S and Shimamoto K. Intracardiac fibroblasts, but not bone marrow derived cells, are the origin of myofibroblasts in myocardial infarct repair. *Cardiovascular Pathology*. 2005;14:241-246.
23. Ruiz-Villalba A, Simón AM, Pogontke C, Castillo MI, Abizanda G, Pelacho B, Sánchez-Domínguez R, Segovia JC, Prósper F and Pérez-Pomares JM. Interacting resident epicardium-derived fibroblasts and recruited bone marrow cells form myocardial infarction scar. *Journal of the American College of Cardiology*. 2015;65:2057-2066.
24. Dobaczewski M, Bujak M, Li N, Gonzalez-Quesada C, Mendoza LH, Wang X-F and Frangogiannis NG. Smad3 Signaling Critically Regulates Fibroblast Phenotype and Function in Healing Myocardial InfarctionNovelty and Significance. *Circulation research*. 2010;107:418-428.
25. Ma Y, Halade GV and Lindsey ML. Extracellular matrix and fibroblast communication following myocardial infarction. *Journal of cardiovascular translational research*. 2012;5:848-857.
26. Van Den Borne SW, Diez J, Blankesteijn WM, Verjans J, Hofstra L and Narula J. Myocardial remodeling after infarction: the role of myofibroblasts. *Nature Reviews Cardiology*. 2010;7:30.
27. Frangogiannis NG, Ren G, Dewald O, Zymek P, Haudek S, Koerting A, Winkelmann K, Michael LH, Lawler J and Entman ML. Critical role of endogenous thrombospondin-1 in preventing expansion of healing myocardial infarcts. *Circulation*. 2005;111:2935-2942.
28. Van Aelst LN, Voss S, Carai P, Van Leeuwen R, Vanhoutte D, Sanders-van Wijk S, Eurlings L, Swinnen M, Verheyen FK and Verbeken E. Osteoglycin prevents cardiac dilatation and dysfunction after myocardial infarction through infarct collagen strengthening. *Circulation research*. 2015;116:425-436.
29. Christia P, Bujak M, Gonzalez-Quesada C, Chen W, Dobaczewski M, Reddy A and Frangogiannis NG. Systematic characterization of myocardial inflammation, repair, and remodeling in a mouse model of reperfused myocardial infarction. *Journal of Histochemistry & Cytochemistry*. 2013;61:555-570.

30. Takemura G, Ohno M, Hayakawa Y, Misao J, Kanoh M, Ohno A, Uno Y, Minatoguchi S, Fujiwara T and Fujiwara H. Role of apoptosis in the disappearance of infiltrated and proliferated interstitial cells after myocardial infarction. *Circulation research*. 1998;82:1130-1138.
31. Lymperopoulos A, Rengo G and Koch WJ. Adrenergic nervous system in heart failure: pathophysiology and therapy. *Circulation research*. 2013;113:739-753.
32. Packer M. The neurohormonal hypothesis: a theory to explain the mechanism of disease progression in heart failure. *Journal of the American College of Cardiology*. 1992;20:248-254.
33. Narula J, Haider N, Arbustini E and Chandrashekhar Y. Mechanisms of disease: apoptosis in heart failure—seeing hope in death. *Nature Reviews Cardiology*. 2006;3:681.
34. Khush KK, Menza R, Nguyen J, Zaroff JG and Goldstein BA. Donor predictors of allograft utilization and recipient outcomes after heart transplantation. *Circulation: Heart Failure*. 2013:CIRCHEARTFAILURE. 112.000165.
35. Mancini D and Colombo PC. Left Ventricular Assist Devices: A Rapidly Evolving Alternative to Transplant. *Journal of the American College of Cardiology*. 2015;65:2542-2555.
36. Niccoli G, Scalone G, Lerman A and Crea F. Coronary microvascular obstruction in acute myocardial infarction. *European heart journal*. 2015;37:1024-1033.
37. McMurray JJ and Pfeffer MA. Heart failure. *Lancet*. 2005;365:1877-89.
38. Golpanian S, Schulman IH, Ebert RF, Heldman AW, DiFede DL, Yang PC, Wu JC, Bolli R, Perin EC and Moyé L. Concise review: review and perspective of cell dosage and routes of administration from preclinical and clinical studies of stem cell therapy for heart disease. *Stem Cells Transl Med*. 2016;5:186-191.
39. Golpanian S, Wolf A, Hatzistergos KE and Hare JM. Rebuilding the damaged heart: mesenchymal stem cells, cell-based therapy, and engineered heart tissue. *Physiological Reviews*. 2016;96:1127-1168.
40. Sanganalmath SK and Bolli R. Cell therapy for heart failure: a comprehensive overview of experimental and clinical studies, current challenges, and future directions. *Circulation research*. 2013;113:810-834.
41. Banerjee MN, Bolli R and Hare JM. Clinical studies of cell therapy in cardiovascular medicine: recent developments and future directions. *Circulation research*. 2018;123:266-287.
42. Gerczuk PZ and Kloner RA. An update on cardioprotection: a review of the latest adjunctive therapies to limit myocardial infarction size in clinical trials. *Journal of the American College of Cardiology*. 2012;59:969-978.
43. Schächinger V, Assmus B, Britten MB, Honold J, Lehmann R, Teupe C, Abolmaali ND, Vogl TJ, Hofmann W-K and Martin H. Transplantation of progenitor cells and regeneration enhancement in acute myocardial infarction: final one-year results of the TOPCARE-AMI Trial. *Journal of the American College of Cardiology*. 2004;44:1690-1699.
44. Wollert KC, Meyer GP, Lotz J, Lichtenberg SR, Lippolt P, Breidenbach C, Fichtner S, Korte T, Hornig B and Messinger D. Intracoronary autologous bone-marrow cell transfer after myocardial infarction: the BOOST randomised controlled clinical trial. *The Lancet*. 2004;364:141-148.
45. Janssens S, Dubois C, Bogaert J, Theunissen K, Deroose C, Desmet W, Kalantzi M, Herbots L, Sinnaeve P and Dens J. Autologous bone marrow-derived stem-cell transfer in patients with ST-segment elevation myocardial infarction: double-blind, randomised controlled trial. *The Lancet*. 2006;367:113-121.
46. Huikuri HV, Kervinen K, Niemelä M, Ylitalo K, Säily M, Koistinen P, Savolainen E-R, Ukkonen H, Pietilä M and Airaksinen JK. Effects of intracoronary injection of mononuclear bone marrow cells on left ventricular function, arrhythmia risk profile, and restenosis after thrombolytic therapy of acute myocardial infarction. *European heart journal*. 2008;29:2723-2732.
47. Schächinger V, Erbs S, Elsässer A, Haberbosch W, Hambrecht R, Hölschermann H, Yu J, Corti R, Mathey DG and Hamm CW. Intracoronary bone marrow–derived progenitor cells in acute myocardial infarction. *New England Journal of Medicine*. 2006;355:1210-1221.

48. Traverse JH, Henry TD, Pepine CJ, Willerson JT, Zhao DX, Ellis SG, Forder JR, Anderson RD, Hatzopoulos AK and Penn MS. Effect of the use and timing of bone marrow mononuclear cell delivery on left ventricular function after acute myocardial infarction: the TIME randomized trial. *Jama*. 2012;308:2380-2389.
49. Traverse JH, Henry TD, Ellis SG, Pepine CJ, Willerson JT, Zhao DX, Forder JR, Byrne BJ, Hatzopoulos AK and Penn MS. Effect of intracoronary delivery of autologous bone marrow mononuclear cells 2 to 3 weeks following acute myocardial infarction on left ventricular function: the LateTIME randomized trial. *Jama*. 2011;306:2110-2119.
50. Sürder D, Manka R, Moccetti T, Lo Cicero V, Emmert MY, Klersy C, Soncin S, Turchetto L, Radrizzani M and Zuber M. Effect of bone marrow–derived mononuclear cell treatment, early or late after acute myocardial infarction: twelve months CMR and long-term clinical results. *Circulation research*. 2016;119:481-490.
51. Nicolau JC, Furtado RH, Rochitte CE, Schettert IT, Dohmann HF, Silva SA and Carvalho AC. Stem Cell Therapy in ST-Elevation Myocardial Infarction With Reduced Ejection Fraction: A Multicenter, Randomized, Double-Blind Trial. From MiHeart/AMI Investigators. 2016.
52. Quyyumi AA, Vasquez A, Kereiakes DJ, Klapholz M, Schaer GL, Abdel-Latif A, Frohwein S, Henry TD, Schatz RA and Dib N. PreSERVE-AMI: a randomized, double-blind, placebo-controlled clinical trial of intracoronary administration of autologous CD34+ cells in patients with left ventricular dysfunction post STEMI. *Circulation research*. 2017;120:324-331.
53. Heldman AW, DiFede DL, Fishman JE, Zambrano JP, Trachtenberg BH, Karantalis V, Mushtaq M, Williams AR, Suncion VY and McNiece IK. Transendocardial mesenchymal stem cells and mononuclear bone marrow cells for ischemic cardiomyopathy: the TAC-HFT randomized trial. *Jama*. 2014;311:62-73.
54. Florea V, Rieger AC, DiFede DL, El-Khorazaty J, Natsumeda M, Banerjee MN, Tompkins BA, Khan A, Schulman IH and Landin AM. Dose Comparison Study of Allogeneic Mesenchymal Stem Cells in Patients With Ischemic Cardiomyopathy (The TRIDENT Study) Novelty and Significance. *Circulation research*. 2017;121:1279-1290.
55. Hare JM, Fishman JE, Gerstenblith G and et al. Comparison of allogeneic vs autologous bone marrow–derived mesenchymal stem cells delivered by transendocardial injection in patients with ischemic cardiomyopathy: The poseidon randomized trial. *JAMA*. 2012;308:2369-2379.
56. Bobis-Wozowicz S, Kmiotek K, Kania K, Karnas E, Labedz-Maslowska A, Sekula M, Kedracka-Krok S, Kolcz J, Boruczkowski D and Madeja Z. Diverse impact of xeno-free conditions on biological and regenerative properties of hUC-MSCs and their extracellular vesicles. *Journal of Molecular Medicine*. 2017;95:205-220.
57. Bartolucci J, Verdugo FJ, González PL, Larrea RE, Abarzua E, Goset C, Rojo P, Palma I, Lamich R and Pedreros PA. Safety and efficacy of the intravenous infusion of umbilical cord mesenchymal stem cells in patients with heart failure: a phase 1/2 randomized controlled trial (RIMECARD trial [randomized clinical trial of intravenous infusion umbilical cord mesenchymal stem cells on cardiopathy]). *Circulation research*. 2017;121:1192-1204.
58. Bateman ME, Strong AL, Gimble JM and Bunnell BA. Using Fat to Fight Disease: A Systematic Review of Non-Homologous Adipose-Derived Stromal/Stem Cell Therapies. *STEM CELLS*. 2018.
59. Perin EC, Sanz-Ruiz R, Sánchez PL, Lasso J, Pérez-Cano R, Alonso-Farto JC, Pérez-David E, Fernández-Santos ME, Serruys PW and Duckers HJ. Adipose-derived regenerative cells in patients with ischemic cardiomyopathy: The PRECISE Trial. *American heart journal*. 2014;168:88-95. e2.
60. Henry TD, Pepine CJ, Lambert CR, Traverse JH, Schatz R, Costa M, Povsic TJ, David Anderson R, Willerson JT and Kesten S. The Athena trials: Autologous adipose-derived regenerative cells for refractory chronic myocardial ischemia with left ventricular dysfunction. *Catheterization and Cardiovascular Interventions*. 2017;89:169-177.

61. Hong KU, Guo Y, Li Q-H, Cao P, Al-Maqtari T, Vajravelu BN, Du J, Book MJ, Zhu X and Nong Y. c-kit+ Cardiac stem cells alleviate post-myocardial infarction left ventricular dysfunction despite poor engraftment and negligible retention in the recipient heart. *PloS one*. 2014;9:e96725.
62. Mirotsou M, Jayawardena TM, Schmeckpeper J, Gnecchi M and Dzau VJ. Paracrine mechanisms of stem cell reparative and regenerative actions in the heart. *Journal of molecular and cellular cardiology*. 2011;50:280-289.
63. Kinnaird T, Stabile E, Burnett M, Shou M, Lee C, Barr S, Fuchs S and Epstein S. Local delivery of marrow-derived stromal cells augments collateral perfusion through paracrine mechanisms. *Circulation*. 2004;109:1543-1549.
64. Gnecchi M, He H, Liang OD, Melo LG, Morello F, Mu H, Noiseux N, Zhang L, Pratt RE and Ingwall JS. Paracrine action accounts for marked protection of ischemic heart by Akt-modified mesenchymal stem cells. *Nature medicine*. 2005;11:367.
65. Gnecchi M, He H, Noiseux N, Liang OD, Zhang L, Morello F, Mu H, Melo LG, Pratt RE, Ingwall JS and Dzau VJ. Evidence supporting paracrine hypothesis for Akt-modified mesenchymal stem cell-mediated cardiac protection and functional improvement. *FASEB journal : official publication of the Federation of American Societies for Experimental Biology*. 2006;20:661-9.
66. Braunwald E. Cell-Based Therapy in Cardiac Regeneration: An Overview. *Circulation research*. 2018;123:132-137.
67. Wysoczynki M, Khan A and Bolli R. New paradigms in cell therapy: repeated dosing, intravenous delivery, immunomodulatory actions, and new cell types. *Circulation research*. 2018;123:138-158.
68. Shu T, Zeng B, Ren X and Li Y. HO-1 modified mesenchymal stem cells modulate MMPs/TIMPs system and adverse remodeling in infarcted myocardium. *Tissue and Cell*. 2010;42:217-222.
69. Tang J, Wang J, Guo L, Kong X, Yang J, Zheng F, Zhang L and Huang Y. Mesenchymal stem cells modified with stromal cell-derived factor 1α improve cardiac remodeling via paracrine activation of hepatocyte growth factor in a rat model of myocardial infarction. *Molecules and cells*. 2010;29:9-19.
70. Paliwal S, Chaudhuri R, Agrawal A and Mohanty S. Regenerative abilities of mesenchymal stem cells through mitochondrial transfer. *Journal of biomedical science*. 2018;25:31.
71. Uemura R, Xu M, Ahmad N and Ashraf M. Bone marrow stem cells prevent left ventricular remodeling of ischemic heart through paracrine signaling. *Circulation research*. 2006;98:1414-21.
72. Tran C and Damaser MS. Stem cells as drug delivery methods: application of stem cell secretome for regeneration. *Advanced drug delivery reviews*. 2015;82:1-11.
73. Gnecchi M, Zhang Z, Ni A and Dzau VJ. Paracrine mechanisms in adult stem cell signaling and therapy. *Circulation research*. 2008;103:1204-1219.
74. Yoshizumi T, Zhu Y, Jiang H, D'Amore A, Sakaguchi H, Tchao J, Tobita K and Wagner WR. Timing effect of intramyocardial hydrogel injection for positively impacting left ventricular remodeling after myocardial infarction. *Biomaterials*. 2016;83:182-93.
75. Baglio SR, Rooijers K, Koppers-Lalic D, Verweij FJ, Lanzón MP, Zini N, Naaijkens B, Perut F, Niessen HW and Baldini N. Human bone marrow-and adipose-mesenchymal stem cells secrete exosomes enriched in distinctive miRNA and tRNA species. *Stem cell research & therapy*. 2015;6:127.
76. Amable PR, Teixeira MVT, Carias RBV, Granjeiro JM and Borojevic R. Protein synthesis and secretion in human mesenchymal cells derived from bone marrow, adipose tissue and Wharton's jelly. *Stem Cell Research & Therapy*. 2014;5:53.
77. Li T-S, Cheng K, Malliaras K, Smith RR, Zhang Y, Sun B, Matsushita N, Blusztajn A, Terrovitis J and Kusuoka H. Direct comparison of different stem cell types and subpopulations reveals superior paracrine potency and myocardial repair efficacy with cardiosphere-derived cells. *Journal of the American College of Cardiology*. 2012;59:942-953.
78. Pires AO, Mendes-Pinheiro B, Teixeira FG, Anjo SI, Ribeiro-Samy S, Gomes ED, Serra SC, Silva NA, Manadas B and Sousa N. Unveiling the differences of secretome of human bone marrow mesenchymal

stem cells, adipose tissue-derived stem cells, and human umbilical cord perivascular cells: a proteomic analysis. *Stem cells and development*. 2016;25:1073-1083.
79. Estrada R, Li N, Sarojini H, An J, Lee MJ and Wang E. Secretome from mesenchymal stem cells induces angiogenesis via Cyr61. *J Cell Physiol*. 2009;219:563-71.
80. Hung SC, Pochampally RR, Chen SC, Hsu SC and Prockop DJ. Angiogenic effects of human multipotent stromal cell conditioned medium activate the PI3K-Akt pathway in hypoxic endothelial cells to inhibit apoptosis, increase survival, and stimulate angiogenesis. *Stem Cells*. 2007;25:2363-70.
81. Feng Y, Huang W, Wani M, Yu X and Ashraf M. Ischemic preconditioning potentiates the protective effect of stem cells through secretion of exosomes by targeting Mecp2 via miR-22. *PloS one*. 2014;9:e88685.
82. Namazi H, Mohit E, Namazi I, Rajabi S, Samadian A, Hajizadeh-Saffar E, Aghdami N and Baharvand H. Exosomes secreted by hypoxic cardiosphere-derived cells enhance tube formation and increase pro-angiogenic miRNA. *Journal of cellular biochemistry*. 2018;119:4150-4160.
83. Danieli P, Malpasso G, Ciuffreda MC, Cervio E, Calvillo L, Copes F, Pisano F, Mura M, Kleijn L and De Boer RA. Conditioned medium from human amniotic mesenchymal stromal cells limits infarct size and enhances angiogenesis. *Stem Cells Transl Med*. 2015;4:448-458.
84. Yu B, Kim HW, Gong M, Wang J, Millard RW, Wang Y, Ashraf M and Xu M. Exosomes secreted from GATA-4 overexpressing mesenchymal stem cells serve as a reservoir of anti-apoptotic microRNAs for cardioprotection. *International journal of cardiology*. 2015;182:349-360.
85. Mirotsou M, Zhang Z, Deb A, Zhang L, Gnecchi M, Noiseux N, Mu H, Pachori A and Dzau V. Secreted frizzled related protein 2 (Sfrp2) is the key Akt-mesenchymal stem cell-released paracrine factor mediating myocardial survival and repair. *Proceedings of the National Academy of Sciences*. 2007;104:1643-1648.
86. Yagi H, Soto-Gutierrez A, Navarro-Alvarez N, Nahmias Y, Goldwasser Y, Kitagawa Y, Tilles AW, Tompkins RG, Parekkadan B and Yarmush ML. Reactive bone marrow stromal cells attenuate systemic inflammation via sTNFR1. *Molecular Therapy*. 2010;18:1857-1864.
87. Mias C, Trouche E, Seguelas MH, Calcagno F, Dignat-George F, Sabatier F, Piercecchi-Marti MD, Daniel L, Bianchi P and Calise D. Ex vivo pretreatment with melatonin improves survival, proangiogenic/mitogenic activity, and efficiency of mesenchymal stem cells injected into ischemic kidney. *Stem cells*. 2008;26:1749-1757.
88. Hoke NN, Salloum FN, Kass DA, Das A and Kukreja RC. Preconditioning by Phosphodiesterase-5 Inhibition Improves Therapeutic Efficacy of Adipose-Derived Stem Cells Following Myocardial Infarction in Mice. *STEM CELLS*. 2012;30:326-335.
89. Potapova IA, Gaudette GR, Brink PR, Robinson RB, Rosen MR, Cohen IS and Doronin SV. Mesenchymal stem cells support migration, extracellular matrix invasion, proliferation, and survival of endothelial cells in vitro. *Stem cells*. 2007;25:1761-1768.
90. Potapova IA, Brink PR, Cohen IS and Doronin SV. Culturing of human mesenchymal stem cells as three-dimensional aggregates induces functional expression of CXCR4 that regulates adhesion to endothelial cells. *Journal of Biological Chemistry*. 2008;283:13100-13107.
91. Cesarz Z and Tamama K. Spheroid culture of mesenchymal stem cells. *Stem cells international*. 2015;2016.
92. Bartosh TJ, Ylöstalo JH, Bazhanov N, Kuhlman J and Prockop DJ. Dynamic compaction of human mesenchymal stem/precursor cells into spheres self-activates caspase-dependent IL1 signaling to enhance secretion of modulators of inflammation and immunity (PGE2, TSG6, and STC1). *Stem Cells*. 2013;31:2443-2456.
93. YlÖstalo JH, Bartosh TJ, Coble K and Prockop DJ. Human mesenchymal stem/stromal cells cultured as spheroids are self-activated to produce prostaglandin E2 that directs stimulated macrophages into an anti-inflammatory phenotype. *Stem cells*. 2012;30:2283-2296.

94. Skiles ML, Hanna B, Rucker L, Tipton A, Brougham-Cook A, Jabbarzadeh E and Blanchette JO. Asc spheroid geometry and culture oxygenation differentially impact induction of preangiogenic behaviors in endothelial cells. *Cell transplantation*. 2015;24:2323-2335.
95. Bassaneze V, Barauna VG, Lavini-Ramos C, Kalil J, Schettert IT, Miyakawa AA and Krieger JE. Shear stress induces nitric oxide–mediated vascular endothelial growth factor production in human adipose tissue mesenchymal stem cells. *Stem cells and development*. 2010;19:371-378.
96. Seib FP, Prewitz M, Werner C and Bornhäuser M. Matrix elasticity regulates the secretory profile of human bone marrow-derived multipotent mesenchymal stromal cells (MSCs). *Biochemical and biophysical research communications*. 2009;389:663-667.
97. Mannello F and Tonti GA. Concise review: no breakthroughs for human mesenchymal and embryonic stem cell culture: conditioned medium, feeder layer, or feeder-free; medium with fetal calf serum, human serum, or enriched plasma; serum-free, serum replacement nonconditioned medium, or ad hoc formula? All that glitters is not gold! *Stem cells*. 2007;25:1603-1609.
98. Shahdadfar A, Frønsdal K, Haug T, Reinholt FP and Brinchmann JE. In vitro expansion of human mesenchymal stem cells: choice of serum is a determinant of cell proliferation, differentiation, gene expression, and transcriptome stability. *Stem cells*. 2005;23:1357-1366.
99. Stastna M and Van Eyk JE. Investigating the Secretome Lessons About the Cells That Comprise the Heart. *Circulation: Cardiovascular Genetics*. 2012;5:o8-o18.
100. Bhang SH, Lee S, Shin J-Y, Lee T-J, Jang H-K and Kim B-S. Efficacious and clinically relevant conditioned medium of human adipose-derived stem cells for therapeutic angiogenesis. *Molecular Therapy*. 2014;22:862-872.
101. Sagaradze GD, Nimiritsky PP, Akopyan ZA, Makarevich PI and Efimenko AY. "Cell-Free Therapeutics" from Components Secreted by Mesenchymal Stromal Cells as a Novel Class of Biopharmaceuticals *Biopharmaceuticals*: IntechOpen; 2018.
102. Teasdale A ED, Nims RW, editors. *ICH Quality Guidelines: An Implementation Guide*: Chichester: Wiley; 2017.
103. Gimona M, Pachler K, Laner-Plamberger S, Schallmoser K and Rohde E. Manufacturing of human extracellular vesicle-based therapeutics for clinical use. *International journal of molecular sciences*. 2017;18:1190.
104. Lindsey ML, Bolli R, Canty JM, Du X-J, Frangogiannis NG, Frantz S, Gourdie RG, Holmes JW, Jones SP and Kloner R. Guidelines for experimental models of myocardial ischemia and infarction. *American Journal of Physiology-Heart and Circulatory Physiology*. 2018.
105. Hasan A, Khattab A, Islam MA, Hweij KA, Zeitouny J, Waters R, Sayegh M, Hossain MM and Paul A. Injectable hydrogels for cardiac tissue repair after myocardial infarction. *Advanced Science*. 2015;2.
106. Peña B, Laughter M, Jett S, Rowland TJ, Taylor MR, Mestroni L and Park D. Injectable Hydrogels for Cardiac Tissue Engineering. *Macromolecular bioscience*. 2018;18:1800079.
107. Nair LS and Laurencin CT. Biodegradable polymers as biomaterials. *Progress in polymer science*. 2007;32:762-798.
108. Waters R, Alam P, Pacelli S, Chakravarti AR, Ahmed RP and Paul A. Stem cell-inspired secretome-rich injectable hydrogel to repair injured cardiac tissue. *Acta biomaterialia*. 2017.
109. Perka C, Spitzer RS, Lindenhayn K, Sittinger M and Schultz O. Matrix-mixed culture: New methodology for chondrocyte culture and preparation of cartilage transplants. *Journal of Biomedical Materials Research: An Official Journal of The Society for Biomaterials and The Japanese Society for Biomaterials*. 2000;49:305-311.
110. Ye Q, Zünd G, Benedikt P, Jockenhoevel S, Hoerstrup SP, Sakyama S, Hubbell JA and Turina M. Fibrin gel as a three dimensional matrix in cardiovascular tissue engineering. *European Journal of Cardio-Thoracic Surgery*. 2000;17:587-591.

111. Li X-Y, Wang T, Jiang X-J, Lin T, Wu D-Q, Zhang X-Z, Okello E, Xu H-X and Yuan M-J. Injectable hydrogel helps bone marrow-derived mononuclear cells restore infarcted myocardium. *Cardiology*. 2010;115:194-199.
112. Li Y, Rodrigues J and Tomas H. Injectable and biodegradable hydrogels: gelation, biodegradation and biomedical applications. *Chemical Society Reviews*. 2012;41:2193-2221.
113. Lee KY and Mooney DJ. Hydrogels for tissue engineering. *Chemical reviews*. 2001;101:1869-1880.
114. Lee S, Tong X and Yang F. The effects of varying poly (ethylene glycol) hydrogel crosslinking density and the crosslinking mechanism on protein accumulation in three-dimensional hydrogels. *Acta biomaterialia*. 2014;10:4167-4174.
115. Sofia SJ, Premnath V and Merrill EW. Poly (ethylene oxide) grafted to silicon surfaces: grafting density and protein adsorption. *Macromolecules*. 1998;31:5059-5070.
116. Alcantar NA, Aydil ES and Israelachvili JN. Polyethylene glycol–coated biocompatible surfaces. *Journal of Biomedical Materials Research: An Official Journal of The Society for Biomaterials, The Japanese Society for Biomaterials, and The Australian Society for Biomaterials and the Korean Society for Biomaterials*. 2000;51:343-351.
117. Elisseeff J, McIntosh W, Anseth K, Riley S, Ragan P and Langer R. Photoencapsulation of chondrocytes in poly (ethylene oxide)-based semi-interpenetrating networks. *Journal of Biomedical Materials Research: An Official Journal of The Society for Biomaterials, The Japanese Society for Biomaterials, and The Australian Society for Biomaterials and the Korean Society for Biomaterials*. 2000;51:164-171.
118. Holmes TC. Novel peptide-based biomaterial scaffolds for tissue engineering. *Trends in biotechnology*. 2002;20:16-21.
119. Branco MC and Schneider JP. Self-assembling materials for therapeutic delivery. *Acta biomaterialia*. 2009;5:817-831.
120. Williams C, Budina E, Stoppel WL, Sullivan KE, Emani S, Emani SM and Black III LD. Cardiac extracellular matrix–fibrin hybrid scaffolds with tunable properties for cardiovascular tissue engineering. *Acta biomaterialia*. 2015;14:84-95.
121. Deng B, Shen L, Wu Y, Shen Y, Ding X, Lu S, Jia J, Qian J and Ge J. Delivery of alginate-chitosan hydrogel promotes endogenous repair and preserves cardiac function in rats with myocardial infarction. *Journal of Biomedical Materials Research Part A*. 2015;103:907-918.
122. Grover GN, Rao N and Christman KL. Myocardial matrix–polyethylene glycol hybrid hydrogels for tissue engineering. *Nanotechnology*. 2013;25:014011.
123. Mukherjee R, Zavadzkas JA, Saunders SM, McLean JE, Jeffords LB, Beck C, Stroud RE, Leone AM, Koval CN and Rivers WT. Targeted myocardial microinjections of a biocomposite material reduces infarct expansion in pigs. *The Annals of thoracic surgery*. 2008;86:1268-1276.
124. Gaharwar AK, Peppas NA and Khademhosseini A. Nanocomposite hydrogels for biomedical applications. *Biotechnology and bioengineering*. 2014;111:441-453.
125. Thoniyot P, Tan MJ, Karim AA, Young DJ and Loh XJ. Nanoparticle–hydrogel composites: Concept, design, and applications of these promising, multi-functional materials. *Advanced Science*. 2015;2:1400010.
126. Shin SR, Jung SM, Zalabany M, Kim K, Zorlutuna P, Kim SB, Nikkhah M, Khabiry M, Azize M and Kong J. Carbon-nanotube-embedded hydrogel sheets for engineering cardiac constructs and bioactuators. *ACS nano*. 2013;7:2369-2380.
127. Baei P, Jalili-Firoozinezhad S, Rajabi-Zeleti S, Tafazzoli-Shadpour M, Baharvand H and Aghdami N. Electrically conductive gold nanoparticle-chitosan thermosensitive hydrogels for cardiac tissue engineering. *Materials Science and Engineering: C*. 2016;63:131-141.
128. Paul A. Nanocomposite hydrogels: an emerging biomimetic platform for myocardial therapy and tissue engineering. *Nanomedicine*. 2015;10:1371-1374.

129. Ravichandran R, Venugopal JR, Sundarrajan S, Mukherjee S, Sridhar R and Ramakrishna S. Minimally invasive injectable short nanofibers of poly (glycerol sebacate) for cardiac tissue engineering. *Nanotechnology*. 2012;23:385102.
130. Babensee JE, Anderson JM, McIntire LV and Mikos AG. Host response to tissue engineered devices. *Advanced drug delivery reviews*. 1998;33:111-139.
131. Garbern JC, Minami E, Stayton PS and Murry CE. Delivery of basic fibroblast growth factor with a pH-responsive, injectable hydrogel to improve angiogenesis in infarcted myocardium. *Biomaterials*. 2011;32:2407-2416.
132. Wu J, Zeng F, Huang X-P, Chung JCY, Konecny F, Weisel RD and Li R-K. Infarct stabilization and cardiac repair with a VEGF-conjugated, injectable hydrogel. *Biomaterials*. 2011;32:579-586.
133. Ruvinov E, Leor J and Cohen S. The promotion of myocardial repair by the sequential delivery of IGF-1 and HGF from an injectable alginate biomaterial in a model of acute myocardial infarction. *Biomaterials*. 2011;32:565-578.
134. Song M, Jang H, Lee J, Kim JH, Kim SH, Sun K and Park Y. Regeneration of chronic myocardial infarction by injectable hydrogels containing stem cell homing factor SDF-1 and angiogenic peptide Ac-SDKP. *Biomaterials*. 2014;35:2436-2445.
135. Kim JH, Jung Y, Kim S-H, Sun K, Choi J, Kim HC, Park Y and Kim SH. The enhancement of mature vessel formation and cardiac function in infarcted hearts using dual growth factor delivery with self-assembling peptides. *Biomaterials*. 2011;32:6080-6088.
136. Johnson NR, Kruger M, Goetsch KP, Zilla P, Bezuidenhout D, Wang Y and Davies NH. Coacervate delivery of growth factors combined with a degradable hydrogel preserves heart function after myocardial infarction. *ACS Biomaterials Science & Engineering*. 2015;1:753-759.
137. Eckhouse SR, Purcell BP, McGarvey JR, Lobb D, Logdon CB, Doviak H, O'neill JW, Shuman JA, Novack CP and Zellars KN. Local hydrogel release of recombinant TIMP-3 attenuates adverse left ventricular remodeling after experimental myocardial infarction. *Science translational medicine*. 2014;6:223ra21-223ra21.
138. Chen CW, Wang LL, Zaman S, Gordon J, Arisi MF, Venkataraman CM, Chung JJ, Hung G, Gaffey AC and Spruce LA. Sustained release of endothelial progenitor cell-derived extracellular vesicles from shear-thinning hydrogels improves angiogenesis and promotes function after myocardial infarction. *Cardiovascular research*. 2018;114:1029-1040.
139. Monaghan MG, Holeiter M, Brauchle E, Layland SL, Lu Y, Deb A, Pandit A, Nsair A and Schenke-Layland K. Exogenous miR-29B delivery through a hyaluronan-based injectable system yields functional maintenance of the infarcted myocardium. *Tissue Engineering Part A*. 2018;24:57-67.
140. Pandey R, Velasquez S, Durrani S, Jiang M, Neiman M, Crocker JS, Benoit JB, Rubinstein J, Paul A and Ahmed RP. MicroRNA-1825 induces proliferation of adult cardiomyocytes and promotes cardiac regeneration post ischemic injury. *American journal of translational research*. 2017;9:3120-3137.
141. Haraguchi K. Nanocomposite hydrogels. *Current Opinion in Solid State and Materials Science*. 2007;11:47-54.
142. Paul A. Nanocomposite hydrogels: an emerging biomimetic platform for myocardial therapy and tissue engineering. *Nanomedicine (London, England)*. 2015;10:1371-4.
143. Pacelli S, Manoharan V, Desalvo A, Lomis N, Jodha KS, Prakash S and Paul A. Tailoring biomaterial surface properties to modulate host-implant interactions: implication in cardiovascular and bone therapy. *Journal of Materials Chemistry B*. 2015.
144. Song F, Li X, Wang Q, Liao L and Zhang C. Nanocomposite Hydrogels and Their Applications in Drug Delivery and Tissue Engineering. *Journal of biomedical nanotechnology*. 2015;11:40-52.
145. Li Y, Dong H, Li Y and Shi D. Graphene-based nanovehicles for photodynamic medical therapy. *International journal of nanomedicine*. 2015;10:2451-9.

146. Montellano A, Da Ros T, Bianco A and Prato M. Fullerene C60 as a multifunctional system for drug and gene delivery. *Nanoscale*. 2011;3:4035-4041.
147. Cho H-B, Nguyen S, Nakayama T, Huynh M, Suematsu H, Suzuki T, Jiang W, Rozali S, Tokoi Y, Park Y-H and Niihara K. Oxidation of nanodiamonds and modulation of their assembly in polymer-based nanohybrids by field-inducement. *J Mater Sci*. 2013;48:4151-4162.
148. Paul A, Hasan A, Kindi HA, Gaharwar AK, Rao VT, Nikkhah M, Shin SR, Krafft D, Dokmeci MR, Shum-Tim D and Khademhosseini A. Injectable graphene oxide/hydrogel-based angiogenic gene delivery system for vasculogenesis and cardiac repair. *ACS nano*. 2014;8:8050-62.
149. Kostarelos K, Bianco A and Prato M. Promises, facts and challenges for carbon nanotubes in imaging and therapeutics. *Nat Nano*. 2009;4:627-633.
150. Krishna KV, Menard-Moyon C, Verma S and Bianco A. Graphene-based nanomaterials for nanobiotechnology and biomedical applications. *Nanomedicine (London, England)*. 2013;8:1669-88.
151. Choy J-H, Choi S-J, Oh J-M and Park T. Clay minerals and layered double hydroxides for novel biological applications. *Applied Clay Science*. 2007;36:122-132.
152. Gaharwar AK, Mihaila SM, Swami A, Patel A, Sant S, Reis RL, Marques AP, Gomes ME and Khademhosseini A. Bioactive silicate nanoplatelets for osteogenic differentiation of human mesenchymal stem cells. *Advanced Materials*. 2013;25:3329-3336.
153. Gaharwar AK, Avery RK, Assmann A, Paul A, McKinley GH, Khademhosseini A and Olsen BD. Shear-thinning nanocomposite hydrogels for the treatment of hemorrhage. *ACS Nano*. 2014;8:9833-42.
154. Min J, Braatz RD and Hammond PT. Tunable staged release of therapeutics from layer-by-layer coatings with clay interlayer barrier. *Biomaterials*. 2014;35:2507-17.
155. Dawson JI, Kanczler JM, Yang XB, Attard GS and Oreffo RO. Clay gels for the delivery of regenerative microenvironments. *Advanced Materials*. 2011;23:3304-3308.
156. Lu S, Lam J, Trachtenberg JE, Lee EJ, Seyednejad H, van den Beucken JJ, Tabata Y, Wong ME, Jansen JA and Mikos AG. Dual growth factor delivery from bilayered, biodegradable hydrogel composites for spatially-guided osteochondral tissue repair. *Biomaterials*. 2014;35:8829-8839.
157. Zhang H, Jia X, Han F, Zhao J, Zhao Y, Fan Y and Yuan X. Dual-delivery of VEGF and PDGF by double-layered electrospun membranes for blood vessel regeneration. *Biomaterials*. 2013;34:2202-2212.
158. Fidelis-de-Oliveira P, Werneck-de-Castro JP, Pinho-Ribeiro V, Shalom BC, Nascimento-Silva JH, Costa e Souza RH, Cruz IS, Rangel RR, Goldenberg RC and Campos-de-Carvalho AC. Soluble factors from multipotent mesenchymal stromal cells have antinecrotic effect on cardiomyocytes in vitro and improve cardiac function in infarcted rat hearts. *Cell transplantation*. 2012;21:1011-21.
159. Gallina C, Turinetto V and Giachino C. A New Paradigm in Cardiac Regeneration: The Mesenchymal Stem Cell Secretome. *Stem cells international*. 2015;2015:765846.
160. Stastna M and Van Eyk JE. Investigating the Secretome: Lessons About the Cells that Comprise the Heart. *Circulation Cardiovascular Genetics*. 2012;5:o8-o18.
161. Pacelli S, Paolicelli P, Pepi F, Garzoli S, Polini A, Tita B, Vitalone A and Casadei M. Gellan gum and polyethylene glycol dimethacrylate double network hydrogels with improved mechanical properties. *J Polym Res*. 2014;21:1-13.
162. Jeong GS, Jun Y, Song JH, Shin SH and Lee S-H. Meniscus induced self organization of multiple deep concave wells in a microchannel for embryoid bodies generation. *Lab on a chip*. 2012;12:159-166.
163. Nikkhah M, Eshak N, Zorlutuna P, Annabi N, Castello M, Kim K, Dolatshahi-Pirouz A, Edalat F, Bae H, Yang Y and Khademhosseini A. Directed endothelial cell morphogenesis in micropatterned gelatin methacrylate hydrogels. *Biomaterials*. 2012;33:9009-18.
164. Konoplyannikov M, Haider KH, Lai VK, Ahmed RP, Jiang S and Ashraf M. Activation of diverse signaling pathways by ex-vivo delivery of multiple cytokines for myocardial repair. *Stem cells and development*. 2013;22:204-15.

165. Prabha S, Sharma B and Labhasetwar V. Inhibition of tumor angiogenesis and growth by nanoparticle-mediated p53 gene therapy in mice. *Cancer gene therapy*. 2012;19:530-7.
166. Tu Y and Zhu L. Enhancing cancer targeting and anticancer activity by a stimulus-sensitive multifunctional polymer-drug conjugate. *Journal of controlled release : official journal of the Controlled Release Society*. 2015;212:94-102.
167. Gallina C, Turinetto V and Giachino C. A New Paradigm in Cardiac Regeneration: The Mesenchymal Stem Cell Secretome. *Stem cells international*. 2015;2015:765846.
168. Nichol JW, Koshy S, Bae H, Hwang CM, Yamanlar S and Khademhosseini A. Cell-laden microengineered gelatin methacrylate hydrogels. *Biomaterials*. 2010;31:5536-5544.
169. Pawar N and Bohidar H. Surface selective binding of nanoclay particles to polyampholyte protein chains. *The Journal of chemical physics*. 2009;131:045103-045103.
170. Chanyshev B, Shainberg A, Isak A, Chepurko Y, Porat E and Hochhauser E. Conditioned medium from hypoxic cells protects cardiomyocytes against ischemia. *Molecular and cellular biochemistry*. 2012;363:167-78.
171. Karantalis V and Hare JM. Use of mesenchymal stem cells for therapy of cardiac disease. *Circulation research*. 2015;116:1413-1430.
172. Ranganath SH, Levy O, Inamdar MS and Karp JM. Harnessing the mesenchymal stem cell secretome for the treatment of cardiovascular disease. *Cell stem cell*. 2012;10:244-258.
173. Tous E, Purcell B, Ifkovits JL and Burdick JA. Injectable acellular hydrogels for cardiac repair. *Journal of cardiovascular translational research*. 2011;4:528-542.
174. Roche ET, Hastings CL, Lewin SA, Shvartsman DE, Brudno Y, Vasilyev NV, O'Brien FJ, Walsh CJ, Duffy GP and Mooney DJ. Comparison of biomaterial delivery vehicles for improving acute retention of stem cells in the infarcted heart. *Biomaterials*. 2014;35:6850-6858.
175. Hasan A, Waters R, Roula B, Dana R, Yara S, Alexandre T and Paul A. Engineered Biomaterials to Enhance Stem Cell-Based Cardiac Tissue Engineering and Therapy. *Macromolecular Bioscience*. 2016;16:958-977.
176. Tang J, Shen D, Caranasos TG, Wang Z, Vandergriff AC, Allen TA, Hensley MT, Dinh P-U, Cores J and Li T-S. Therapeutic microparticles functionalized with biomimetic cardiac stem cell membranes and secretome. *Nature communications*. 2017;8:13724.
177. Luo L, Tang J, Nishi K, Yan C, Dinh P-U, Cores J, Kudo T, Zhang J, Li T-S and Cheng K. Fabrication of synthetic mesenchymal stem cells for the treatment of acute myocardial infarction in micenovelty and significance. *Circulation research*. 2017;120:1768-1775.
178. Pacelli S, Paolicelli P, Dreesen I, Kobayashi S, Vitalone A and Casadei MA. Injectable and photocross-linkable gels based on gellan gum methacrylate: A new tool for biomedical application. *International Journal of Biological Macromolecules*. 2015;72:1335-1342.
179. Paul A, Hasan A, Kindi HA, Gaharwar AK, Rao VT, Nikkhah M, Shin SR, Krafft D, Dokmeci MR and Shum-Tim D. Injectable graphene oxide/hydrogel-based angiogenic gene delivery system for vasculogenesis and cardiac repair. *ACS nano*. 2014;8:8050-8062.
180. Su D, Jiang L, Chen X, Dong J and Shao Z. Enhancing the Gelation and Bioactivity of Injectable Silk Fibroin Hydrogel with Laponite Nanoplatelets. *ACS applied materials & interfaces*. 2016;8:9619-9628.
181. Mulyasasmita W, Cai L, Hori Y and Heilshorn SC. Avidity-controlled delivery of angiogenic peptides from injectable molecular-recognition hydrogels. *Tissue Engineering Part A*. 2014;20:2102-2114.
182. Whitlow J, Pacelli S and Paul A. Polymeric Nanohybrids as a New Class of Therapeutic Biotransporters. *Macromolecular Chemistry and Physics*. 2016.
183. Pacelli S, Manoharan V, Desalvo A, Lomis N, Jodha KS, Prakash S and Paul A. Tailoring biomaterial surface properties to modulate host-implant interactions: implication in cardiovascular and bone therapy. *Journal of Materials Chemistry B*. 2016;4:1586-1599.

184. Krishna KV, Ménard-Moyon C, Verma S and Bianco A. Graphene-based nanomaterials for nanobiotechnology and biomedical applications. *Nanomedicine : nanotechnology, biology, and medicine*. 2013;8:1669-1688.
185. Waters R, Pacelli S, Maloney R, Medhi I, Ahmed RPH and Paul A. Stem cell secretome-rich nanoclay hydrogel: a dual action therapy for cardiovascular regeneration. *Nanoscale*. 2016;8:7371-7376.
186. Ding X, Gao J, Wang Z, Awada H and Wang Y. A shear-thinning hydrogel that extends in vivo bioactivity of FGF2. *Biomaterials*. 2016;111:80-89.
187. Gibbs D, Black C, Hulsart-Billstrom G, Shi P, Scarpa E, Oreffo R and Dawson J. Bone induction at physiological doses of BMP through localization by clay nanoparticle gels. *Biomaterials*. 2016;99:16-23.
188. Corrente F, Amara HMA, Pacelli S, Paolicelli P and Casadei MA. Novel injectable and in situ cross-linkable hydrogels of dextran methacrylate and scleroglucan derivatives: Preparation and characterization. *Carbohydrate polymers*. 2013;92:1033-1039.
189. Watson BM, Kasper FK, Engel PS and Mikos AG. Synthesis and characterization of injectable, biodegradable, phosphate-containing, chemically cross-linkable, thermoresponsive macromers for bone tissue engineering. *Biomacromolecules*. 2014;15:1788-1796.
190. Huang CC, Pan WY, Tseng MT, Lin KJ, Yang YP, Tsai HW, Hwang SM, Chang Y, Wei HJ and Sung HW. Enhancement of cell adhesion, retention, and survival of HUVEC/cbMSC aggregates that are transplanted in ischemic tissues by concurrent delivery of an antioxidant for therapeutic angiogenesis. *Biomaterials*. 2016;74:53-63.
191. Durrani S, Haider KH, Ahmed RPH, Jiang S and Ashraf M. Cytoprotective and Proangiogenic Activity of Ex-Vivo Netrin-1 Transgene Overexpression Protects the Heart Against Ischemia/Reperfusion Injury. *Stem Cells and Development*. 2012;21:1769-1778.
192. Paul A, Binsalamah ZM, Khan AA, Abbasia S, Elias CB, Shum-Tim D and Prakash S. A nanobiohybrid complex of recombinant baculovirus and Tat/DNA nanoparticles for delivery of Ang-1 transgene in myocardial infarction therapy. *Biomaterials*. 2011;32:8304-8318.
193. Arif M, Pandey R, Alam P, Jiang S, Sadayappan S, Paul A and Ahmed RPH. MicroRNA-210-mediated proliferation, survival, and angiogenesis promote cardiac repair post myocardial infarction in rodents. *Journal of molecular medicine (Berlin, Germany)*. 2017.
194. Paul A, Hasan A, Kindi HA, Gaharwar AK, Rao VTS, Nikkhah M, Shin SR, Krafft D, Dokmeci MR, Shum-Tim D and Khademhosseini A. Injectable Graphene Oxide/Hydrogel-Based Angiogenic Gene Delivery System for Vasculogenesis and Cardiac Repair. *ACS Nano*. 2014;8:8050-8062.
195. Haider HK, Lee Y-J, Jiang S, Ahmed RPH, Ryon M and Ashraf M. Phosphodiesterase inhibition with tadalafil provides longer and sustained protection of stem cells. *American Journal of Physiology - Heart and Circulatory Physiology*. 2010;299:H1395-H1404.
196. Frith JE, Thomson B and Genever PG. Dynamic three-dimensional culture methods enhance mesenchymal stem cell properties and increase therapeutic potential. *Tissue Engineering Part C: Methods*. 2009;16:735-749.
197. Shearier E, Xing Q, Qian Z and Zhao F. Physiologically Low Oxygen Enhances Biomolecule Production and Stemness of Mesenchymal Stem Cell Spheroids. *Tissue Engineering Part C: Methods*. 2016;22:360-369.
198. Okada M, Oba Y and Yamawaki H. Endostatin stimulates proliferation and migration of adult rat cardiac fibroblasts through PI3K/Akt pathway. *European Journal of Pharmacology*. 2015;750:20-26.
199. Isobe K, Kuba K, Maejima Y, Suzuki J-i, Kubota S and Isobe M. Inhibition of endostatin/collagen XVIII deteriorates left ventricular remodeling and heart failure in rat myocardial infarction model. *Circulation Journal*. 2010;74:109-119.
200. Sonnenberg S, Rane AA, Liu CJ, Rao N, Agmon G, Suarez S, Wang R, Munoz A, Bajaj V, Zhang S, Braden R, Schup-Magoffin PJ, Kwan OL, DeMaria AN, Cochran JR and Christman KL. Delivery of an

engineered HGF fragment in an extracellular matrix-derived hydrogel prevents negative LV remodeling post-myocardial infarction. *Biomaterials*. 2015;45:56-63.
201. Nakamura T, Mizuno S, Matsumoto K, Sawa Y, Matsuda H and Nakamura T. Myocardial protection from ischemia/reperfusion injury by endogenous and exogenous HGF. *The Journal of clinical investigation*. 2000;106:1511-1519.
202. Nakamura T, Matsumoto K, Mizuno S, Sawa Y, Matsuda H and Nakamura T. Hepatocyte growth factor prevents tissue fibrosis, remodeling, and dysfunction in cardiomyopathic hamster hearts. *American Journal of Physiology-Heart and Circulatory Physiology*. 2005;288:H2131-H2139.
203. Taniyama Y, Morishita R, Aoki M, Hiraoka K, Yamasaki K, Hashiya N, Matsumoto K, Nakamura T, Kaneda Y and Ogihara T. Angiogenesis and antifibrotic action by hepatocyte growth factor in cardiomyopathy. *Hypertension*. 2002;40:47-53.
204. Ueda H, Nakamura T, Matsumoto K, Sawa Y, Matsuda H and Nakamura T. A potential cardioprotective role of hepatocyte growth factor in myocardial infarction in rats. *Cardiovascular research*. 2001;51:41-50.
205. Marsano A, Maidhof R, Luo J, Fujikara K, Konofagou EE, Banfi A and Vunjak-Novakovic G. The effect of controlled expression of VEGF by transduced myoblasts in a cardiac patch on vascularization in a mouse model of myocardial infarction. *Biomaterials*. 2013;34:393-401.
206. Wu J, Zeng F, Huang X-P, Chung JC-Y, Konecny F, Weisel RD and Li R-K. Infarct stabilization and cardiac repair with a VEGF-conjugated, injectable hydrogel. *Biomaterials*. 2011;32:579-586.
207. Yang Y, Shi C, Hou X, Zhao Y, Chen B, Tan B, Deng Z, Li Q, Liu J, Xiao Z, Miao Q and Dai J. Modified VEGF targets the ischemic myocardium and promotes functional recovery after myocardial infarction. *Journal of Controlled Release*. 2015;213:27-35.
208. Zhao T, Zhao W, Chen Y, Ahokas RA and Sun Y. Vascular endothelial growth factor (VEGF)-A: Role on cardiac angiogenesis following myocardial infarction. *Microvascular Research*. 2010;80:188-194.
209. Cohn JN, Ferrari R and Sharpe N. Cardiac remodeling--concepts and clinical implications: a consensus paper from an international forum on cardiac remodeling. Behalf of an International Forum on Cardiac Remodeling. *Journal of the American College of Cardiology*. 2000;35:569-82.
210. Kurrelmeyer K, Kalra D, Bozkurt B, Wang F, Dibbs Z, Seta Y, Baumgarten G, Engle D, Sivasubramanian N and Mann DL. Cardiac remodeling as a consequence and cause of progressive heart failure. *Clinical cardiology*. 1998;21:14-19.
211. Awada HK, Hwang MP and Wang Y. Towards comprehensive cardiac repair and regeneration after myocardial infarction: Aspects to consider and proteins to deliver. *Biomaterials*. 2016;82:94-112.
212. Deroanne CF, Lapiere CM and Nusgens BV. In vitro tubulogenesis of endothelial cells by relaxation of the coupling extracellular matrix-cytoskeleton. *Cardiovascular research*. 2001;49:647-658.
213. Swendeman S, Mendelson K, Weskamp G, Horiuchi K, Deutsch U, Scherle P, Hooper A, Rafii S and Blobel CP. VEGF-A stimulates ADAM17-dependent shedding of VEGFR2 and crosstalk between VEGFR2 and ERK signaling. *Circulation research*. 2008;103:916-918.
214. Guidolin D, Albertin G and Ribatti D. Exploring in vitro angiogenesis by image analysis and mathematical modeling. *Microscopy: science, technology, applications and education*. 2010;2:876-884.
215. Davies J. *Replacing animal models: a practical guide to creating and using culture-based biomimetic alternatives*: John Wiley & Sons; 2012.
216. Annabi N, Tamayol A, Uquillas JA, Akbari M, Bertassoni LE, Cha C, Camci-Unal G, Dokmeci MR, Peppas NA and Khademhosseini A. 25th Anniversary Article: Rational Design and Applications of Hydrogels in Regenerative Medicine. *Advanced materials (Deerfield Beach, Fla)*. 2014;26:85-124.
217. Mahdavinia GR, Ettehadi S, Amini M and Sabzi M. Synthesis and characterization of hydroxypropyl methylcellulose-g-poly (acrylamide)/LAPONITE® RD nanocomposites as novel magnetic-and pH-sensitive carriers for controlled drug release. *RSC Advances*. 2015;5:44516-44523.

218. Pacelli S, Paolicelli P, Moretti G, Petralito S, Di Giacomo S, Vitalone A and Casadei MA. Gellan gum methacrylate and laponite as an innovative nanocomposite hydrogel for biomedical applications. *European Polymer Journal*. 2016;77:114-123.
219. Xavier JR, Thakur T, Desai P, Jaiswal MK, Sears N, Cosgriff-Hernandez E, Kaunas R and Gaharwar AK. Bioactive nanoengineered hydrogels for bone tissue engineering: a growth-factor-free approach. *ACS nano*. 2015;9:3109-3118.
220. Gaharwar AK, Avery RK, Assmann A, Paul A, McKinley GH, Khademhosseini A and Olsen BD. Shear-thinning nanocomposite hydrogels for the treatment of hemorrhage. *ACS nano*. 2014;8:9833-9842.
221. Gaharwar AK, Kishore V, Rivera C, Bullock W, Wu CJ, Akkus O and Schmidt G. Physically Crosslinked Nanocomposites from Silicate-Crosslinked PEO: Mechanical Properties and Osteogenic Differentiation of Human Mesenchymal Stem Cells. *Macromolecular bioscience*. 2012;12:779-793.
222. Appel EA, Tibbitt MW, Webber MJ, Mattix BA, Veiseh O and Langer R. Self-assembled hydrogels utilizing polymer–nanoparticle interactions. *Nature communications*. 2015;6.
223. Timmers L, Lim SK, Hoefer IE, Arslan F, Lai RC, van Oorschot AAM, Goumans MJ, Strijder C, Sze SK, Choo A, Piek JJ, Doevendans PA, Pasterkamp G and de Kleijn DPV. Human mesenchymal stem cell-conditioned medium improves cardiac function following myocardial infarction. *Stem Cell Research*. 2011;6:206-214.
224. Khan M, Nickoloff E, Abramova T, Johnson J, Verma SK, Krishnamurthy P, Mackie AR, Vaughan E, Garikipati VN and Benedict CL. Embryonic stem cell-derived exosomes promote endogenous repair mechanisms and enhance cardiac function following myocardial infarction. *Circulation research*. 2015:CIRCRESAHA. 115.305990.
225. Yang Y, Cheng H-W, Qiu Y, Dupee D, Noonan M, Lin Y-D, Fisch S, Unno K, Sereti K-I and Liao R. MicroRNA-34a Plays a Key Role in Cardiac Repair and Regeneration Following Myocardial InfarctionNovelty and Significance. *Circulation research*. 2015;117:450-459.
226. Kai D, Wang Q-L, Wang H-J, Prabhakaran MP, Zhang Y, Tan Y-Z and Ramakrishna S. Stem cell-loaded nanofibrous patch promotes the regeneration of infarcted myocardium with functional improvement in rat model. *Acta Biomaterialia*. 2014;10:2727-2738.
227. Hastings CL, Roche ET, Ruiz-Hernandez E, Schenke-Layland K, Walsh CJ and Duffy GP. Drug and cell delivery for cardiac regeneration. *Advanced drug delivery reviews*. 2015;84:85-106.
228. Lu M, Xing H, Yang Z, Sun Y, Yang T, Zhao X, Cai C, Wang D and Ding P. Recent advances on extracellular vesicles in therapeutic delivery: Challenges, solutions, and opportunities. *European Journal of Pharmaceutics and Biopharmaceutics*. 2017;119:381-395.
229. Valadi H, Ekström K, Bossios A, Sjöstrand M, Lee JJ and Lötvall JO. Exosome-mediated transfer of mRNAs and microRNAs is a novel mechanism of genetic exchange between cells. *Nature cell biology*. 2007;9:654.
230. Armstrong JP, Holme MN and Stevens MM. Re-engineering extracellular vesicles as smart nanoscale therapeutics. *ACS nano*. 2017;11:69-83.
231. Sahoo S and Losordo DW. Exosomes and cardiac repair after myocardial infarction. *Circulation research*. 2014;114:333-344.
232. Seeger FH, Zeiher AM and Dimmeler S. MicroRNAs in stem cell function and regenerative therapy of the heart. *Arteriosclerosis, thrombosis, and vascular biology*. 2013;33:1739-1746.
233. Van der Pol E, Böing AN, Harrison P, Sturk A and Nieuwland R. Classification, functions, and clinical relevance of extracellular vesicles. *Pharmacological reviews*. 2012;64:676-705.
234. Xu J, Wu W, Zhang L, Dorset-Martin W, Morris MW, Mitchell ME and Liechty KW. The role of microRNA-146a in the pathogenesis of the diabetic wound-healing impairment: correction with mesenchymal stem cell treatment. *Diabetes*. 2012;61:2906-2912.

235. Cheng HS, Sivachandran N, Lau A, Boudreau E, Zhao JL, Baltimore D, Delgado-Olguin P, Cybulsky MI and Fish JE. MicroRNA-146 represses endothelial activation by inhibiting pro-inflammatory pathways. *EMBO molecular medicine*. 2013;5:1017-1034.
236. Ibrahim AG-E, Cheng K and Marbán E. Exosomes as critical agents of cardiac regeneration triggered by cell therapy. *Stem cell reports*. 2014;2:606-619.
237. Huang W, Tian S-S, Hang P-Z, Sun C, Guo J and Du Z-M. Combination of microRNA-21 and microRNA-146a attenuates cardiac dysfunction and apoptosis during acute myocardial infarction in mice. *Molecular Therapy-Nucleic Acids*. 2016;5.
238. Vizoso F, Eiro N, Cid S, Schneider J and Perez-Fernandez R. Mesenchymal stem cell secretome: toward cell-free therapeutic strategies in regenerative medicine. *International journal of molecular sciences*. 2017;18:1852.
239. Lötvall J, Hill AF, Hochberg F, Buzás EI, Di Vizio D, Gardiner C, Gho YS, Kurochkin IV, Mathivanan S and Quesenberry P. Minimal experimental requirements for definition of extracellular vesicles and their functions: a position statement from the International Society for Extracellular Vesicles. 2014.
240. Koppers-Lalic D, Hogenboom MM, Middeldorp JM and Pegtel DM. Virus-modified exosomes for targeted RNA delivery; a new approach in nanomedicine. *Advanced drug delivery reviews*. 2013;65:348-356.
241. Stepanova V, Jayaraman PS, Zaitsev SV, Lebedeva T, Bdeir K, Kershaw R, Holman KR, Parfyonova YV, Semina EV, Beloglazova IB, Tkachuk VA and Cines DB. Urokinase-type Plasminogen Activator (uPA) Promotes Angiogenesis by Attenuating Proline-rich Homeodomain Protein (PRH) Transcription Factor Activity and De-repressing Vascular Endothelial Growth Factor (VEGF) Receptor Expression. *The Journal of biological chemistry*. 2016;291:15029-45.
242. Montuori N and Ragno P. Role of uPA/uPAR in the modulation of angiogenesis. *Chemical immunology and allergy*. 2014;99:105-22.
243. Formiga FR, Tamayo E, Simón-Yarza T, Pelacho B, Prosper F and Blanco-Prieto MJ. Angiogenic therapy for cardiac repair based on protein delivery systems. *Heart failure reviews*. 2012;17:449-473.
244. Cochain C, Channon KM and Silvestre J-S. Angiogenesis in the infarcted myocardium. *Antioxidants & redox signaling*. 2013;18:1100-1113.
245. Awada H, Johnson N and Wang Y. *Dual Delivery of Vascular Endothelial Growth Factor and Hepatocyte Growth Factor Coacervate Displays Strong Angiogenic Effects*; 2014.
246. Schober A, Nazari-Jahantigh M, Wei Y, Bidzhekov K, Gremse F, Grommes J, Megens RT, Heyll K, Noels H and Hristov M. MicroRNA-126-5p promotes endothelial proliferation and limits atherosclerosis by suppressing Dlk1. *Nature medicine*. 2014;20:368.
247. Jakob P, Doerries C, Briand S, Mocharla P, Kränkel N, Besler C, Mueller M, Manes C, Templin C and Baltes C. Loss of angiomiR-126 and 130a in angiogenic early outgrowth cells from patients with chronic heart failure: role for impaired in vivo neovascularization and cardiac repair capacity. *Circulation*. 2012:CIRCULATIONAHA. 112.093906.
248. Lucas T, Bonauer A and Dimmeler S. RNA therapeutics in cardiovascular disease. *Circulation research*. 2018;123:205-220.
249. Frangogiannis NG. The inflammatory response in myocardial injury, repair, and remodelling. *Nature Reviews Cardiology*. 2014;11:255.
250. Harada M, Qin Y, Takano H, Minamino T, Zou Y, Toko H, Ohtsuka M, Matsuura K, Sano M and Nishi J-i. G-CSF prevents cardiac remodeling after myocardial infarction by activating the Jak-Stat pathway in cardiomyocytes. *Nature medicine*. 2005;11:305.
251. Srinivas G, Anversa P and Frishman WH. Cytokines and myocardial regeneration: a novel treatment option for acute myocardial infarction. *Cardiology in review*. 2009;17:1-9.

252. Tong Z, Jiang B, Wu Y, Liu Y, Li Y, Gao M, Jiang Y, Lv Q and Xiao X. MiR-21 protected cardiomyocytes against doxorubicin-induced apoptosis by targeting BTG2. *International journal of molecular sciences*. 2015;16:14511-14525.
253. Huang Z, Wu S, Kong F, Cai X, Ye B, Shan P and Huang W. Micro RNA-21 protects against cardiac hypoxia/reoxygenation injury by inhibiting excessive autophagy in H9c2 cells via the Akt/mTOR pathway. *Journal of cellular and molecular medicine*. 2017;21:467-474.
254. Xiao X, Lu Z, Lin V, May A, Shaw DH, Wang Z, Che B, Tran K, Du H and Shaw PX. MicroRNA miR-24-3p Reduces Apoptosis and Regulates Keap1-Nrf2 Pathway in Mouse Cardiomyocytes Responding to Ischemia/Reperfusion Injury. *Oxidative Medicine and Cellular Longevity*. 2018;2018.
255. Seeger T, Xu Q-F, Muhly-Reinholz M, Fischer A, Kremp E-M, Zeiher AM and Dimmeler S. Inhibition of let-7 augments the recruitment of epicardial cells and improves cardiac function after myocardial infarction. *Journal of molecular and cellular cardiology*. 2016;94:145-152.
256. Frangogiannis NG, Mendoza LH, Lewallen M, Michael LH, Smith CW and Entman ML. Induction and suppression of interferon-inducible protein 10 in reperfused myocardial infarcts may regulate angiogenesis. *The FASEB Journal*. 2001;15:1428-1430.
257. Kapur SK and Katz AJ. Review of the adipose derived stem cell secretome. *Biochimie*. 2013;95:2222-2228.
258. Wang Je, Wang G, Sun Y, Wang Y, Yang Y, Yuan Y, Li Y and Liu C. In Situ formation of pH-/thermo-sensitive nanohybrids via friendly-assembly of poly (N-vinylpyrrolidone) onto LAPONITE®. *RSC Advances*. 2016;6:31816-31823.
259. Perin EC, Dohmann HF, Borojevic R, Silva SA, Sousa AL, Mesquita CT, Rossi MI, Carvalho AC, Dutra HS and Dohmann HJ. Transendocardial, autologous bone marrow cell transplantation for severe, chronic ischemic heart failure. *Circulation*. 2003;107:2294-2302.
260. Assmus B, Honold J, Schächinger V, Britten MB, Fischer-Rasokat U, Lehmann R, Teupe C, Pistorius K, Martin H and Abolmaali ND. Transcoronary transplantation of progenitor cells after myocardial infarction. *New England Journal of Medicine*. 2006;355:1222-1232.
261. Perin E, Willerson J, Pepine C, Henry T, Ellis S, Zhao D, Silva G, Lai D, Thomas J and Kronenberg M. Cardiovascular Cell Therapy Research Network (CCTRN) Effect of transendocardial delivery of autologous bone marrow mononuclear cells on functional capacity, left ventricular function, and perfusion in chronic heart failure: the FOCUS-CCTRN trial. *Jama*. 2012;307:1717-1726.
262. Mathiasen AB, Qayyum AA, Jørgensen E, Helqvist S, Fischer-Nielsen A, Kofoed KF, Haack-Sørensen M, Ekblond A and Kastrup J. Bone marrow-derived mesenchymal stromal cell treatment in patients with severe ischaemic heart failure: a randomized placebo-controlled trial (MSC-HF trial). *European heart journal*. 2015;36:1744-1753.
263. Bolli R, Chugh AR, D'Amario D, Loughran JH, Stoddard MF, Ikram S, Beache GM, Wagner SG, Leri A and Hosoda T. Cardiac stem cells in patients with ischaemic cardiomyopathy (SCIPIO): initial results of a randomised phase 1 trial. *The Lancet*. 2011;378:1847-1857.
264. Hare JM, Fishman JE, Gerstenblith G, Velazquez DLD, Zambrano JP, Suncion VY, Tracy M, Ghersin E, Johnston PV and Brinker JA. Comparison of allogeneic vs autologous bone marrow–derived mesenchymal stem cells delivered by transendocardial injection in patients with ischemic cardiomyopathy: the POSEIDON randomized trial. *Jama*. 2012;308:2369-2379.
265. Makkar RR, Smith RR, Cheng K, Malliaras K, Thomson LE, Berman D, Czer LS, Marbán L, Mendizabal A and Johnston PV. Intracoronary cardiosphere-derived cells for heart regeneration after myocardial infarction (CADUCEUS): a prospective, randomised phase 1 trial. *The Lancet*. 2012;379:895-904.
266. Bartunek J, Terzic A, Davison BA, Filippatos GS, Radovanovic S, Beleslin B, Merkely B, Musialek P, Wojakowski W and Andreka P. Cardiopoietic cell therapy for advanced ischaemic heart failure: results at 39 weeks of the prospective, randomized, double blind, sham-controlled CHART-1 clinical trial. *European heart journal*. 2016;38:648-660.

267. Wollert KC, Meyer GP, Müller-Ehmsen J, Tschöpe C, Bonarjee V, Larsen AI, May AE, Empen K, Chorianopoulos E and Tebbe U. Intracoronary autologous bone marrow cell transfer after myocardial infarction: the BOOST-2 randomised placebo-controlled clinical trial. *European heart journal*. 2017;38:2936-2943.
268. Hare JM, Traverse JH, Henry TD, Dib N, Strumpf RK, Schulman SP, Gerstenblith G, DeMaria AN, Denktas AE and Gammon RS. A randomized, double-blind, placebo-controlled, dose-escalation study of intravenous adult human mesenchymal stem cells (prochymal) after acute myocardial infarction. *Journal of the American College of Cardiology*. 2009;54:2277-2286.
269. Butler J, Epstein SE, Greene SJ, Quyyumi AA, Sikora S, Kim RJ, Anderson AS, Wilcox JE, Tankovich NI and Lipinski MJ. Intravenous allogeneic mesenchymal stem cells for non-ischemic cardiomyopathy: safety and efficacy results of a phase II-A randomized trial. *Circulation Research*. 2016:CIRCRESAHA. 116.309717.
270. Segers VF and Lee RT. Protein therapeutics for cardiac regeneration after myocardial infarction. *Journal of cardiovascular translational research*. 2010;3:469-477.
271. Sluijter JP, Condorelli G, Davidson SM, Engel FB, Ferdinandy P, Hausenloy DJ, Lecour S, Madonna R, Ovize M and Ruiz-Meana M. Novel therapeutic strategies for cardioprotection. *Pharmacology & therapeutics*. 2014;144:60-70.
272. Urbanek K, Rota M, Cascapera S, Bearzi C, Nascimbene A, De Angelis A, Hosoda T, Chimenti S, Baker M and Limana F. Cardiac stem cells possess growth factor-receptor systems that after activation regenerate the infarcted myocardium, improving ventricular function and long-term survival. *Circulation research*. 2005;97:663-673.
273. Padin-Iruegas ME, Misao Y, Davis ME, Segers VF, Esposito G, Tokunou T, Urbanek K, Hosoda T, Rota M and Anversa P. Cardiac progenitor cells and biotinylated insulin-like growth factor-1 nanofibers improve endogenous and exogenous myocardial regeneration after infarction. *Circulation*. 2009;120:876-887.
274. Kerkelä R, Karsikas S, Szabo Z, Serpi R, Magga J, Gao E, Alitalo K, Anisimov A, Sormunen R and Pietilä I. Activation of hypoxia response in endothelial cells contributes to ischemic cardioprotection. *Molecular and cellular biology*. 2013:MCB. 00432-13.
275. Carmeliet P and Jain RK. Molecular mechanisms and clinical applications of angiogenesis. *Nature*. 2011;473:298.
276. Losordo DW and Dimmeler S. Therapeutic angiogenesis and vasculogenesis for ischemic disease: part II: cell-based therapies. *Circulation*. 2004;109:2692-2697.
277. Johnson NR and Wang Y. Controlled delivery of sonic hedgehog morphogen and its potential for cardiac repair. *PloS one*. 2013;8:e63075.
278. Engel FB, Hsieh PC, Lee RT and Keating MT. FGF1/p38 MAP kinase inhibitor therapy induces cardiomyocyte mitosis, reduces scarring, and rescues function after myocardial infarction. *Proceedings of the National Academy of Sciences*. 2006;103:15546-15551.
279. Formiga FR, Pelacho B, Garbayo E, Imbuluzqueta I, Díaz-Herráez P, Abizanda G, Gavira JJ, Simón-Yarza T, Albiasu E and Tamayo E. Controlled delivery of fibroblast growth factor-1 and neuregulin-1 from biodegradable microparticles promotes cardiac repair in a rat myocardial infarction model through activation of endogenous regeneration. *Journal of Controlled Release*. 2014;173:132-139.
280. Kardami E, Detillieux K, Ma X, Jiang Z, Santiago J-J, Jimenez SK and Cattini PA. Fibroblast growth factor-2 and cardioprotection. *Heart failure reviews*. 2007;12:267-277.
281. Uchinaka A, Kawaguchi N, Mori S, Hamada Y, Miyagawa S, Saito A, Sawa Y and Matsuura N. Tissue inhibitor of metalloproteinase-1 and-3 improves cardiac function in an ischemic cardiomyopathy model rat. *Tissue Engineering Part A*. 2014;20:3073-3084.
282. Zachary I and Gliki G. Signaling transduction mechanisms mediating biological actions of the vascular endothelial growth factor family. *Cardiovascular research*. 2001;49:568-581.

283. Hellstrom M, Lindahl P, Abramsson A and Betsholtz C. Role of PDGF-B and PDGFR-beta in recruitment of vascular smooth muscle cells and pericytes during embryonic blood vessel formation in the mouse. *Development*. 1999;126:3047-3055.
284. Hsieh PC, Davis ME, Gannon J, MacGillivray C and Lee RT. Controlled delivery of PDGF-BB for myocardial protection using injectable self-assembling peptide nanofibers. *The Journal of clinical investigation*. 2006;116:237-248.
285. Gerritsen ME. HGF and VEGF: a dynamic duo. 2005.
286. Tang J-M, Wang J-N, Zhang L, Zheng F, Yang J-Y, Kong X, Guo L-Y, Chen L, Huang Y-Z and Wan Y. VEGF/SDF-1 promotes cardiac stem cell mobilization and myocardial repair in the infarcted heart. *Cardiovascular research*. 2011;91:402-411.
287. Yamaguchi J-i, Kusano KF, Masuo O, Kawamoto A, Silver M, Murasawa S, Bosch-Marce M, Masuda H, Losordo DW and Isner JM. Stromal cell–derived factor-1 effects on ex vivo expanded endothelial progenitor cell recruitment for ischemic neovascularization. *Circulation*. 2003;107:1322-1328.
288. Bromage DI, Davidson SM and Yellon DM. Stromal derived factor 1α: a chemokine that delivers a two-pronged defence of the myocardium. *Pharmacology & therapeutics*. 2014;143:305-315.
289. Penn M, Pastore J, Miller T and Aras R. SDF-1 in myocardial repair. *Gene therapy*. 2012;19:583.
290. Cai Z, Manalo DJ, Wei G, Rodriguez ER, Fox-Talbot K, Lu H, Zweier JL and Semenza GL. Hearts from rodents exposed to intermittent hypoxia or erythropoietin are protected against ischemia-reperfusion injury. *Circulation*. 2003;108:79-85.
291. Fiordaliso F, Chimenti S, Staszewsky L, Bai A, Carlo E, Cuccovillo I, Doni M, Mengozzi M, Tonelli R and Ghezzi P. A nonerythropoietic derivative of erythropoietin protects the myocardium from ischemia–reperfusion injury. *Proceedings of the National Academy of Sciences*. 2005;102:2046-2051.
292. Moon C, Krawczyk M, Ahn D, Ahmet I, Paik D, Lakatta EG and Talan MI. Erythropoietin reduces myocardial infarction and left ventricular functional decline after coronary artery ligation in rats. *Proceedings of the National Academy of Sciences*. 2003;100:11612-11617.
293. Ye L, Du X, Xia J, Jiang P, Wang J, Fan H and Liu Z. An experimental study of recombinant human erythropoietin on the treatment of acute myocardial infarction in rats. *Zhonghua yi xue za zhi*. 2006;86:2776-2780.
294. Urao N, Okigaki M, Yamada H, Aadachi Y, Matsuno K, Matsui A, Matsunaga S, Tateishi K, Nomura T and Takahashi T. Erythropoietin-mobilized endothelial progenitors enhance reendothelialization via Akt-endothelial nitric oxide synthase activation and prevent neointimal hyperplasia. *Circulation research*. 2006;98:1405-1413.
295. Lin X, Fujita M, Kanemitsu N, Kimura Y, Tambara K, Premaratne GU, Nagasawa A, Ikeda T, Tabata Y and Komeda M. Sustained-release erythropoietin ameliorates cardiac function in infarcted rat-heart without inducing polycythemia. *Circulation Journal*. 2007;71:132-137.
296. Smart N, Risebro CA, Melville AA, Moses K, Schwartz RJ, Chien KR and Riley PR. Thymosin β4 induces adult epicardial progenitor mobilization and neovascularization. *Nature*. 2007;445:177.
297. Lemmens K, Doggen K and De Keulenaer GW. Role of neuregulin-1/ErbB signaling in cardiovascular physiology and disease: implications for therapy of heart failure. *Circulation*. 2007;116:954-960.
298. Liu X, Gu X, Li Z, Li X, Li H, Chang J, Chen P, Jin J, Xi B and Chen D. Neuregulin-1/erbB-activation improves cardiac function and survival in models of ischemic, dilated, and viral cardiomyopathy. *Journal of the American College of Cardiology*. 2006;48:1438-1447.
299. Bersell K, Arab S, Haring B and Kühn B. Neuregulin1/ErbB4 signaling induces cardiomyocyte proliferation and repair of heart injury. *Cell*. 2009;138:257-270.
300. Galindo CL, Ryzhov S and Sawyer DB. Neuregulin as a heart failure therapy and mediator of reverse remodeling. *Current heart failure reports*. 2014;11:40-49.

301. Ikonomidis JS, Hendrick JW, Parkhurst AM, Herron AR, Escobar PG, Dowdy KB, Stroud RE, Hapke E, Zile MR and Spinale FG. Accelerated LV remodeling after myocardial infarction in TIMP-1-deficient mice: effects of exogenous MMP inhibition. *American Journal of Physiology-Heart and Circulatory Physiology*. 2005;288:H149-H158.
302. Roten L, Nemoto S, Simsic J, Coker ML, Rao V, Baicu S, Defreyte G, Soloway PJ, Zile MR and Spinale FG. Effects of gene deletion of the tissue inhibitor of the matrix metalloproteinase-type 1 (TIMP-1) on left ventricular geometry and function in mice. *Journal of molecular and cellular cardiology*. 2000;32:109-120.
303. Fedak PW, Altamentova SM, Weisel RD, Nili N, Ohno N, Verma S, Lee T-YJ, Kiani C, Mickle DA and Strauss BH. Matrix remodeling in experimental and human heart failure: a possible regulatory role for TIMP-3. *American Journal of Physiology-Heart and Circulatory Physiology*. 2003;284:H626-H634.
304. Fedak PW, Smookler DS, Kassiri Z, Ohno N, Leco KJ, Verma S, Mickle DA, Watson KL, Hojilla CV and Cruz W. TIMP-3 deficiency leads to dilated cardiomyopathy. *Circulation*. 2004;110:2401-2409.
305. Kassiri Z, Defamie V, Hariri M, Oudit GY, Anthwal S, Dawood F, Liu P and Khokha R. Simultaneous transforming growth factor β-tumor necrosis factor activation and cross-talk cause aberrant remodeling response and myocardial fibrosis in Timp3-deficient heart. *Journal of Biological Chemistry*. 2009;284:29893-29904.
306. Krishnamurthy P, Rajasingh J, Lambers E, Qin G, Losordo DW and Kishore R. IL-10 inhibits inflammation and attenuates left ventricular remodeling after myocardial infarction via activation of STAT3 and suppression of HuR. *Circulation research*. 2009;104:e9-e18.
307. Manukyan MC, Alvernaz CH, Poynter JA, Wang Y, Brewster BD, Weil BR, Abarbanell AM, Herrmann JL, Crowe BJ and Keck AC. Interleukin-10 protects the ischemic heart from reperfusion injury via the STAT3 pathway. *Surgery*. 2011;150:231-239.
308. Murakami M and Simons M. Fibroblast growth factor regulation of neovascularization. *Current opinion in hematology*. 2008;15:215.
309. Christia P and Frangogiannis NG. Targeting inflammatory pathways in myocardial infarction. *European journal of clinical investigation*. 2013;43:986-995.
310. Li R-C, Tao J, Guo Y-B, Wu H-D, Liu R-F, Bai Y, Lv Z-Z, Luo G-Z, Li L-L and Wang M. In vivo suppression of microRNA-24 prevents the transition toward decompensated hypertrophy in aortic-constricted mice. *Circulation research*. 2013;112:601-605.
311. Qian L, Van Laake LW, Huang Y, Liu S, Wendland MF and Srivastava D. miR-24 inhibits apoptosis and represses Bim in mouse cardiomyocytes. *Journal of Experimental Medicine*. 2011;208:549-560.
312. Aurora AB, Mahmoud AI, Luo X, Johnson BA, van Rooij E, Matsuzaki S, Humphries KM, Hill JA, Bassel-Duby R and Sadek HA. MicroRNA-214 protects the mouse heart from ischemic injury by controlling Ca 2+ overload and cell death. *The Journal of clinical investigation*. 2012;122.
313. van Balkom BW, De Jong OG, Smits M, Brummelman J, den Ouden K, de Bree PM, van Eijndhoven MA, Pegtel DM, Stoorvogel W and Würdinger T. Endothelial cells require miR-214 to secrete exosomes that suppress senescence and induce angiogenesis in human and mouse endothelial cells. *Blood*. 2013:blood-2013-02-478925.
314. Hu S, Huang M, Li Z, Jia F, Ghosh Z, Lijkwan MA, Fasanaro P, Sun N, Wang X and Martelli F. MicroRNA-210 as a novel therapy for treatment of ischemic heart disease. *Circulation*. 2010;122:S124-S131.
315. Barile L, Lionetti V, Cervio E, Matteucci M, Gherghiceanu M, Popescu LM, Torre T, Siclari F, Moccetti T and Vassalli G. Extracellular vesicles from human cardiac progenitor cells inhibit cardiomyocyte apoptosis and improve cardiac function after myocardial infarction. *Cardiovascular research*. 2014;103:530-541.
316. Mocharla P, Briand S, Giannotti G, Dörries C, Jakob P, Paneni F, Lüscher T and Landmesser U. AngiomiR-126 expression and secretion from circulating CD34+ and CD14+ PBMCs: role for proangiogenic effects and alterations in type 2 diabetics. *Blood*. 2013;121:226-236.

317. Katare R, Riu F, Mitchell K, Gubernator M, Campagnolo P, Cui Y, Fortunato O, Avolio E, Cesselli D and Beltrami AP. Transplantation of human pericyte progenitor cells improves the repair of infarcted heart through activation of an angiogenic program involving micro-RNA-132. *Circulation research*. 2011:CIRCRESAHA. 111.251546.
318. Shapiro P. Ras-MAP kinase signaling pathways and control of cell proliferation: relevance to cancer therapy. *Critical reviews in clinical laboratory sciences*. 2002;39:285-330.
319. Yu B, Gong M, Wang Y, Millard RW, Pasha Z, Yang Y, Ashraf M and Xu M. Cardiomyocyte protection by GATA-4 gene engineered mesenchymal stem cells is partially mediated by translocation of miR-221 in microvesicles. *PloS one*. 2013;8:e73304.
320. Qin Y, Yu Y, Dong H, Bian X, Guo X and Dong S. MicroRNA 21 inhibits left ventricular remodeling in the early phase of rat model with ischemia-reperfusion injury by suppressing cell apoptosis. *International journal of medical sciences*. 2012;9:413.

APPENDIX A: Figures

Chapter 1: No Figures

Chapter 2: Figure 2.1

Chapter 3: Figures 3.1-3.4 and Figures S3.1-S3.3

Chapter 4: Figures 4.1-4.5 and Figures S4.1- S4.10

Chapter 5: Figure 5.1-5.5 and Figure S5.1

Chapter 6: No Figures

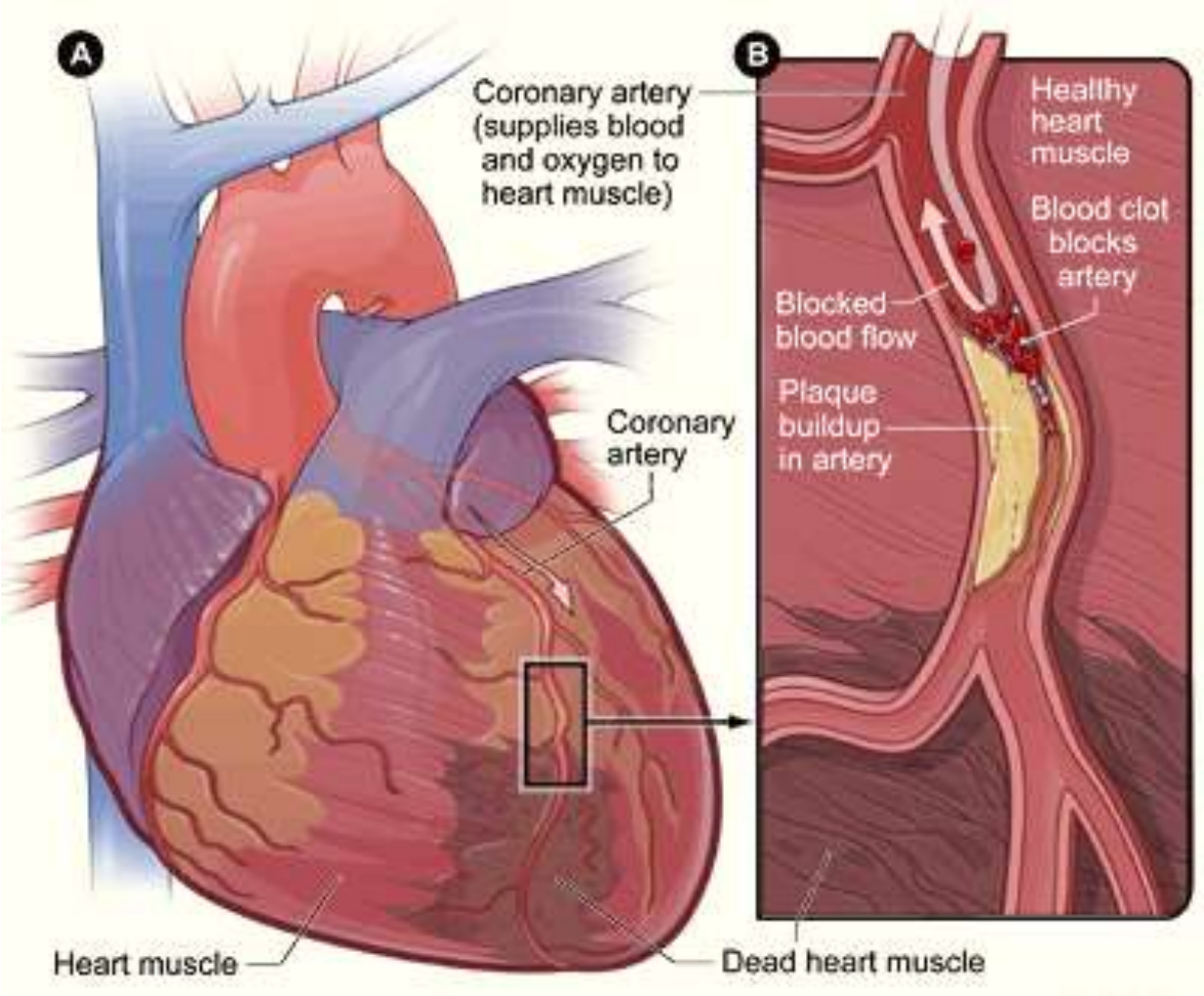

Figure 2.1 Schematic diagram of an acute myocardial infarction.

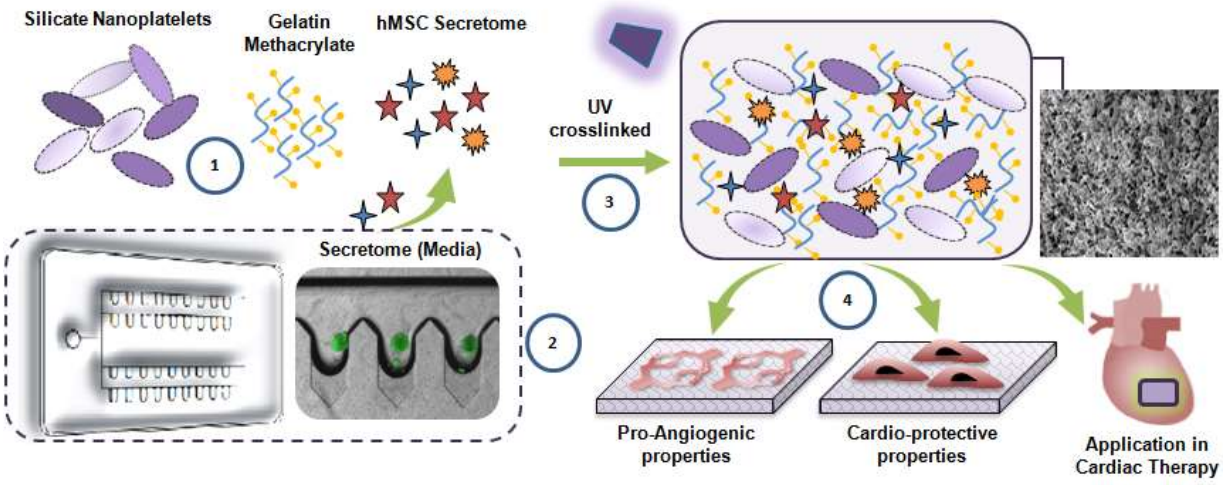

Figure 3.1 Development of hMSC secretome-loaded hydrogel treatment schematic. 1) Photo-crosslinkable nanocomposite hydrogels comprised of silicate nanoplatelets, gelatin methacrylate and hMSC derived growth factors (secretome). 2) Microbioreactor with deep concave wells to harness hMSC secretome. 3) Photo-crosslinked nanocomposite hydrogel encapsulating secretome. 4) The hydrogel can promote endothelial proliferation, migration and significantly attenuate cardiac cell apoptosis under stressed (hypoxic and serum starved) conditions.

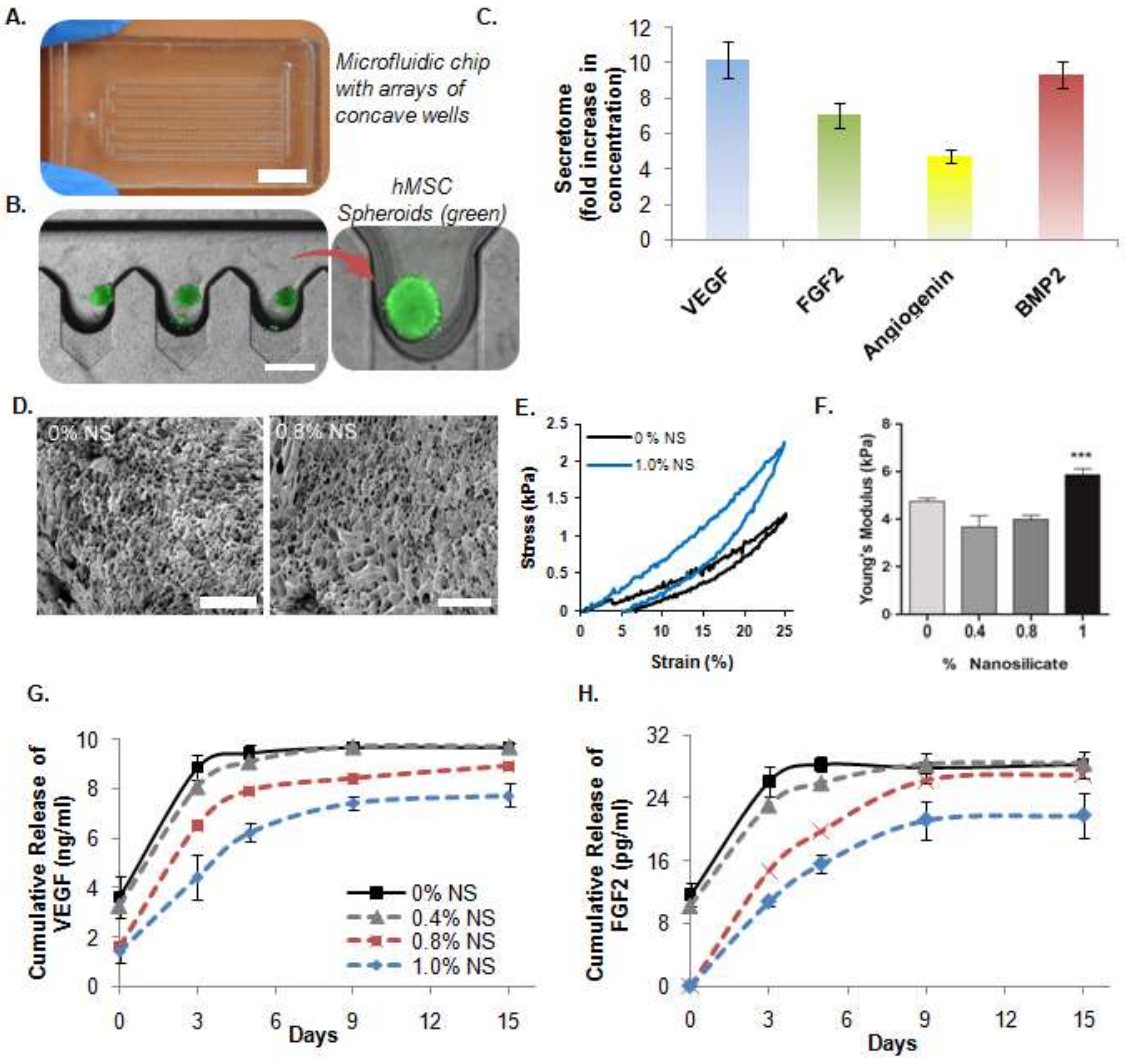

Figure 3.2 *In vitro* characterization of the developed nanocomposite hydrogel carrying secretome of hMSC spheroids. A) Microfluidic chip with concave microwell array. Optical microscopy image of the microfluidic chip (Scale bar: 1mm). B) hMSC spheroid formation in the deep concave microwell arrayed microfluidic chip. Scale bar indicate 500 μm. C) After 48h, the conditioned media (secretome) was harvested from the microfluidic chip leaving behind the spheroids. hMSC spheroids secreted higher concentration of growth factors (VEGF, FGF, Angiogenin and BMP2) compared to 2D culture in plates as quantified by ELISA. D) Scanning electron microscopic images of 0% and 0.8% NS hydrogels demonstrate the porous microstructures of the hydrogel. Scale bar: 100 μm E-F) Cyclic stress versus strain curves and corresponding compressive modulus of the hydrogel showing the effect of Laponite concentration over the mechanical properties G-H) Effect of NS concentration on release of VEGF and FGF2 growth factors from different NS hydrogel formulations over time. *** = P<0.001, n=3.

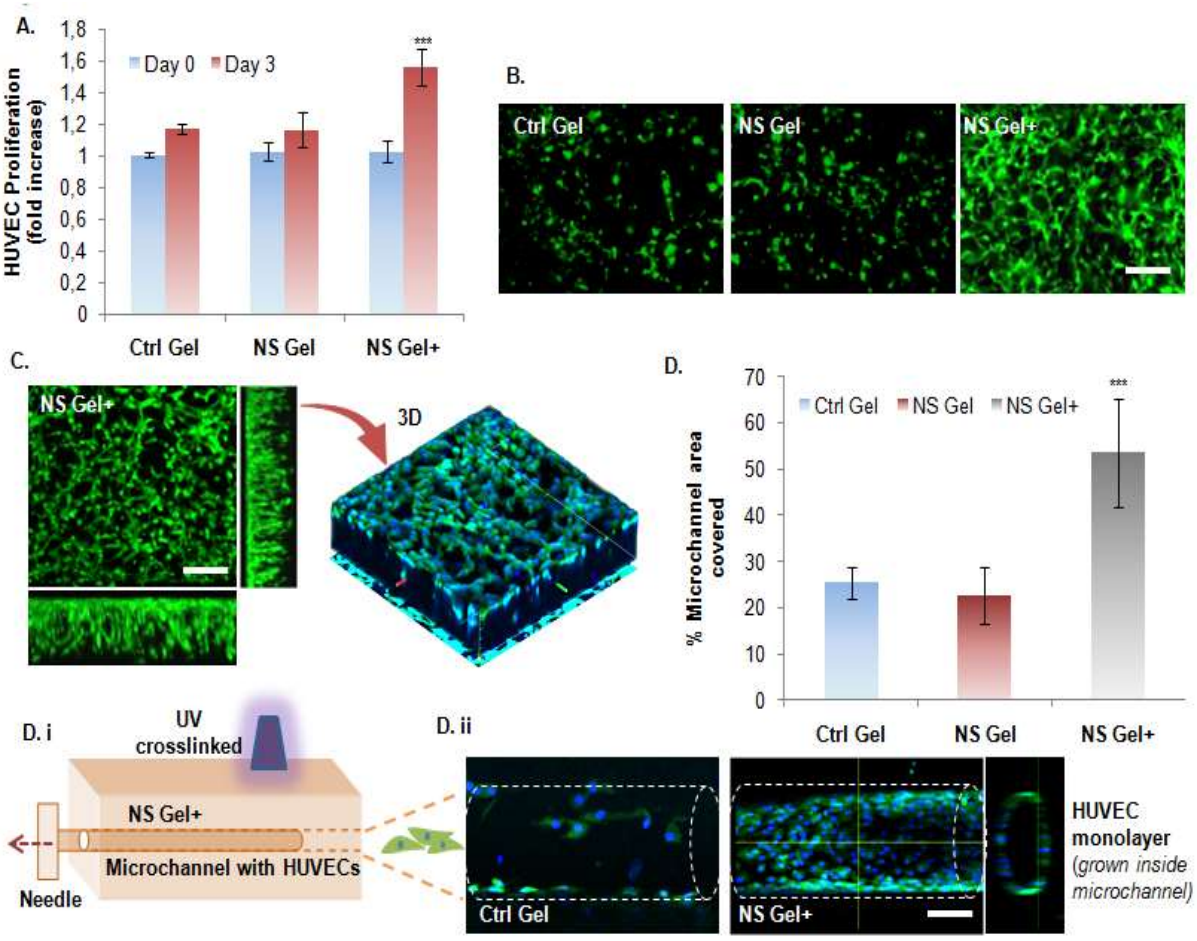

Figure 3.3 Angiogenic potential the developed bioactive nanocomposite hydrogel. A) Proliferation of HUVECs in 3D hydrogels with (NS Gel+) and without secretome (NS Gel). As a control group, hydrogel without NS (Ctrl Gel) was used. Cell proliferation was detected by MTS colorimetric assay while data (n=3) presented in the graph were normalized with data from the control gel group at Day 0. NS+ Gel group showed significantly higher proliferation compared to other groups. B) Representative photomicrographs of calcein stained HUVECs encapsulated in each hydrogel group. Importantly, HUVEC in NS+ Gel group also demonstrated highly branched tube-like structures which were absent in other groups. C) Confocal fluorescence microscope image of HUVECs grown in 3D NS+ hydrogel, with blue nuclei stained with DAPI. The image confirms proliferation of the HUVEC all throughout the thickness of the hydrogel with highly branched tube-like microstructures. D) i-ii. HUVEC adhesion and migration assay inside microchannels fabricated from the different hydrogel groups. The microchannel was made by needle (200 μm) insertions and photocrosslinking. Data are expressed as mean value± Standard Deviation (SD). *** = P<0.001 compared to Control Gel, n=3. Scale bars: 100μm.

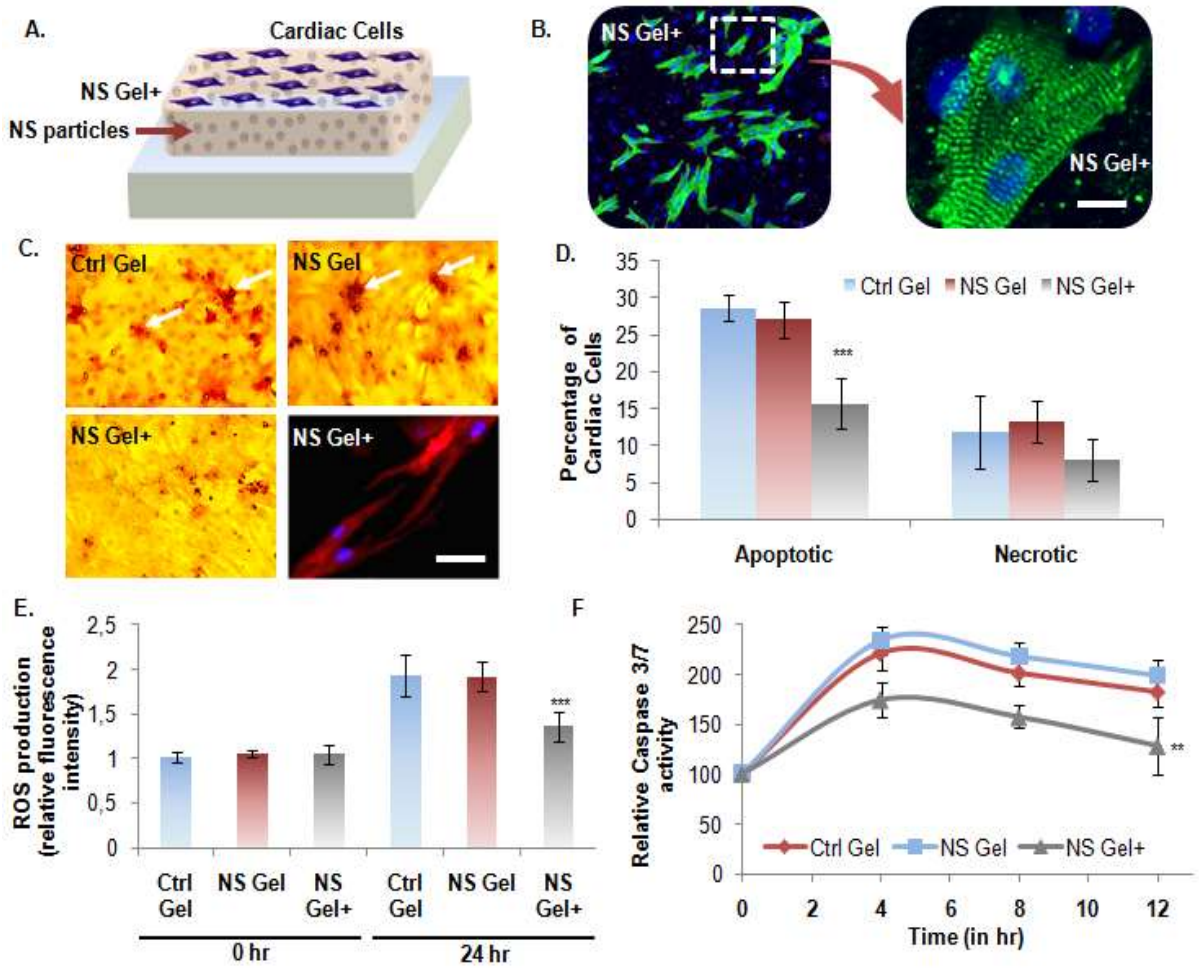

Figure 3.4 Cardioprotective nature of the developed bioactive nanocomposite hydrogel. A) Schematic of culturing neonatal CMs on nanocomposite hydrogels. B) Fluorescence microscope images of CMs grown in standard condition on NS+ hydrogel. The cells were immunostained with cardiac specific marker, sarcomeric α-actinin, and nuclei with DAPI (Scale bar: 10μm). C-D) Apoptosis assay on CMs under stressed condition by Deadend Colorimetric TUNEL assay. (Scale: bar: 50μm). Number of apoptotic cells per well was quantified and represented in graph as percentage apoptotic cells per group. MTS assay was also performed to quantify the percentage of necrotic cells. The picture on lower right panel shows CM cells grown on the NS+ hydrogel under the above mentioned stressed condition still retained expression of intact cardiac marker, sarcomeric α-actinin. E) Detection of ROS-induced apoptosis. Intracellular ROS quantified in terms of relative fluorescence intensities normalized to Ctrl gel value at 0h. F-G) To investigate the anti-apoptotic effects of the NS+ hydrogel, Caspase-3/7 activity was measured as an early indicator of apoptosis using Apo-ONE® homogeneous caspase-3/7 assay Kit (Promega, Madison, WI, USA). Data are expressed as mean value± Standard Deviation (SD). *** = P<0.001 and ** = P<0.01 compared to Control Gel, n=3.

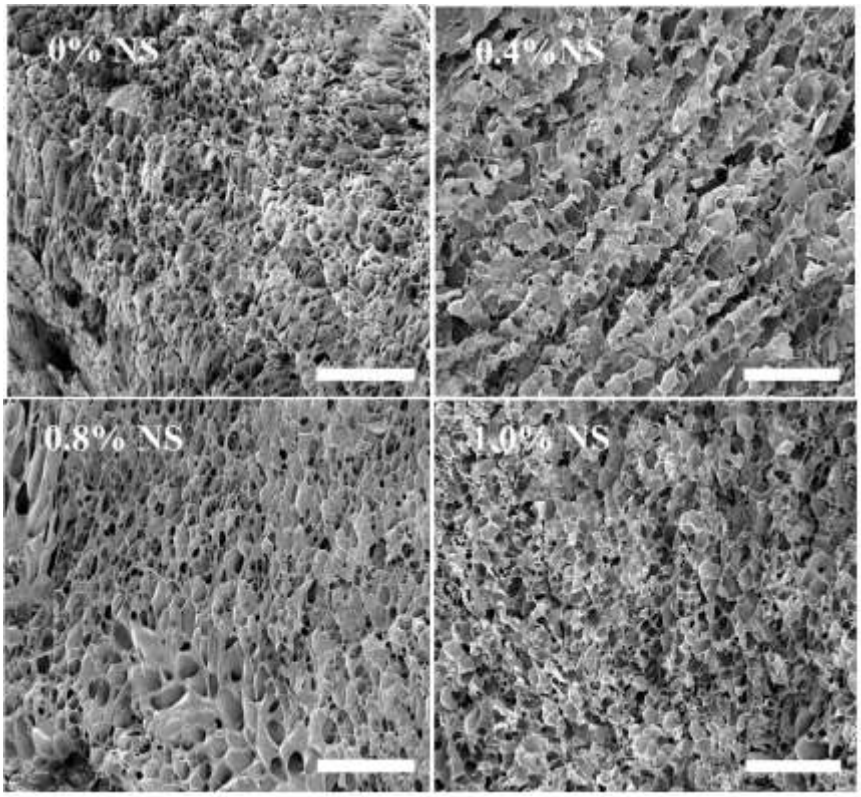

Figure S3.1. SEM images of Gel-MA nanocomposite hydrogels having different concentration of Laponite Scale bar: 100 μm.

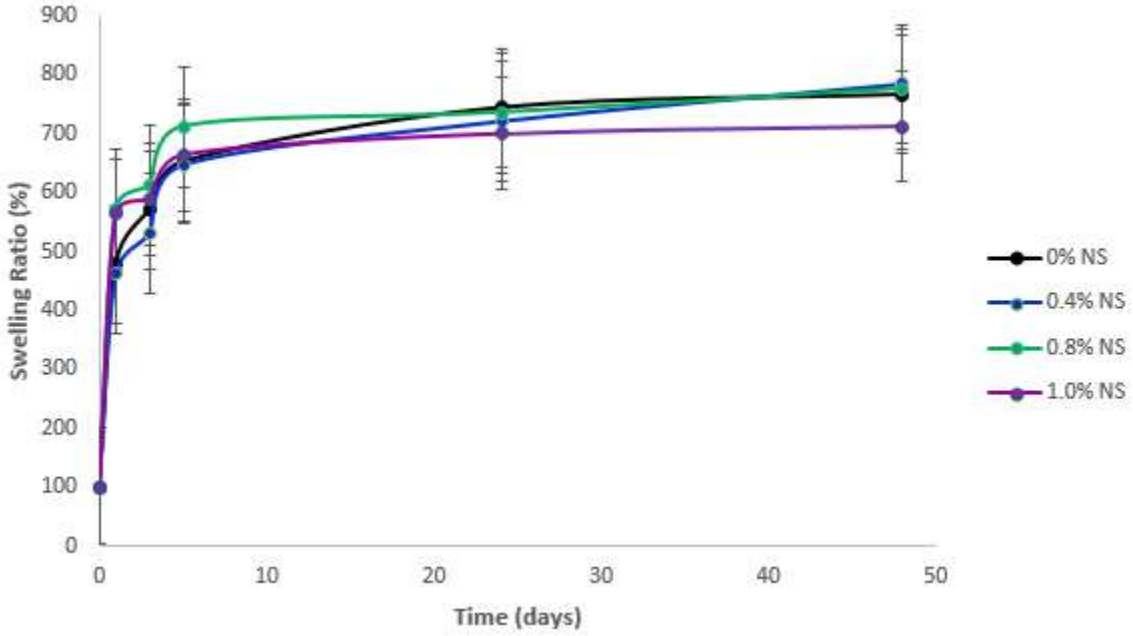

Figure S3.2. Swelling equilibrium profiles of the different nanocomposite hydrogels over time. The study was carried out in PBS (pH 7.4) n=4.

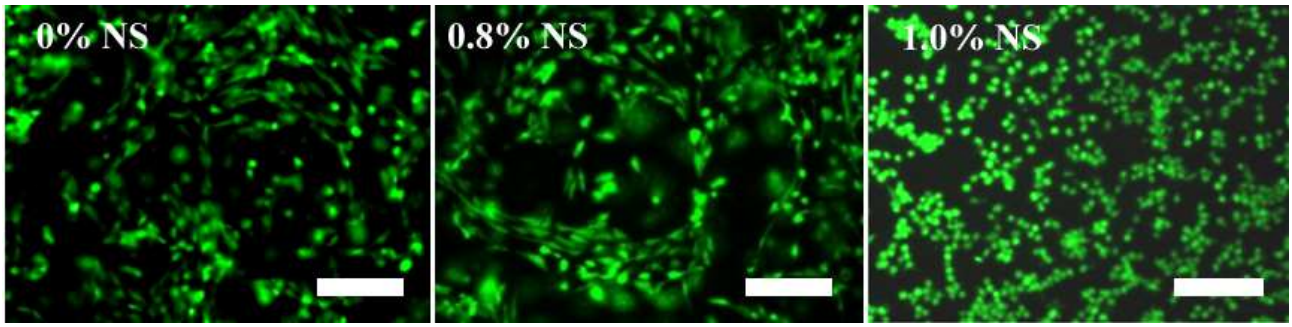

Figure S3.3 Calcein staining of HUVECs in 3D GelMA nanocomposite hydrogels having different concentration of Laponite. Scale bar: 100 µm

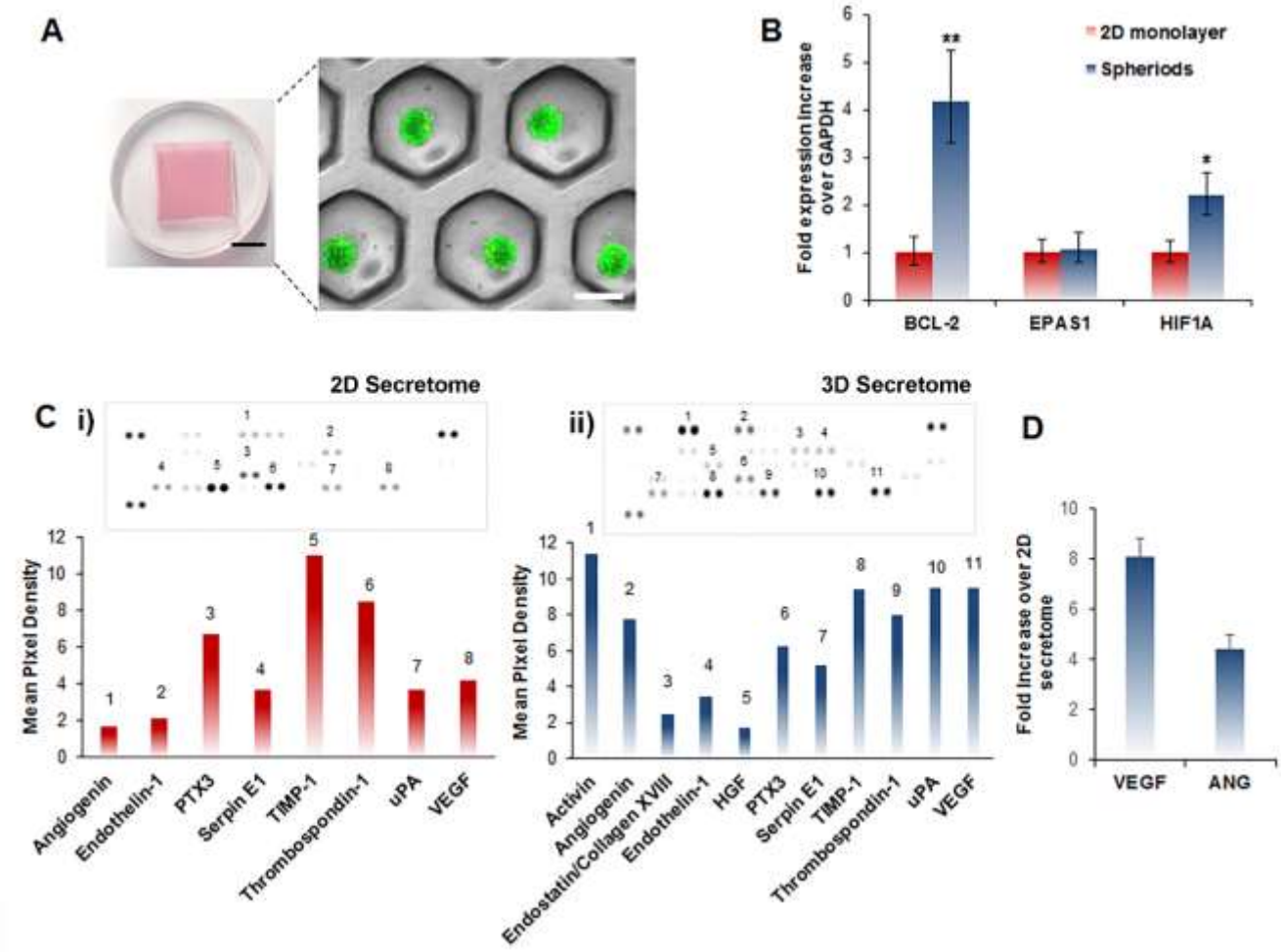

Figure 4.1 Preparation and characterization of secretome isolated from both hASC spheroids (3D secretome) and hASC monolayer (2D secretome). **A)** Microwell culture dish used for hASCs spheroid culture and characteristic fluorescent microscopy image of resultant spheroids superimposed on an equivalent bright-field image. Calcein and ethidium bromide was used to visualize live and dead cells, respectively. (Black scale bar: 1 mm, white scale bar: 200 µm). **B)** Gene expression analysis of hASCs culture in a traditional monolayer and in spheroids using qPCR. The data in the graph represents fold changes in the expression levels of anti-apoptotic and stress related genes between the two groups. Data are expressed as mean value ± standard deviation * $p<0.05$, ** $p<0.01$, ($n = 3$). **C) i)** Human angiogenic dot blot array of 2D hASCs monolayer derived secretome and corresponding quantification of the mean pixel density quantified using ImageJ software. **ii)** Human angiogenic dot blot array of hASCs spheroid-derived secretome, and the corresponding quantification of the mean pixel density quantified using ImageJ software. The presence of key cardioprotective and angiogenic factors such as endostatin/collagen XVIII and hepatocyte growth factor (HGF) were only detected in the secretome derived from hASCs spheroid. **D)** ELISA quantification of the concentration of VEGF and angiogenin (ANG), present in the secretome. The data are represented as the fold increase in growth factor concentration in the secretome derived from hASCs spheroids with respect to the secretome isolated from the monolayer hASCs culture. Data are expressed as mean value ± standard deviation (n=3).

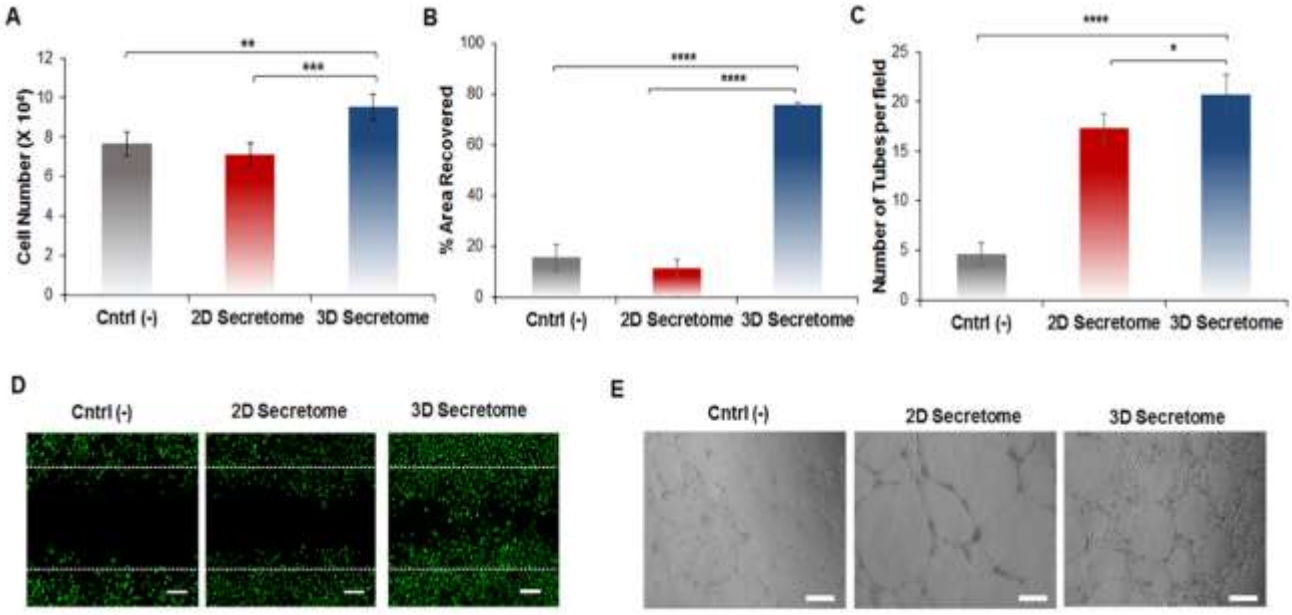

Figure 4.2 *In vitro* superior angiogenic potential of hASCs spheroid-derived secretome. **A)** The proliferation of HUVECs was carried out in endothelial growth medium without VEGF and hFGF-B. Cells were treated with hASCs monolayer derived secretome (2D secretome), and hASCs spheroid-derived secretome (3D secretome) for 24 hours. As control group (Cntrl (-)), cells were cultured without growth factors. HUVECs number was determined using an MTS assay. Data are reported as mean ± standard deviation (n=5). **B)** Quantification of the % of area covered by HUVECs after 16 hours in the different groups. The analysis was carried out by quantifying the area occupied by the HUVECs within the wound area post 16hour incubation using ImageJ software. **C)** Quantification of complete tube formation after 24 hours in the different groups. Data are expressed as mean of tubes formed in each group ± standard deviation (n=3). * $p<0.05$, ** $p<0.01$, *** $p<0.001$, **** $p<0.001$. **D)** Fluorescent images of HUVECs stained with calcein showing their migration within the scratch area in the different groups after 16 hours. Scale bar: 100 μm. Data are reported as mean ± standard deviation (n=3). **E)** Representative bright-field images of a Matrigel tube formation assay for the different groups after 10 hours. Scale bar: 200 μm.

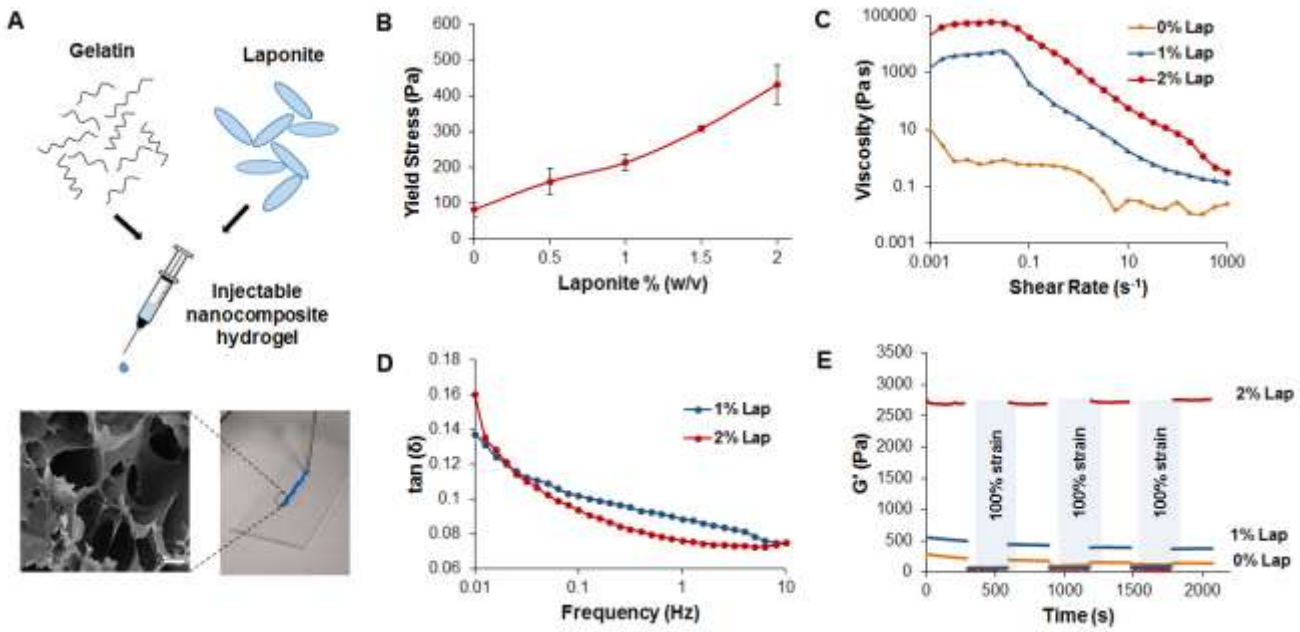

Figure 4.3 Effect of Laponite® on the rheological properties of the nanocomposite hydrogel. **A)** Schematic representation of the injectable hydrogel main components and representative image of the injectable nanocomposite hydrogel using a 22 gauge needle along with SEM image illustrating the hydrogel porosity. Scale bar: 100 µm **B)** Yield stress values of the nanocomposite hydrogel plotted as a function of the Laponite® concentration. Data are expressed as mean ± standard deviation (n=3). **C)** Viscosity curves showing an increase in the viscosity as the Laponite® concentration increases **D)** Representative Tan δ (G"/G') profiles as a function of the frequency (0.01-10 Hz) for the different system containing a different concentration of Laponite®. A decrease in the tan δ was observed for the system containing Laponite® 2% w/v, which is indicative of a higher degree of physical crosslinking. **E)** Recovery properties of the hydrogels were assessed by monitoring the storage moduli of the hydrogels while subjecting them to alternating high (100%) and low (1%) strain. Laponite® was found to greatly enhance the thixotropic behavior of the hydrogels.

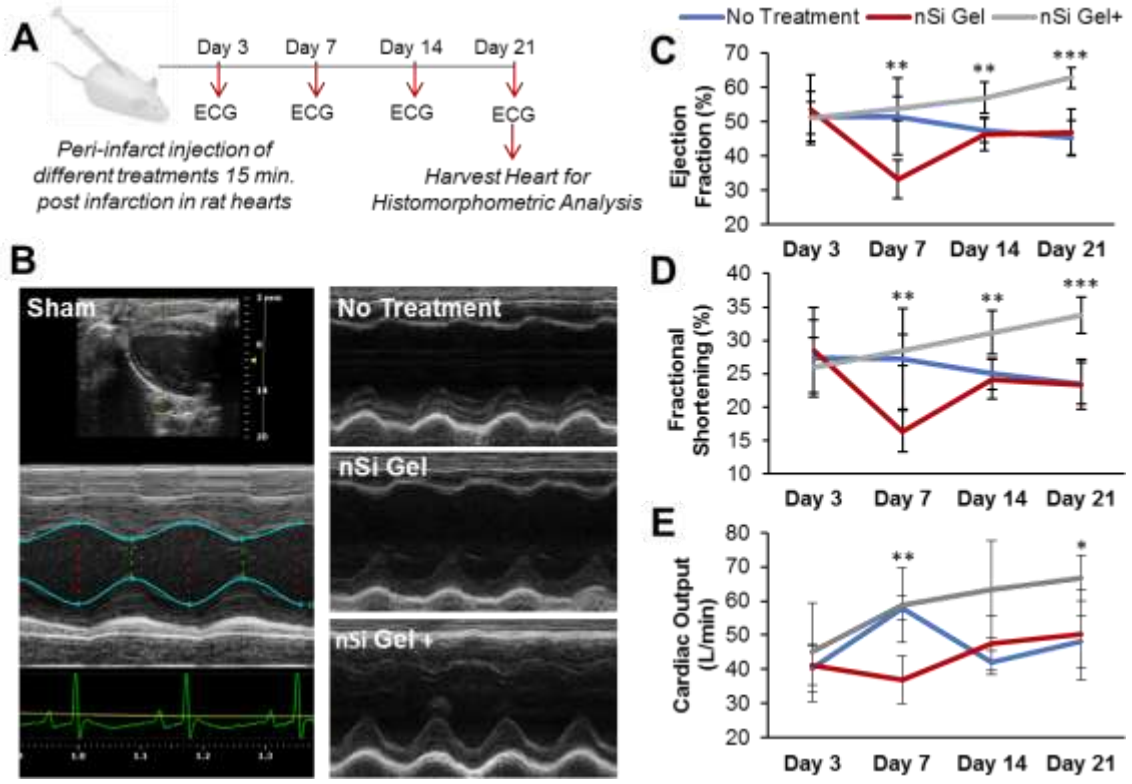

Figure 4.4 Positive effect of the secretome loaded nanocomposite hydrogel on cardiac function *in vivo*. **A)** Schematic representing the design of the study. Specifically, either phosphate buffer saline (No Treatment), the nanocomposite hydrogel (nSi Gel), or the secretome loaded nanocomposite hydrogel (nSi Gel+) were injected into the peri-infarct region of rat hearts with an induced acute myocardial infarction 15 minutes post infarction. Subsequent echocardiographs were taken at day 3, 7, 14, and 21 followed by histomorphometric studies of the rat hearts. **B)** Representative echocardiograph data for each test group used to calculate the cardiac function parameters. **C)** Calculated heart ejection fractions (EF %) at each time point. A significant increase in the nSi Gel+ group EF% was observed when compared to the nSi Gel group. **D)** Fractional shortening (FS %) calculations at each time point. The nSi Gel+ showed a substantial increase in FS% in comparison to the nSi Gel group at each time point except at day 3. **E)** Cardiac output (L/min) was monitored for each group throughout the study. The cardiac output for the nSi Gel+ group was significantly greater than the nSi Gel group on days 7 and 21. Data are expressed as mean value ± standard deviation f, * $p<0.05$, ** $p<0.01$, *** $p<0.001$, ($n = 5$).

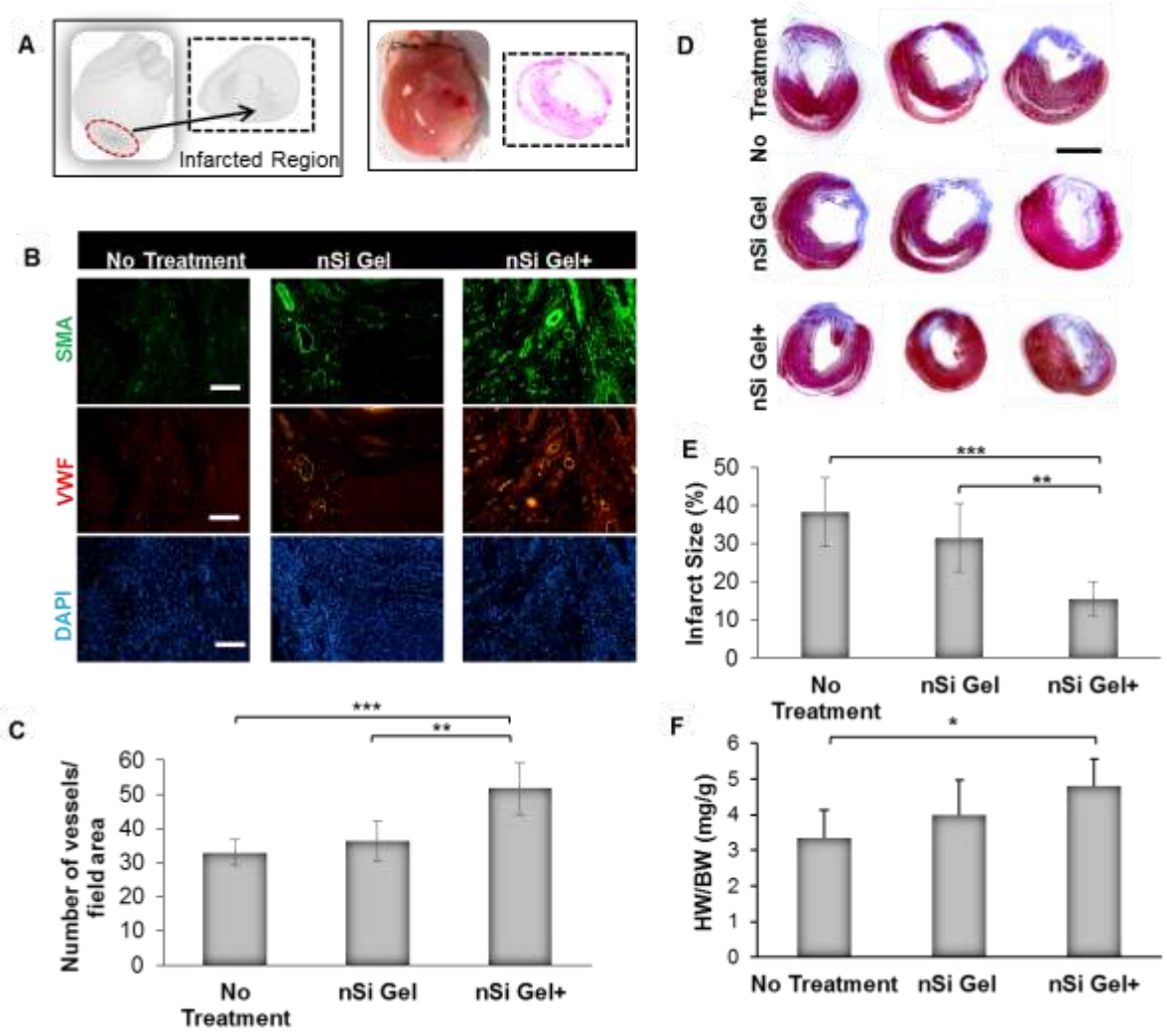

Figure 4.5 Assessment of the *in vivo* proangiogenic and scar area reduction capability of the secretome loaded nanocomposite hydrogel. **A)** An illustration (left) and image (right) of the infarcted region of the acute myocardial infarction model where either phosphate buffer saline (No Treatment), nanocomposite hydrogel (nSi Gel), or secretome loaded nanocomposite hydrogel (nSi Gel+) was injected. **B)** Representative micrographs of immunohistochemically stained sections of the peri-infarct region highlighting cell nuclei (DAPI), endothelial cells (vWF) and mural cells (SMA), 21 days post treatment injection. Scale bar: 100 µm. **C)** Quantification of vessels stained positive for vWF+ and SMA indicating a significant increase in the blood vessel density in the hearts that received the nSi Gel and nSi Gel+ treatment. **D)** Characteristic Masson's trichrome stained cross-sections of the rat hearts displaying the scar formation in each group. Scale bar: 5 mm. **E)** The percentage of the myocardium that was replaced with infarcted tissue was quantified for each test group. A significant decrease in infarct size was observed in the nSi Gel and nSi Gel+ group. **F)** The heart weight to body weight ratio (HW/BW) was calculated for each group and a significant increase in the ratio was observed in the nSi Gel+ group when compared to the control. Data expressed as mean value ± standard deviation * $p<0.05$, ** $p<0.01$, *** $p<0.001$, ($n = 5$).

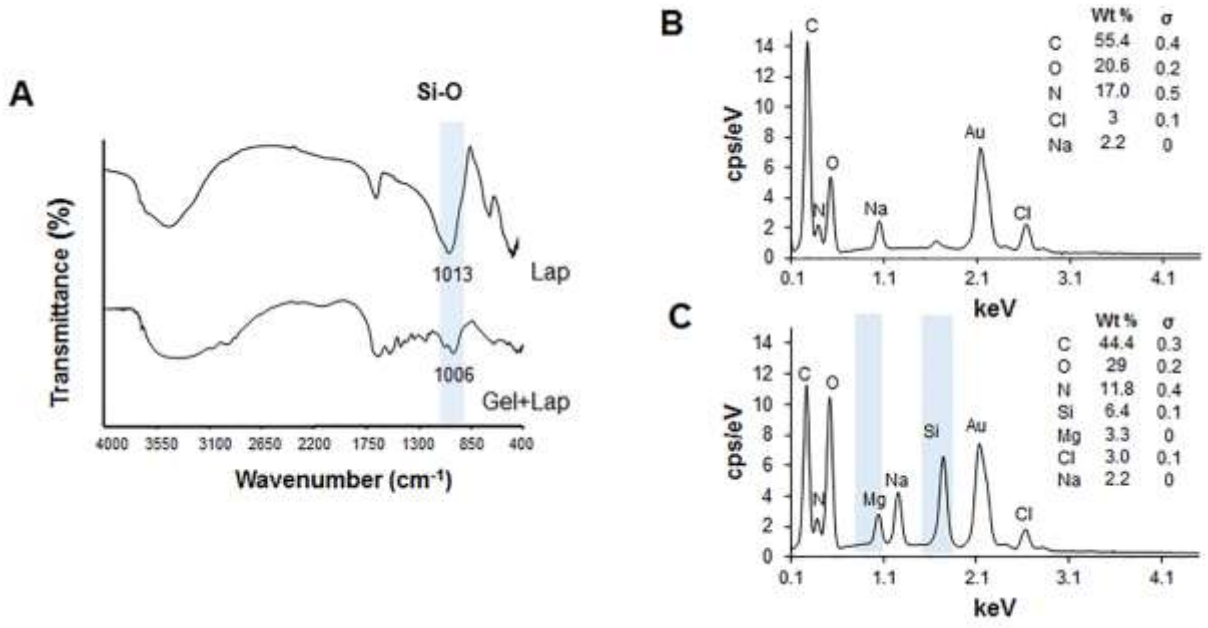

Figure S 4.1. Characterization of the injectable nanocomposite hydrogel **A)** FT-IR spectra of Laponite and the nanocomposite hydrogel confirming the gelatin Laponite interactions due to the shift observed in the stretching of the Si-O bond highlighted in blue. **B)** EDX analysis of gelatin hydrogel and **C)** nanocomposite hydrogel confirming the presence of the Laponite by the detection of Mg and Si.

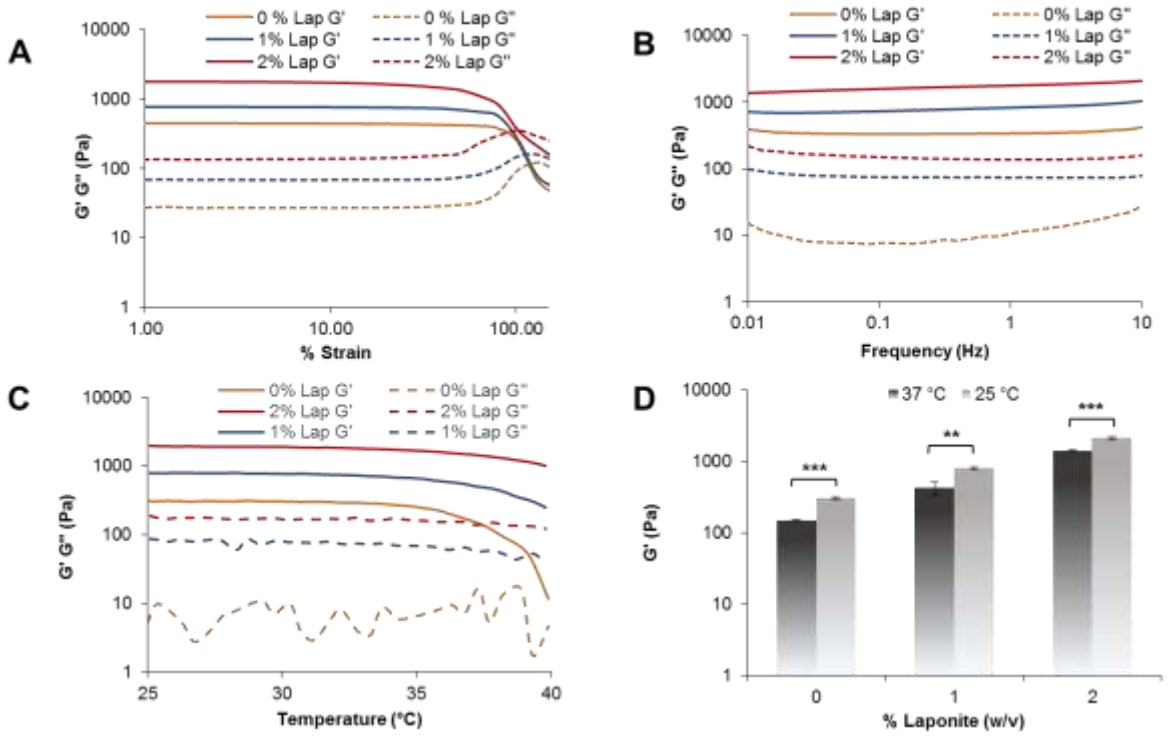

Figure S4.2. Effect of Laponite on nanocomposite hydrogel stiffness. **A)** Strain sweeps at 1 Hz to determine the linear viscoelastic region of each hydrogel. **B)** Frequency sweeps of each hydrogel obtained in the range of frequencies from 0.01 to 10 Hz at 25 °C. **C)** Temperature sweeps at 1 Hz to monitor the stiffness of the hydrogel at physiological temperatures. **D)** Storage modulus (G') of each hydrogel at 25 °C and 37 °C (n=3). Data is expressed as mean value ± st. dev., ** $p<0.01$, *** $p<0.001$.

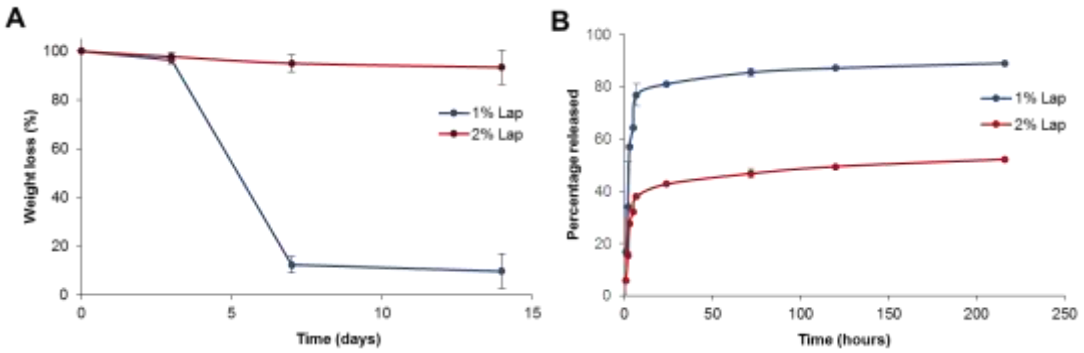

Figure S4.3. Influence of Laponite concentration on the injectable hydrogel stability and protein release. **A)** Degradation profiles of the nanocomposite hydrogels in PBS at 37 °C. **B)** Release of the model protein myoglobin from the nanocomposite hydrogel in PBS at 37 °C. Data is expressed as mean value ± st. dev. (n=5).

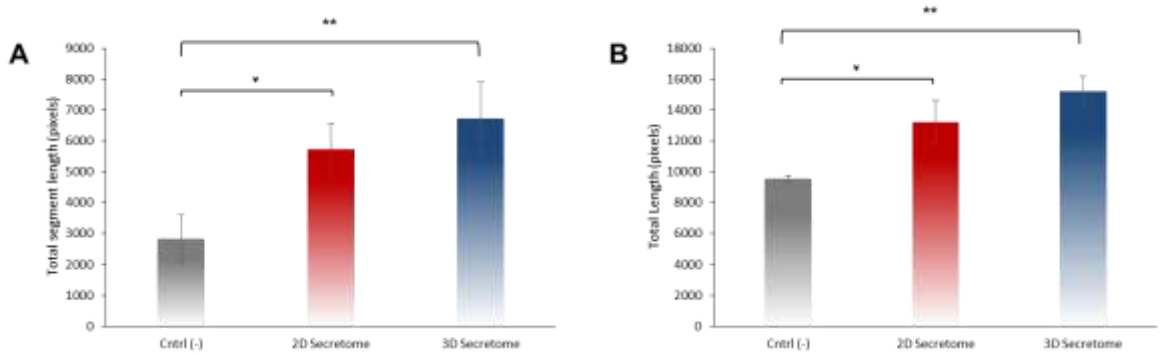

Figure S4.4. Effect of secretome on *in vitro* tube network length using tube formation assay. **A)** The total segment length of each HUVEC tube network after the addition of secretome in tube formation assay. **B)** The total length of the tube network formed during *in vitro* tube formation assay after adding secretome. Data is expressed as mean value ± st. dev. (n=3), * $p<0.05$, ** $p<0.01$.

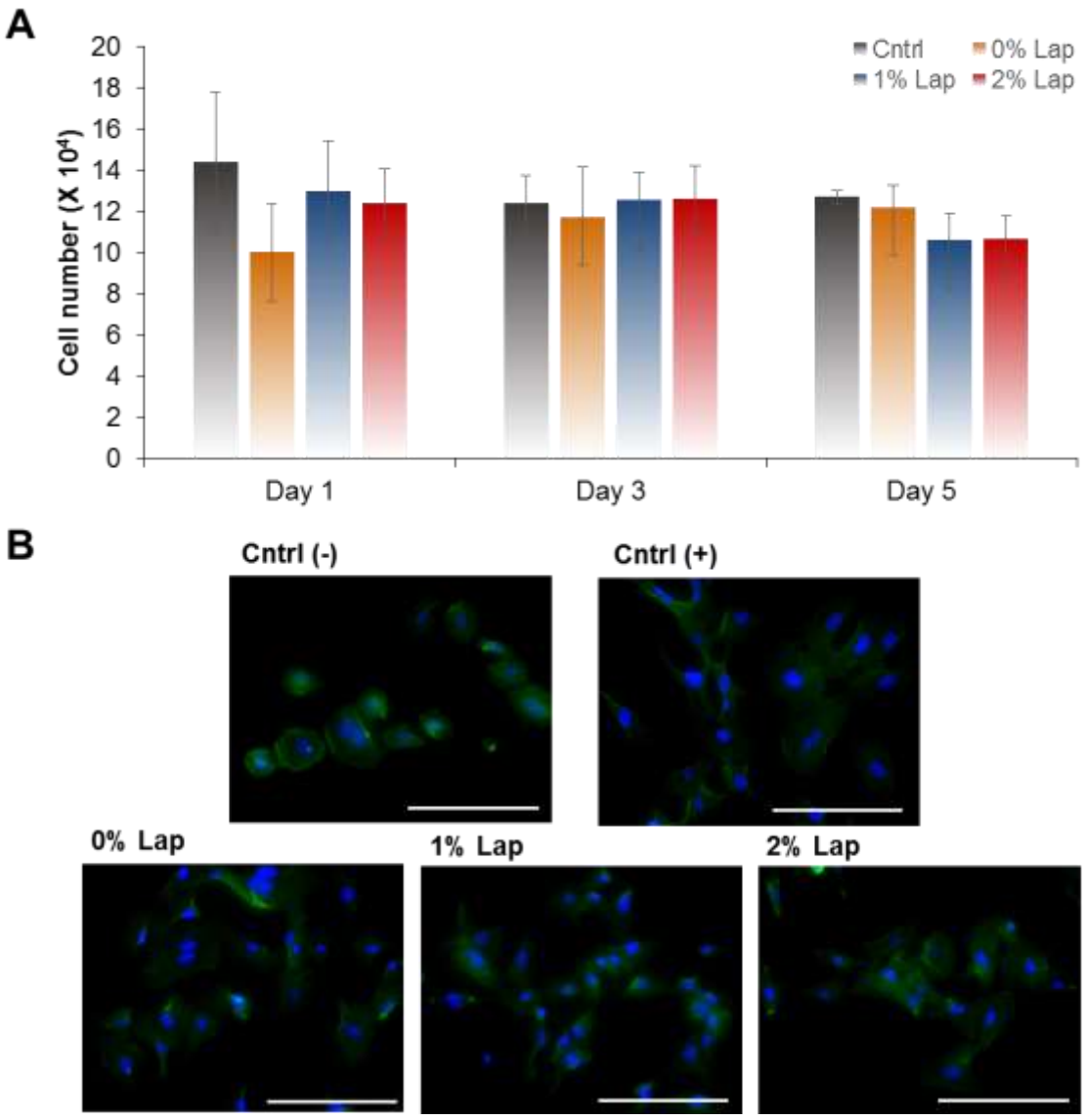

Figure S4.5. Biocompatiblity assessment of the injectable nanocomposite hydrogels **A)** Quantification of HUVECs using an MTS assay after 1 day, 3 days, and 5 days of incubation with the respective nanocomposite hydrogel. Positive control group (Cntrl) received only complete endothelial growth media. Data is expressed as mean value ± st. dev. (n=5). **B)** Immunofluorescent images of HUVECs counterstained for F-actin and nuclei after 24 hour incubation with media containing 10% of the respective nanocomposite hydrogel. Complete endothelial growth media was used as a positive control (Cntrl+) and the negative control (Cntrl-) received camptothecin (50 nM) in the media. Scale bar: 200 µm.

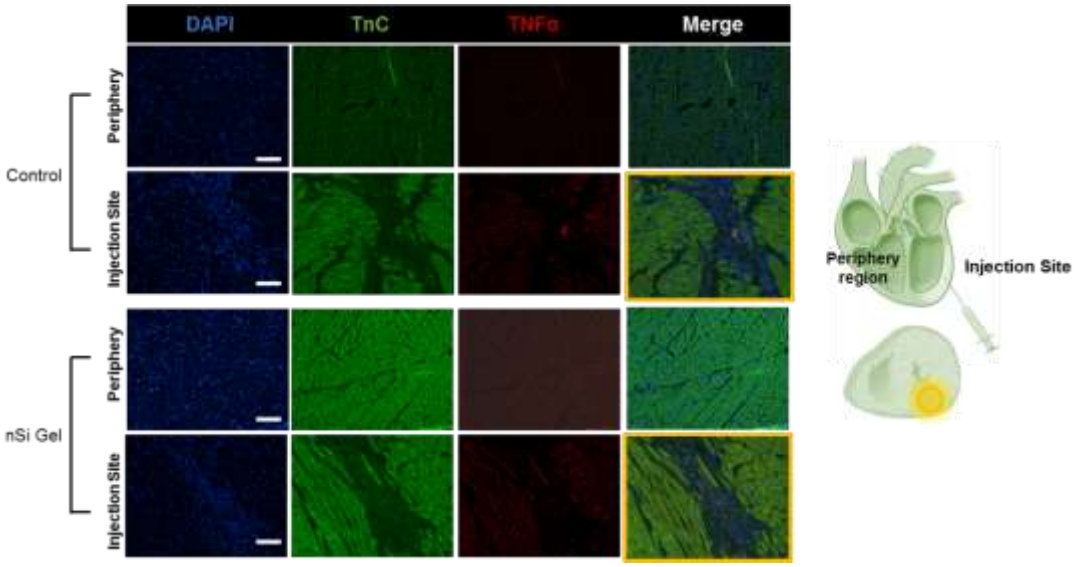

Figure S4.6. *In vivo* assessment of pro-inflammatory markers post nanocomposite hydrogel injections. Immunohistochemical analysis of the injection site and peripheral tissue of healthy rats that received either a PBS injection or a nanocomposite hydrogel injection was carried out. No visual difference in pro-inflammatory marker TNFα was seen among the regions of the two groups. Scale bar: 20 µm.

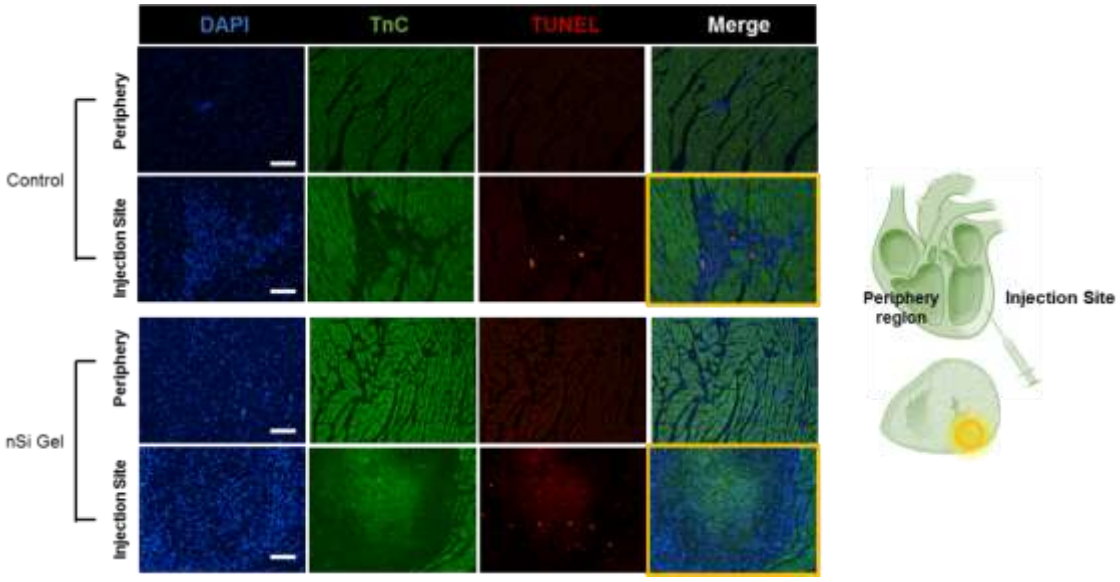

Figure S4.7. Cardiac damage assessment post *in vivo* nanocomposite hydrogel injections. Immunohistochemical analysis of the injection site and peripheral tissue of healthy rats that received either a PBS injection or a nanocomposite hydrogel injection was carried out. No visual difference in cardiac apoptotic marker TUNEL was seen among the regions of the two groups. Scale bar: 20 µm.

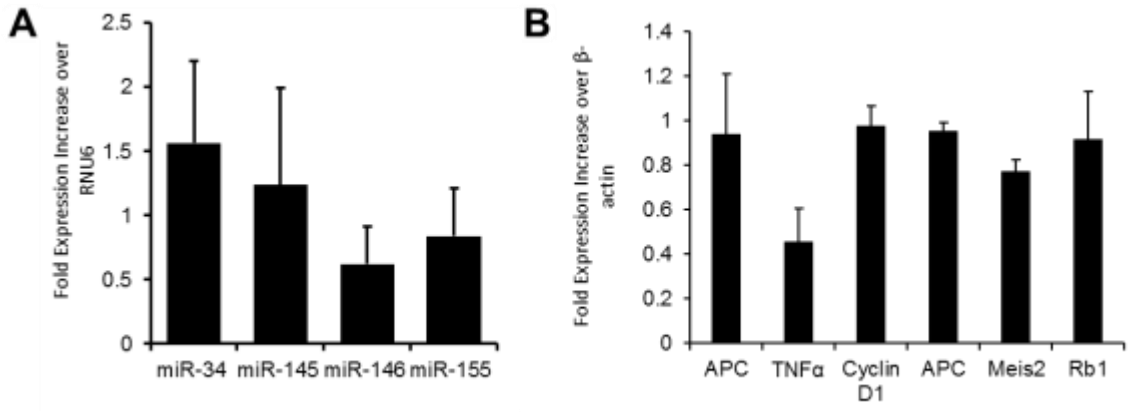

C

Gene	Primer Sequences			
APC	F	5'	TAGGAAAAGCAGCGCAGACA	3'
	R		GGACTCTGGGCTCCACTAGA	
TNFα	F	5'	ACTCCCAGAAAAGCAAGCAA	3'
	R		CGAGCAGGAATGAGAAGAGG	
Cyclin D1	F	5'	CCTGGACCGTTTCTTGTCTC	3'
	R		CCATTTGAGCTTGTTCACCA	
Rb1	F	5'	GTCTGCCAACACCCACAAAA	3'
	R		ATCCTTCGATGTCAAAGCGC	
Meis2	F	5'	TGATAACTTCTGCCACCGGT	3'
	R		GGTTGCATCATCGTGGTCTC	
miR-34a Rat	F	5'	TGGCAGTGTCTTAGCTGGTTGT	3'
miR-145 Rat	F	5'	GTCCAGTTTTCCCAGGAATCCCT	3'
miR-146a Rat	F	5'	TGAGAACTGAATTCCATGGGTT	3'
miR-155 Rat	F	5'	TTAATGCTAATTGTGATAGGGGT	3'

Figure S4.8. *In vivo* biocompatibility of the injectable nanocomposite hydrogel. Healthy rat models that either received an injection of the nanocomposite hydrogel or no treatment were tested **A)** Expression of cardiac stress and inflammatory marker specific miRNA was assessed using qPCR. The data represents the fold increase in the expression of the miRNA within animals that received the nanocomposite hydrogel injections with respect to the animals that did not. The data from each group was normalized to RNU6. No significant difference among the groups was determined. **B)** Gene expression of cardiac stress, cell cycle and inflammatory genes were quantified using qPCR. The data represents the fold increase in the gene expression within animals that received the nanocomposite hydrogel injections with respect to the animals that did not. The data from each group was normalized to GAPDH prior to the fold increase calculations. **C)** Specific primers used for each gene and miRNA. No significant difference in gene expression was detected among the groups (n=5).

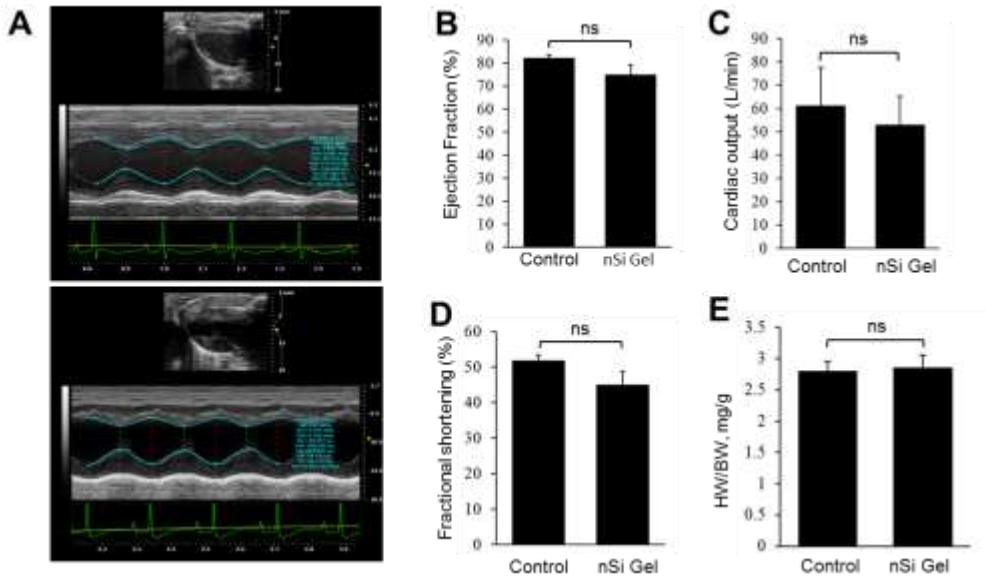

Figure S4.9. Retention of cardiac function post intramyocardial injection of nanocomposite hydrogel. Healthy rats received an intramyocardial injection of either PBS (control) or the nanocomposite hydrogel (nSi Gel) **A)** Representative echocardiograph data used to calculate the cardiac function parameters for each test group is shown. **B)** Calculated heart ejection fractions (EF%) showed no significant change among the groups. **C)** No significant change in the calculated fractional shortening (FS%) was detected **D)** Cardiac output (L/min) was monitored for each group and showed no substantial difference. **E)** The heart weight to body weight ratio was calculated for each group and no significant increase in the ratio was observed between groups. Data is expressed as mean value ± st.dev. (n=5).

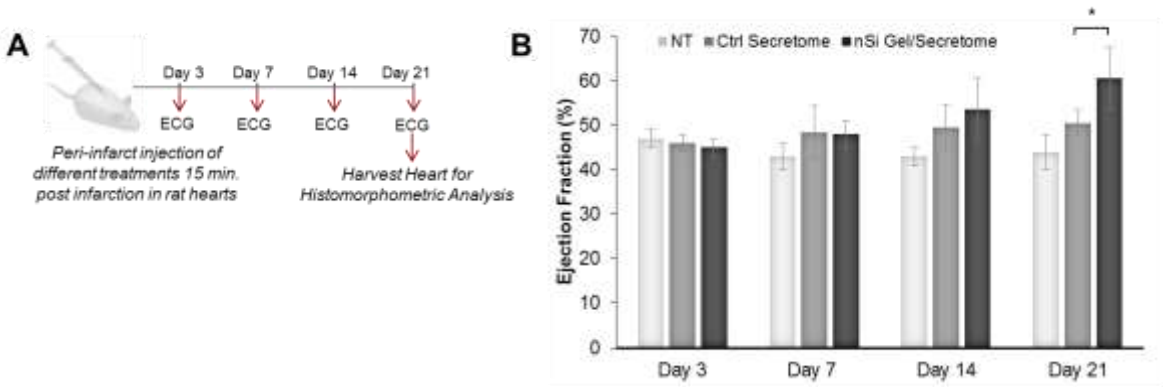

Figure S4.10. *In vivo* cardiac function assessment after secretome delivery with and without the nanocomposite hydrogel. **A)** Schematic representing the design of the study. Specifically, either phosphate buffer saline (No Treatment), the secretome solution (Ctrl Secretome), or the secretome loaded nanocomposite hydrogel (nSi Gel/Secretome) were injected into the peri-infarct region of rat hearts with an induced acute myocardial infarction 15 minutes post infarction. Subsequent echocardiographs were taken at day 3, 7, 14, and 21. **B)** Calculated heart ejection fractions (EF%) at each time point. A significant increase in the nSi Gel/Secretome group EF% was observed when compared to the Ctrl Secretome group at day 21. Data are expressed as mean value ± standard deviation f, * $p<0.05$, ($n = 5$).

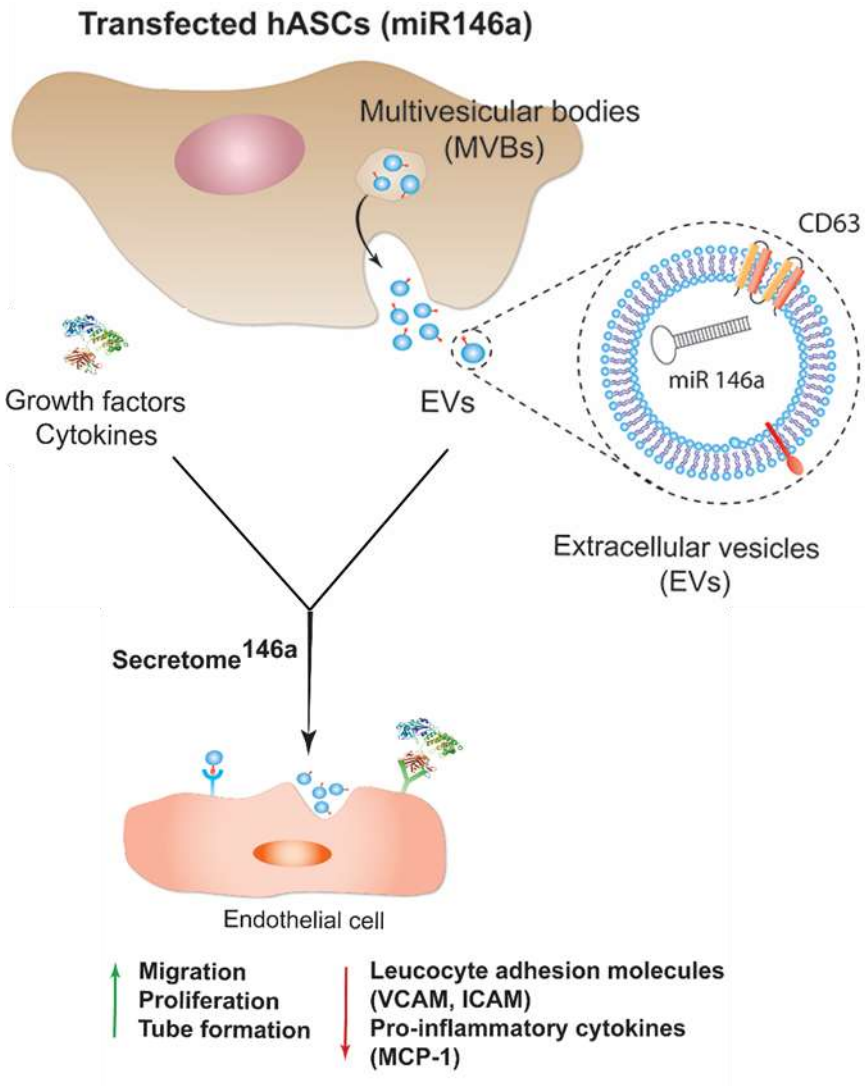

Figure 5.1 Schematic representing the process of hASCs transfection with miR-146a. Upon transfection, hASCs start secreting enriched extracellular vesicles containing miR-146a. The enriched secretome will possess a proangiogenic and anti-inflammatory effect on endothelial cells due to the presence of the miR-146a carried in the exosome subpopulation of EVs. Abbreviations: human adipose-derived stem cells (hASCs), multi-vescular body (MVB), vascular cell adhesion protein (VCAM), intercellular adhesion molecule (ICAM), and monocyte chemoattractant protein-1 (MCP-1).

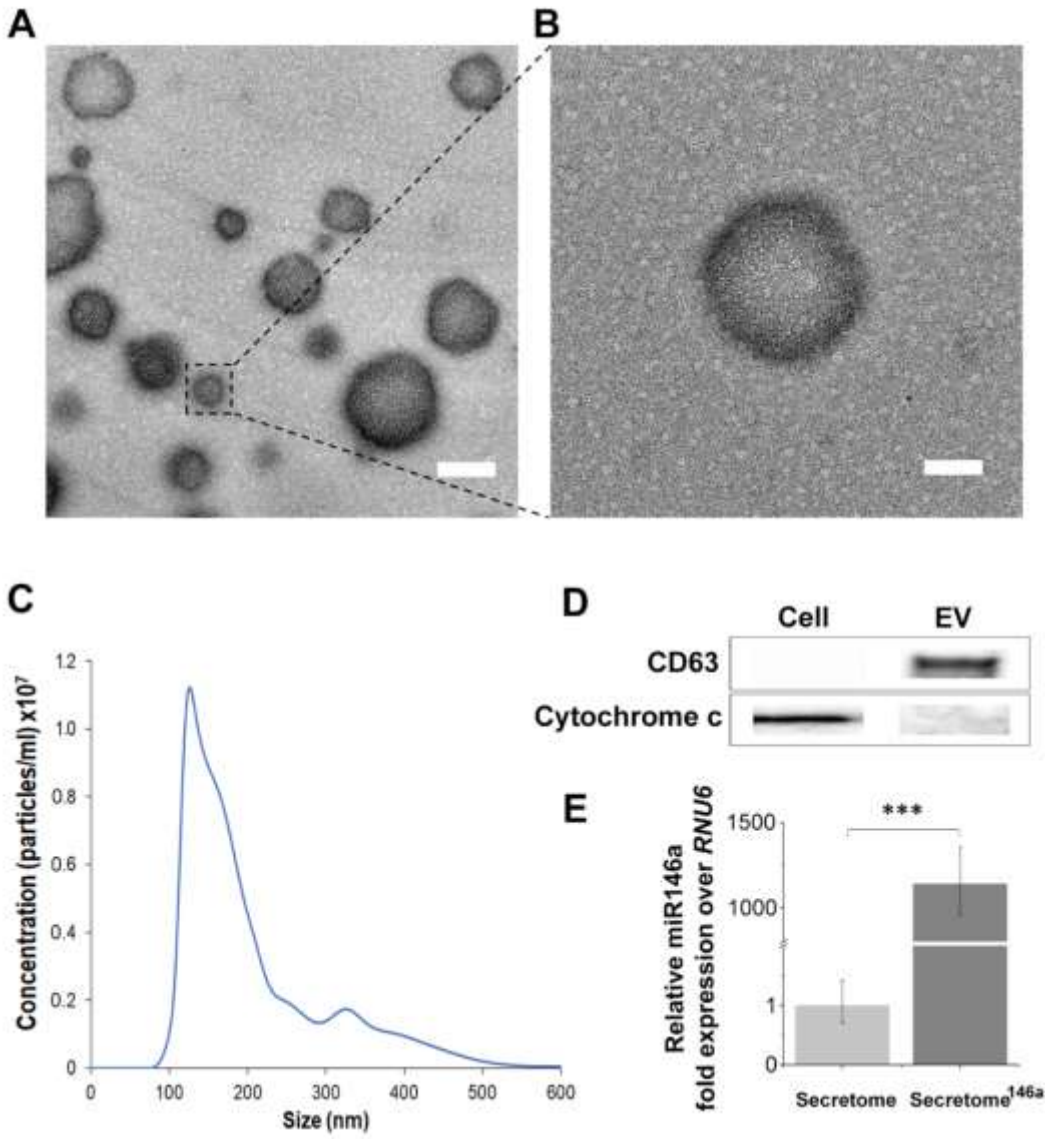

Figure 5.2. Characterization of EVs-derived from transfected hASCs. **A)** TEM images of the extracellular vesicles secreted by hASCs. Scale bar = 200 nm. **B)** Corresponding higher magnification where it is evident the presence of the double bilayer of the exosomes. Scale bar =100 nm. **C)** Representative size distribution curve obtained by the NTA analysis of the extracellular vesicle population secreted by hASCs. It is evident a bimodal distribution with the larger population displaying a smaller size in the range of 150-200 nm. **D)** Western blot analysis was carried out to test the presence of specific protein markers in the exosome population compared to the whole cell lysate. **E)** Relative fold expression of miR-146a in the exosomes obtained from the transfected hASCs. Results are normalized based on the level expression in the control group using *RNU6* as the housekeeping gene.

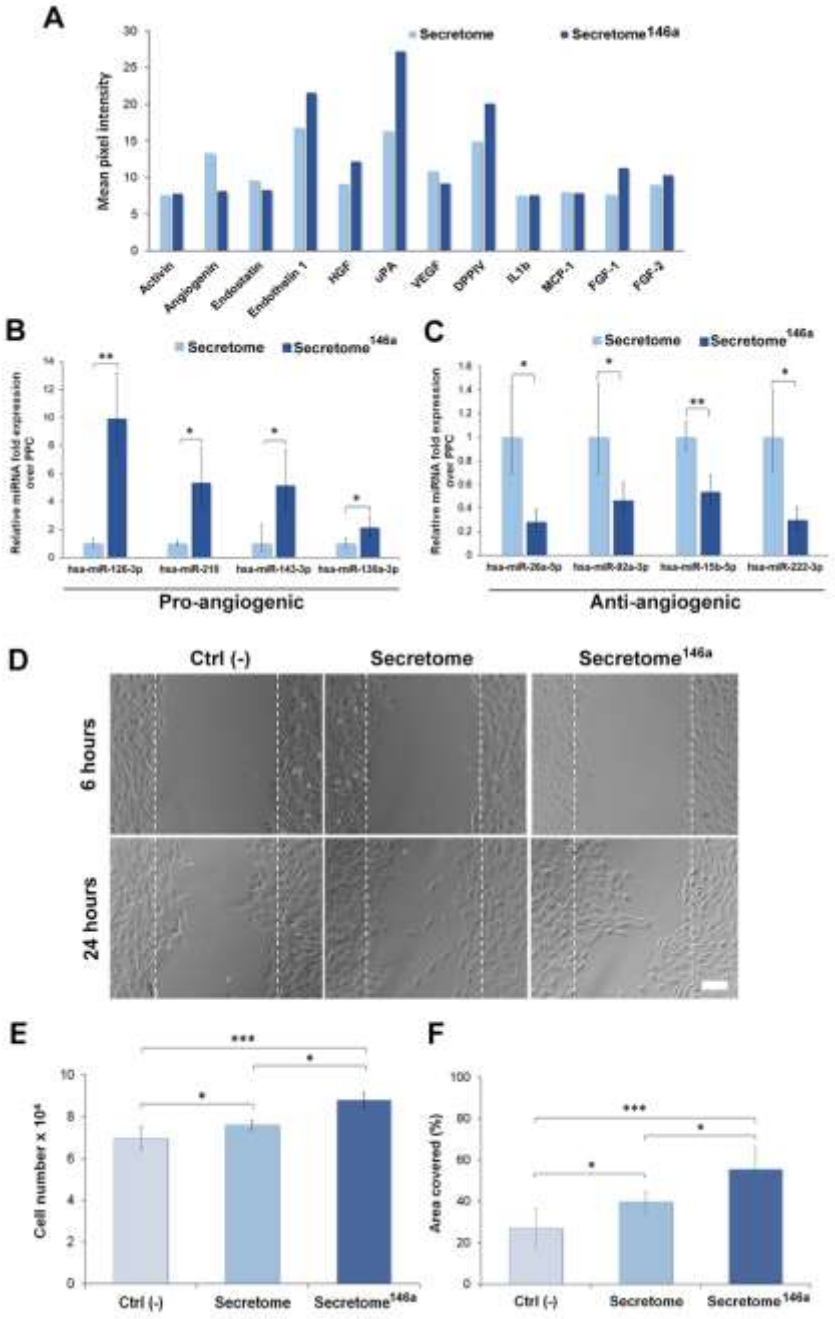

Figure 5.3. Comparison of the growth factor composition and angiogenic properties of the secretome derived from transfected vs non-transfected hASCs with miR-146a. The group named secretome^{146a} refers to hASCs transfected with the miR-146a. **A)** Angiogenic array analysis displaying the difference in the secreted amount of several angiogenic growth factors. **B)** qPCR analysis of the main proangiogenic miRNA found in the EVs of the two types of secretome. **C)** qPCR analysis of the main anti-angiogenic miRNA found in the EVs of the two types of secretome. **D)** Representative bright field images of the scratch assay carried out at 6 and 24 hours for the free different groups. The dotted white lines define the original area of the scratch. Scale bar = 200 µm.

E) HUVEC cell proliferation monitored after 24 hours using an MTS assay (n=5). Cells were treated with different type of secretome and compared to the cells cultured without the addition of any angiogenic growth factor (Ctrl (-)). **F)** Corresponding quantification of the area covered by the HUVECs over 24 hours of migration. Image J analysis was used to quantify the percentage of area covered (n=10). Results are reported as mean ± deviation standard. * = $p<0.05$, ** = $p<0.01$ *** = $p<0.001$.

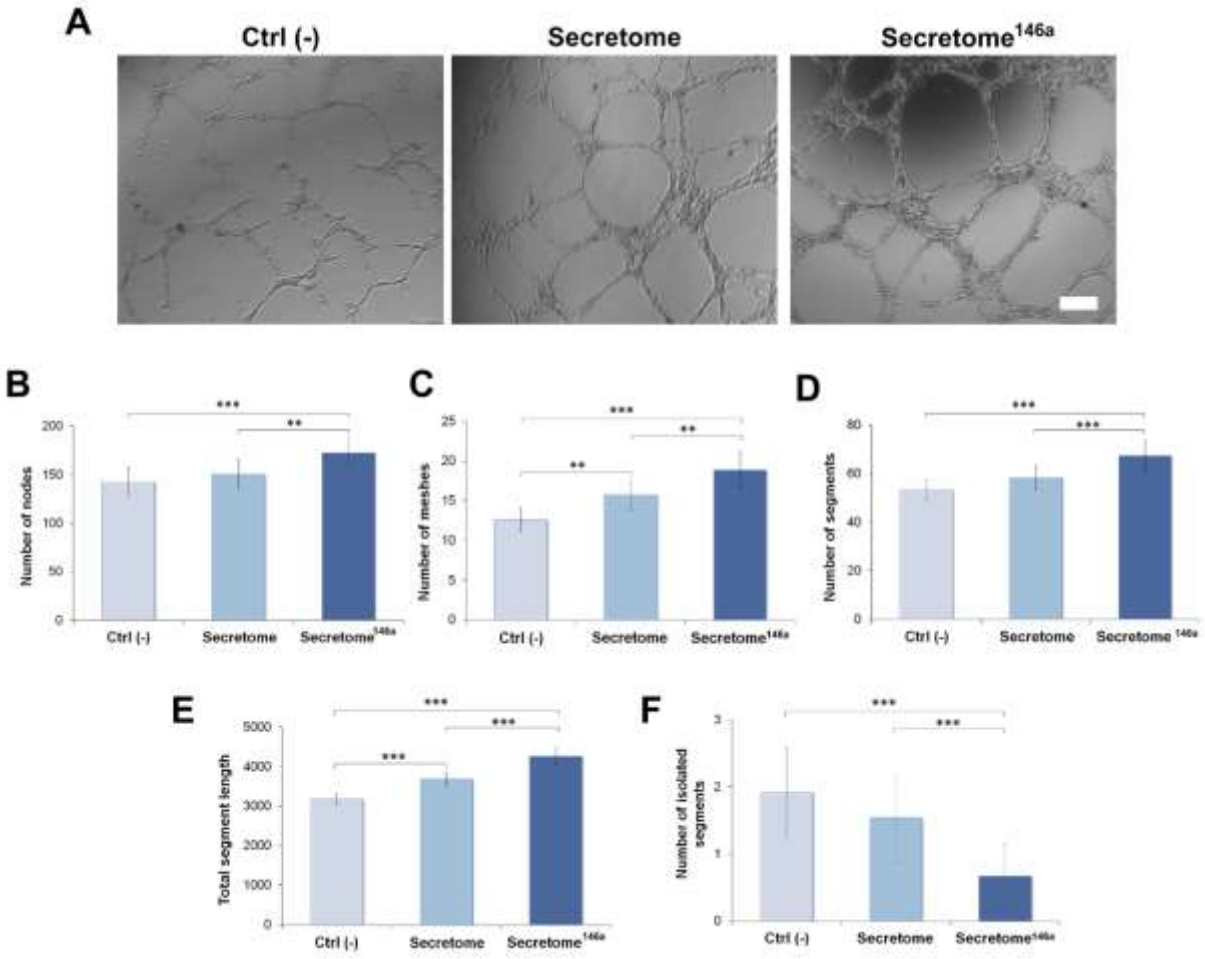

Figure 5.4. Tube formation assay of HUVEC to test the proangiogenic properties of the secretome. **A)** Bright field images of HUVECs cultured on Matrigel and treated with different types of secretome. The negative control group (Ctrl (-)) was represented by endothelial cells cultured without any angiogenic growth factor. Scale bar = 200 µm. Image J quantification of several parameters regarding the network structure including **B)** number of nodes **C)** number of meshes **D)** number of segments **E)** total segments length in the network, and **F)** number of isolated segments. The results are reported as mean ± deviation standard (n=10). * = $p<0.05$, ** = $p<0.01$ *** = $p<0.001$.

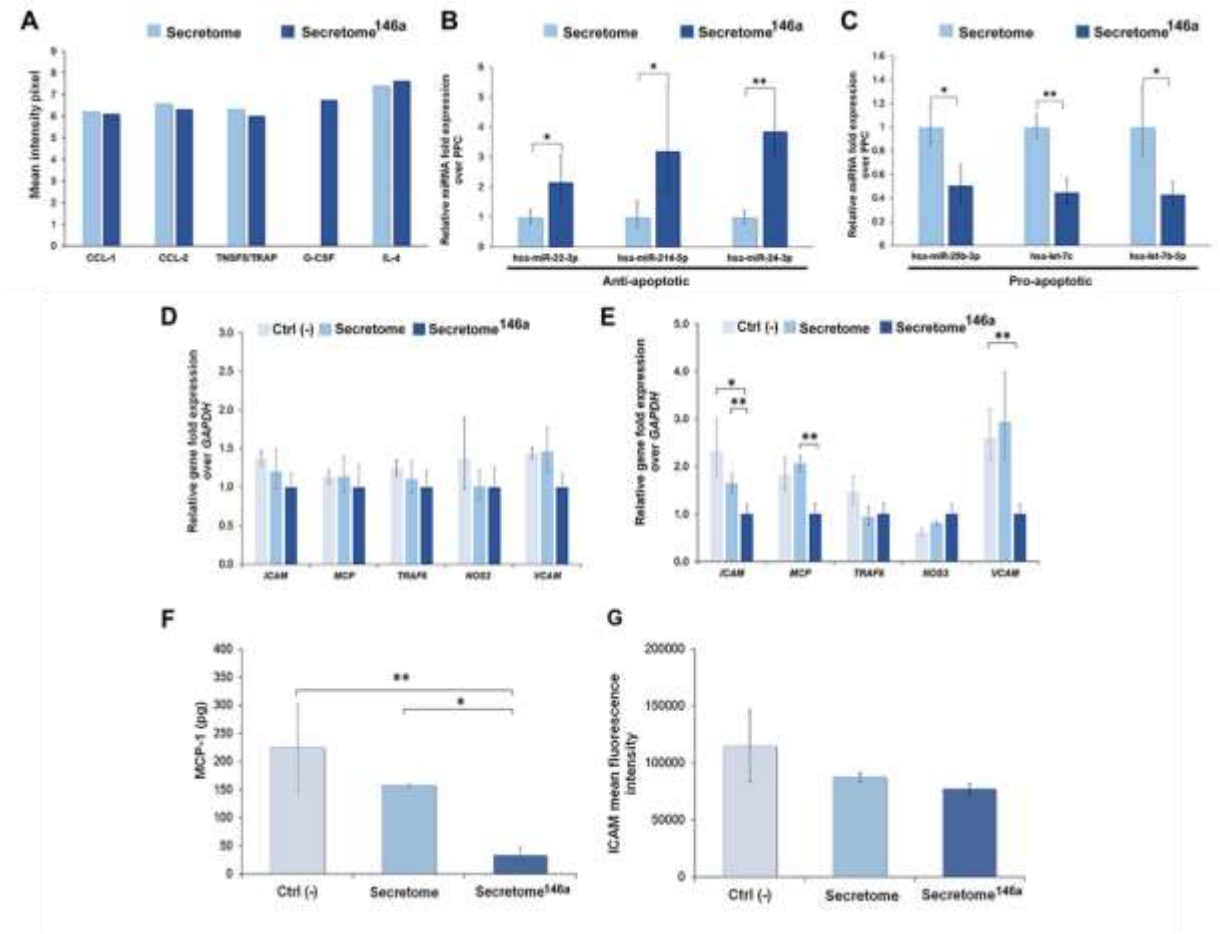

Figure 5.5. Assessment of the anti-inflammatory response of the secretome^{146a}. **A)** Cytokine array results of the different types of cytokines found in the two different types of secretome. **B)** Anti-apoptotic miRNA found in the EVs of the two types of secretome. **C)** Pro-apoptotic miRNA found in the EVs of the two types of secretome. **D-E)** qPCR analysis of main genes involved in the inflammatory response of HUVECs upon exposure to IL-1β. Gene profiles of *ICAM*, *MCP-1*, *TRAF6*, *NOS3* and *VCAM*, were studied at 4 and 24 hours. **F)** Quantification of MCP-1 secreted by HUVECs after being exposed to IL-1β and subsequent treatment with the different types of secretome. **G)** FACs analysis reporting the mean fluorescent intensity of positive fluorescent stained HUVECs expressing the cellular molecular adhesion protein ICAM. Results are reported as mean ± deviation standard. * = $p<0.05$, ** = $p<0.01$ *** = $p<0.001$.

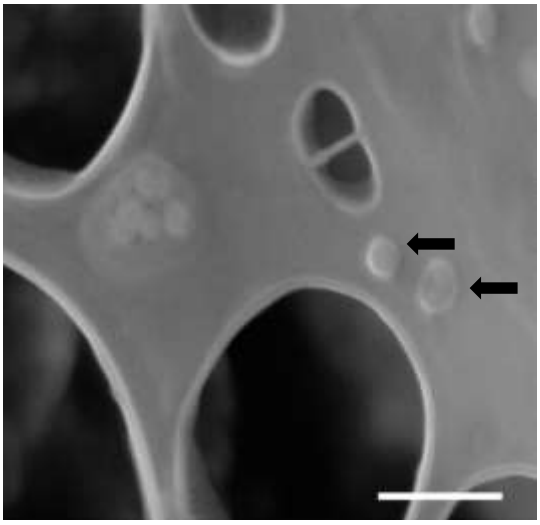

Figure S5.1 SEM image displaying the morphological structure of EV (highlighted by the black arrows). Scale bar= 500 nm.

APPENDIX B: Tables

Chapter 1: No Tables

Chapter 2: Tables 2.1-2.2

Chapter 3: No Tables

Chapter 4: No Tables

Chapter 5: No Tables

Chapter 6: No Tables

Table 2.1 Clinical Trials Assessing Adult Stem Cell Therapy for AMI and IHD

Trial	Follow-Up	n	Cell Type, Dose, and Treatment Groups	Delivery Method	End Point Evaluation	LVEF	LV Volumes	Scar Size
Perin et al.[259]	4 mo	21	25.5×106 BMMNCs vs control	TESI	Echo	↑	↓ESV	NA
TOPCARE CHD Assmus et al. [260]	3 mo	75	22×106 CPCs vs 205×106 BMMNCs vs control	IC	LVG	BMMNC ↑EF	NS	NS
FOCUS CCTRN Perin et al.[261]	6 mo	92	100×106 BMMNCs vs placebo	TESI	Echo SPECT	NS	NS	NS
MSC-HF Mathiasen et al.[262]	6 mo	55	77×106 BM-MSC vs placebo	TESI	cMRI or CT	↑	↓ ESV	↓
SCIPIO Bolli et al.[263]	4 mo	23	1×106 CSCs vs control	IC	Echo/cMRI	↑	NA	↓
POSEIDON Hare et al.[264]	13 mo	30	20, 100, or 200×106 BM-MSCs (allo vs auto)	TESI	cMRI	NS	Allo: ↓EDV	↓
CADUCEUS Makkar et al.[265]	6 mo	31	12.5–25×106 CDCs vs control	IC	cMRI	NS	NS	↓
CHART-1 Bartunek et al.[266]	39 wk	351	9.7×108 – 1.2×109 Cardiopoietic cells vs sham	TESI	Echo	NS	NS	NA
TAC-HFT Heldman et al.[53]	12 mo	65	100×106 BM-MSCs vs 100×106 BMMNCs vs placebo	TESI	cMRI/CT	NS	NS	MSC: ↓
RIMECARD Bartolucci et al.[57]	12 mo	30	1×106 /kg UC-MSC vs placebo	IV	Echo/cMRI	↑	↑EDV	NA
ATHENA Trials Henry et al.[60]	12 mo	31	80×106 vs 40×106 ARDCs vs placebo	TESI	Echo	NS	NS	NA
TOPCARE-AMI Schächinger et al.[43]	12 mo	59	CPCs; BMMNCs 7. 3×106	IC	LVG	↑	↓ ESV	↓

BOOST Wollert et al.[44]	6 mo	60	2.4×109 BMMNCs vs control	IC	cMRI	↑	NS	NA
REPAIR-AMI Schächinger et al.[47]	4 mo	204	198×106 BMMNCs vs placebo	IC	LVG	↑	NS	NA
TIME Traverse et al.[48]	6 mo	120	150×106 BMMNCs vs placebo	IC	cMRI	NS	NS	NS
LateTime Traverse et al.[49]	6 mo	87	150×106 BMMNCs vs placebo	IC	cMRI	NS	NS	NS
SWISS AMI Sürder et al.[50]	12 mo	192	153×106 BMMNCs vs control	IC	cMRI	NS	NS	NS
BOOST-2 Wollert et al.[267]	6 mo	188	20.6×108 vs 7.0×108 BMMNCs vs placebo	IC	cMRI	NS	NS	NS
Pre-SERVE-AMI Quyyumi et al.[52]	12 mo	161	14.9×106 CD34+ vs placebo	IC	cMRI	NS	NS	NS
Hare et al.[268]	6 mo	34	BM MSC, allogeneic 0.5×106 1.6×106 5×106	IV	Echo/cMRI	↑ EF		
Bartolucci et al.[57]	12 mo	15	UC MSC, allogeneic 1×106	IV	Echo/cMRI	↑ EF		
Butler et al.[269]	90 d	10	BM MSC, allogeneic 1×106	IV	cMRI	↑ EF		

Table 2.2 Key Paracrine Molecules for Cardiac Regeneration

Protein	Main cardiac functions	Refs.
Insulin-like growth factor-1 (IGF-1)	Anti-apoptotic; promote stem cell growth and differentiation	270-273
Hypoxia-inducible factor-1a (HIF-1a)	Trigger release of angiogenic growth factors and nitric oxide	244, 274-276
Sonic hedgehog (Shh)	Induce cardiac morphogenesis; anti-apoptotic	243, 277
Fibroblast growth factor-1 (FGF-1)	Initiation of angiogenesis; stimulate cardiomyocyte proliferation	243, 276, 278, 279
Fibroblast growth factor-2 (FGF-2)	Initiation of angiogenesis; upregulate proliferation, migration, and survival of endothelial cells; induce chemotaxis; anti-apoptotic	243, 244, 275, 276, 280, 281
Vascular endothelial growth factor-A (VEGF-A	Initiation of angiogenesis; upregulate proliferation, migration, and survival of endothelial cells; trigger nitric oxide release	243, 244, 275, 276, 282
Platelet-derived growth factor-BB (PDGF-BB)	Upregulate proliferation and chemotaxis of pericytes; promote angiogenesis and neovessel maturation; anti-apoptotic	270, 275, 283, 284
Hepatocyte growth factor (HGF)	Angiogenic, anti-apoptotic; chemotactic on stem/progenitor cells	133, 272, 285
Granulocyte colony-stimulating factor (G-CSF)	Chemotactic on stem/progenitor cells; anti-apoptotic; angiogenic	250, 251
Stromal cell-derived factor 1-a (SDF1-a)	Chemotactic on stem/progenitor cells; angiogenic	134, 286-289
Erythropoietin (EPO)	Chemotactic on stem/progenitor cells; angiogenic; anti-apoptotic	290-295
Thymosin-b4	Chemotactic on stem/progenitor cells; angiogenic	270, 296
Neuregulin-1 (NRG-1)	Induce cardiomyocyte proliferation; anti-apoptotic	297-300
Tissue inhibitor of metalloproteinases-1 (TIMP-1)	Inhibit MMP activity and ECM degradation; anti-apoptotic	281, 301, 302
Tissue inhibitor of metalloproteinases-3 (TIMP-3)	Inhibit MMP activity and ECM degradation; anti-apoptotic; anti-inflammatory	137, 281, 302-305
Interleukin-10 (IL-10)	Anti-inflammatory; anti-apoptotic	306, 307
Monocyte chemoattractant protein-1 (MCP-1)	Pro-inflammatory; angiogenic; chemoattractant	308, 309
miR-24	Targets the proapoptotic Bcl-2-like protein 11 (Bim); anti-apoptotic	310, 311
miR-214	Targets the proapoptotic Bcl-2-like protein 11 (Bim); anti-apoptotic	312, 313

miR-210	Targets antiangiogenic receptor tyrosine kinase ephrin-A3 and proapoptotic tyrosine-protein phosphatase non-receptor type 1 (PTP-1B); angiogenic, anti-apoptotic	[314, 315]
miR-126	Targets phosphoinositol-3 kinase regulatory subunit 2 (PIK3R2); angiogenic	[316]
miR-132	Inhibits RAS GTPase-activating protein (Ras p21 protein activator); angiogenic	[317]
miR-146	downregulates *NRAS*; anti-apoptotic, angiogenic	[235, 318]
miR-22	Inhibits methyl CpG binding protein 2 (Mecp2); anti-apoptotic	[81]
miR-221	Inhibits levels of p53 up-regulated modulator of apoptosis (PUMA); anti-apoptotic	[319]
miR-21	suppression of Fas ligand targeting PDCD4; anti-apoptotic	[320]